Warm DM Scenario for galaxy formation: constraining the WDM candidates

N. Menci
Osservatorio Astronomico di Roma - INAF

Outline

Unsolved issues in CDM on small scales: Solutions based on Astrophysics vs Solutions based on Warm Dark Matter

Some properties of WDM galaxy formation

Constraining the Warm Dark Matter particle mass: getting rid of uncertainties due to modelling of astrophysical processes

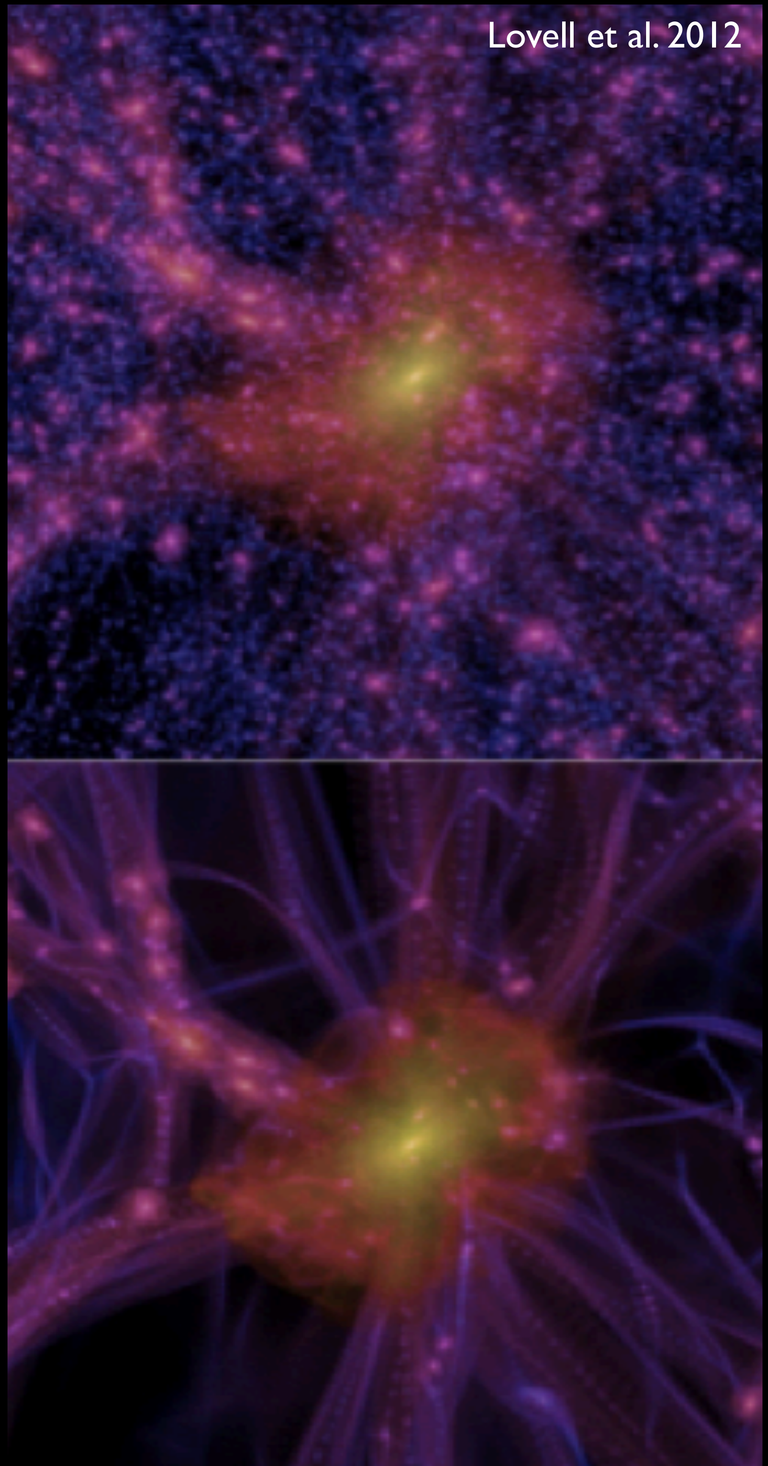

Cosmic Structures form from the collapse of overdense regions in the DM primordial density field, and grow by gravitational instability

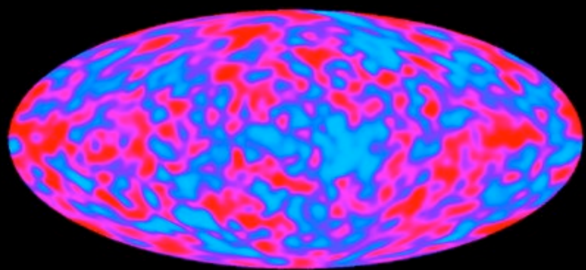

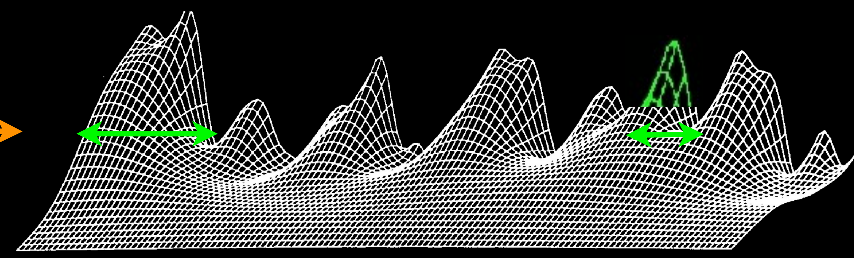

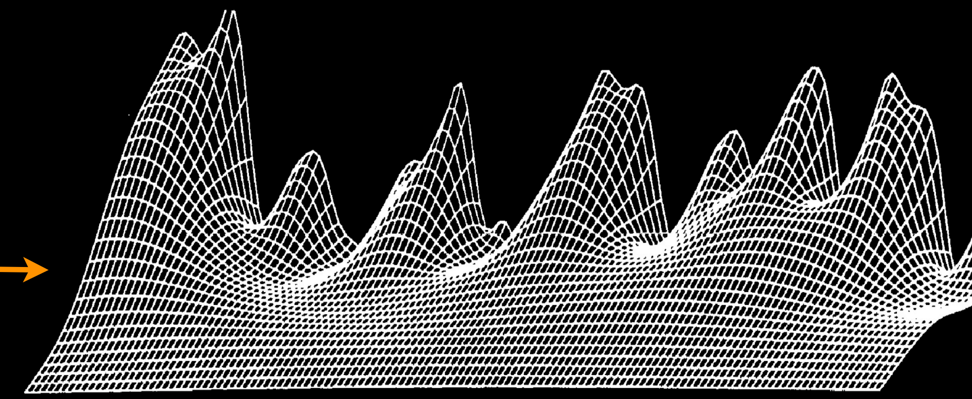

R=2π/k

$$M = \frac{4\,\pi}{3}\,\rho\,R^3$$

$$\langle \delta_M^2 \rangle = \sigma^2(M)\,g(t)$$

Gaussian Random field

$$\delta = \frac{\delta\rho}{\rho}$$

$$p(\delta_k) = \frac{1}{\sqrt{2\pi}\,\sigma_k}\,e^{-\frac{\delta_k^2}{2\,\sigma_k^2}}$$

Mean (square) value of perturbations of size R(~1/k) enclosing a mass M

$$P(k) = \frac{1}{V}\,\langle|\delta_k|^2\rangle$$

$$\sigma_M^2 = \frac{1}{(2\pi)^3\,V}\int^{M\leftrightarrow k} dk\,k^2\,P(k)$$

$$\sigma_M^2 \leftrightarrow P(k)$$

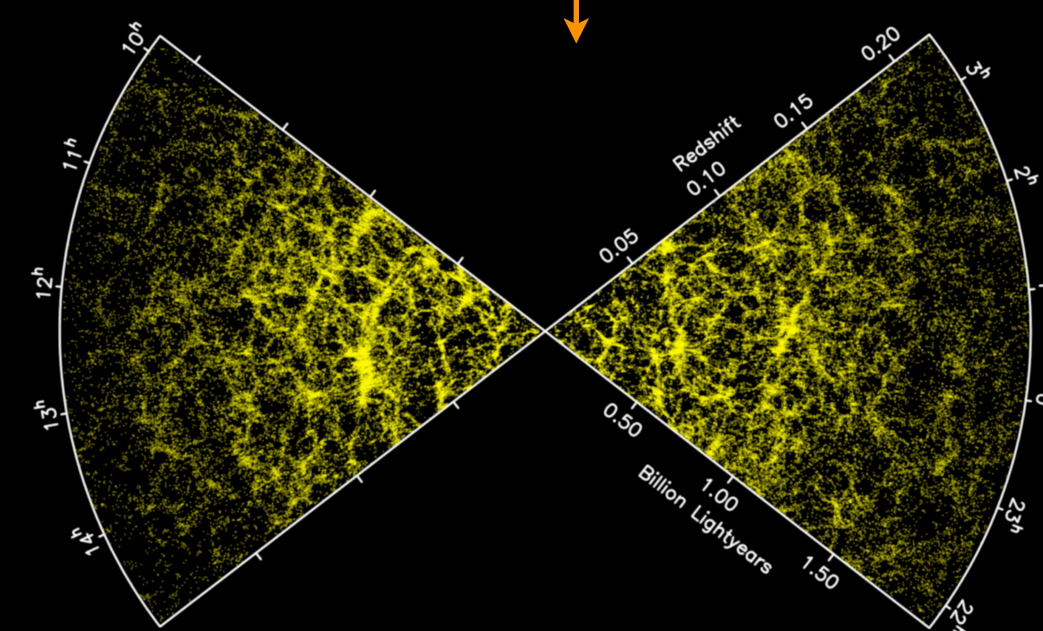

Variance σ(M) quantifies the typical amplitude of density perturbations on a given mass scale

The Variance of the perturbation field

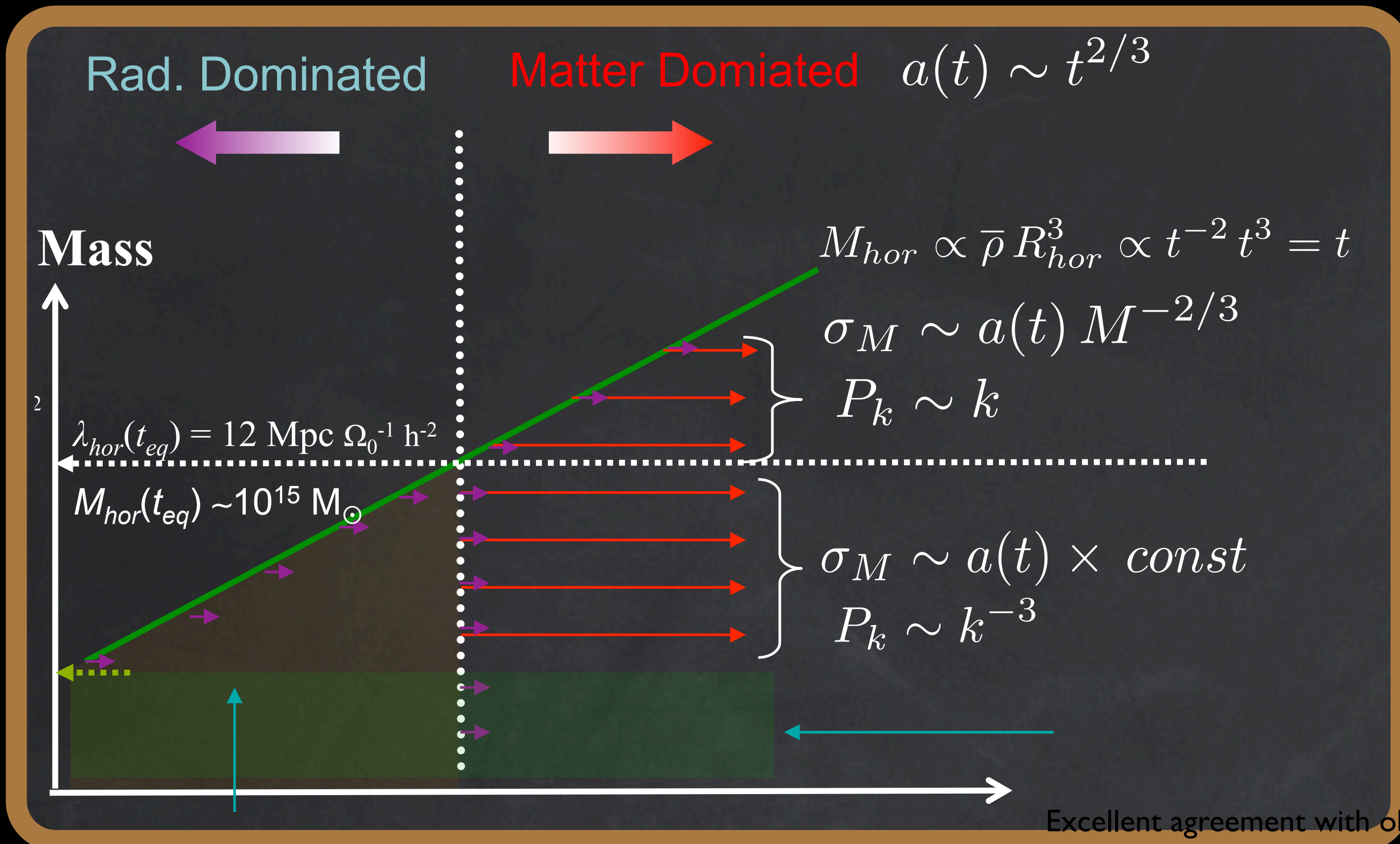

Cold Dark Matter

non relativistic at decoupling

no dissipation down to small scales < 10^6 $M_\odot$

Variance is an ever-increasing inverse function of the mass scale.

Huge number of small-scale structures

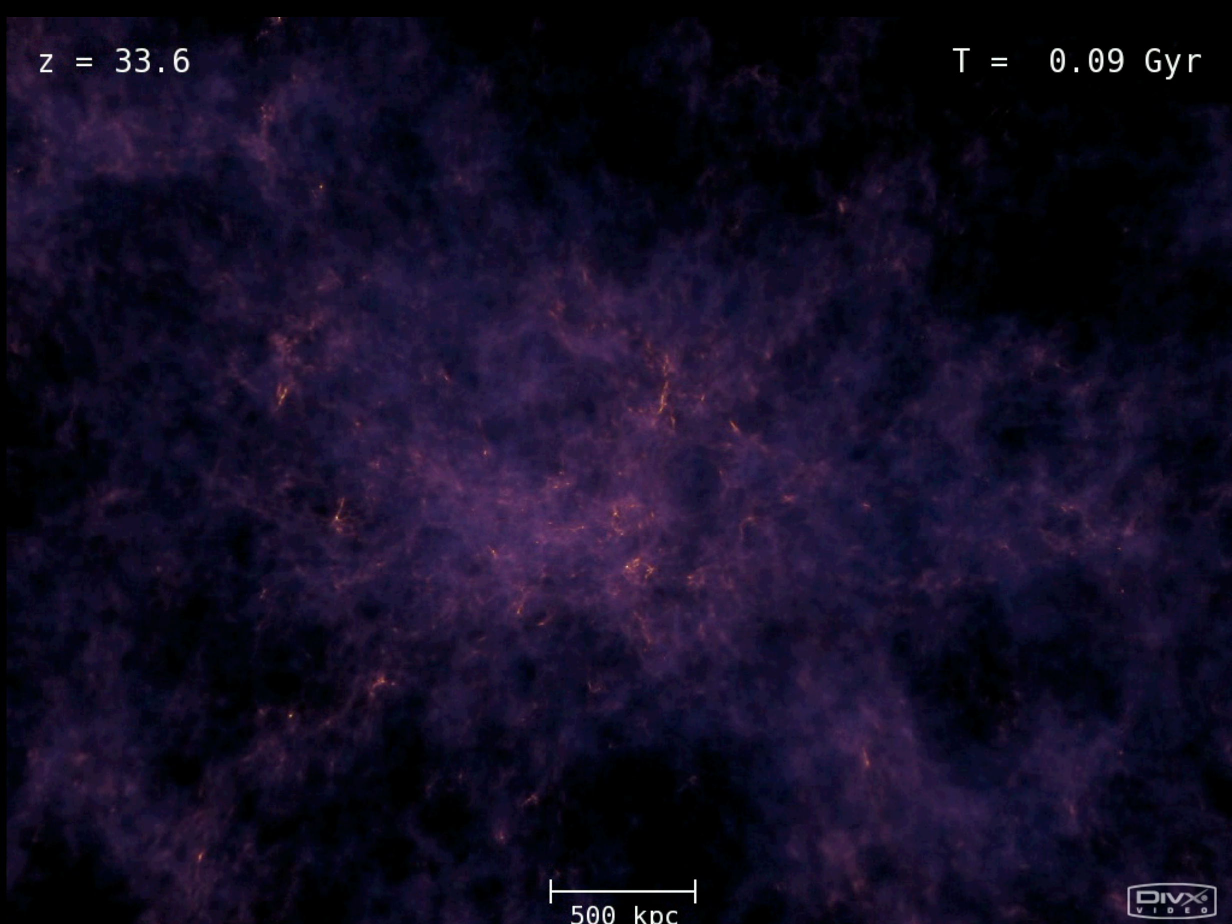

Springel et al. 2009

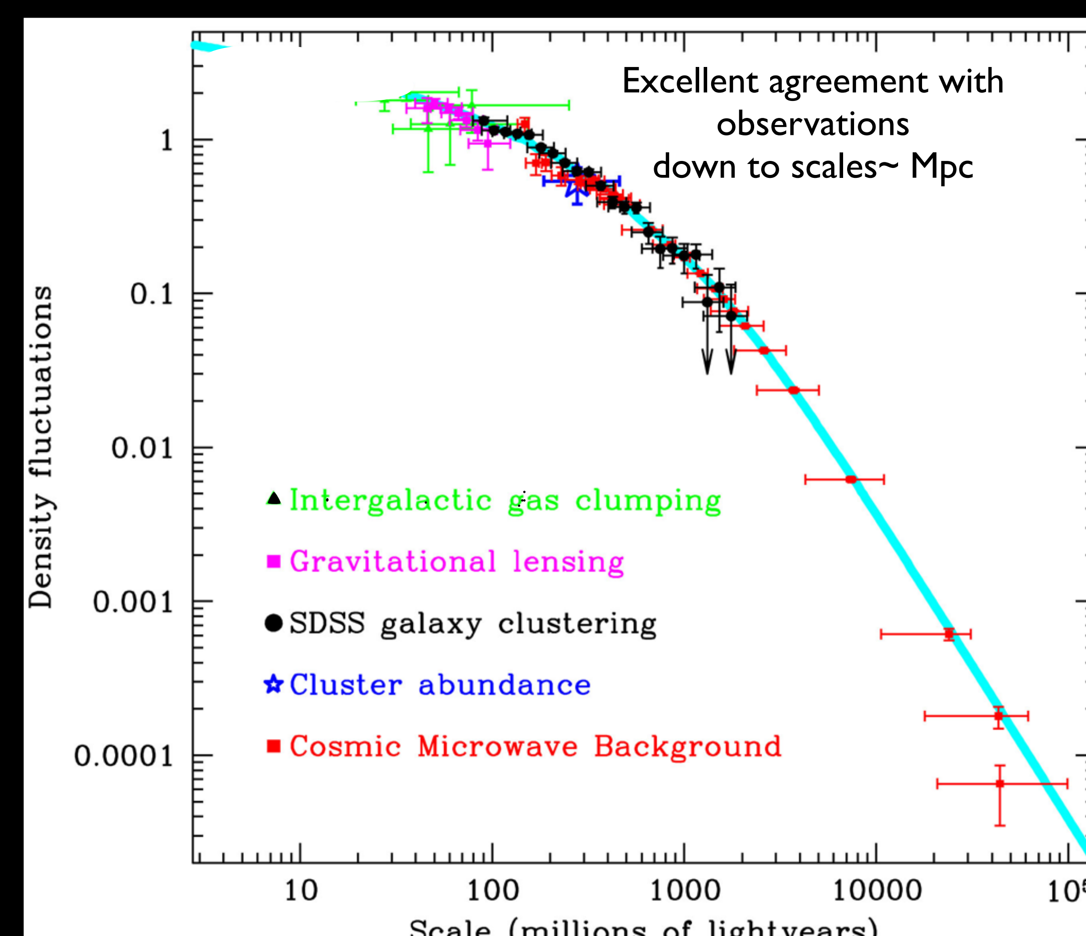

Dissipation, free-streaming scale

$$r_{fs} = \int_0^t \frac{v(t)}{R(t)}$$

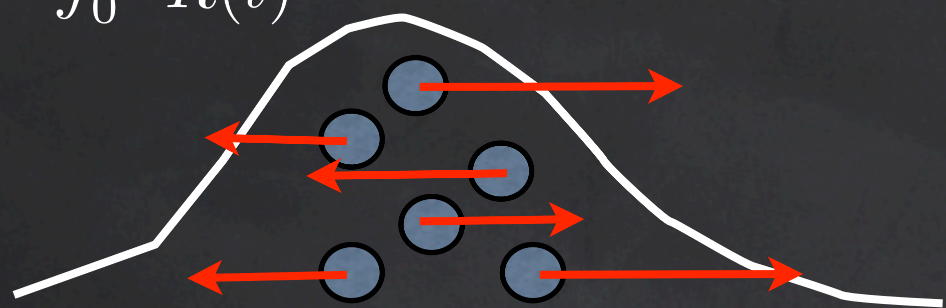

$$\sigma_\chi \propto a^{-1}\, m_\chi^{-1/2}$$

$$M_{fs} = 4 \times 10^{15} \left(\frac{m_\nu}{30\ \mathrm{eV}} \right)^{-2} M_\odot$$

Lighter and faster Dark Matter particles stream out of density perturbations

CDM: the free streaming length is much smaller than any scale involved in galaxy formation (≪Mpc)

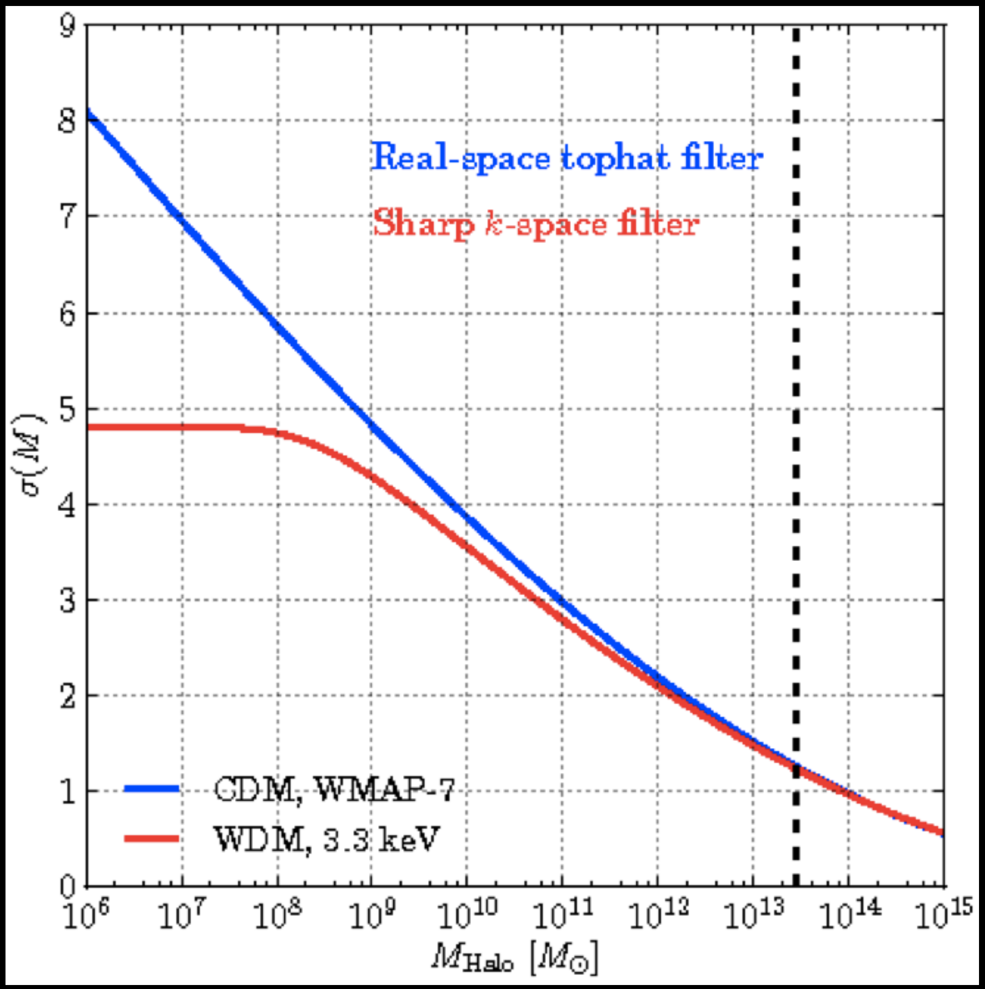

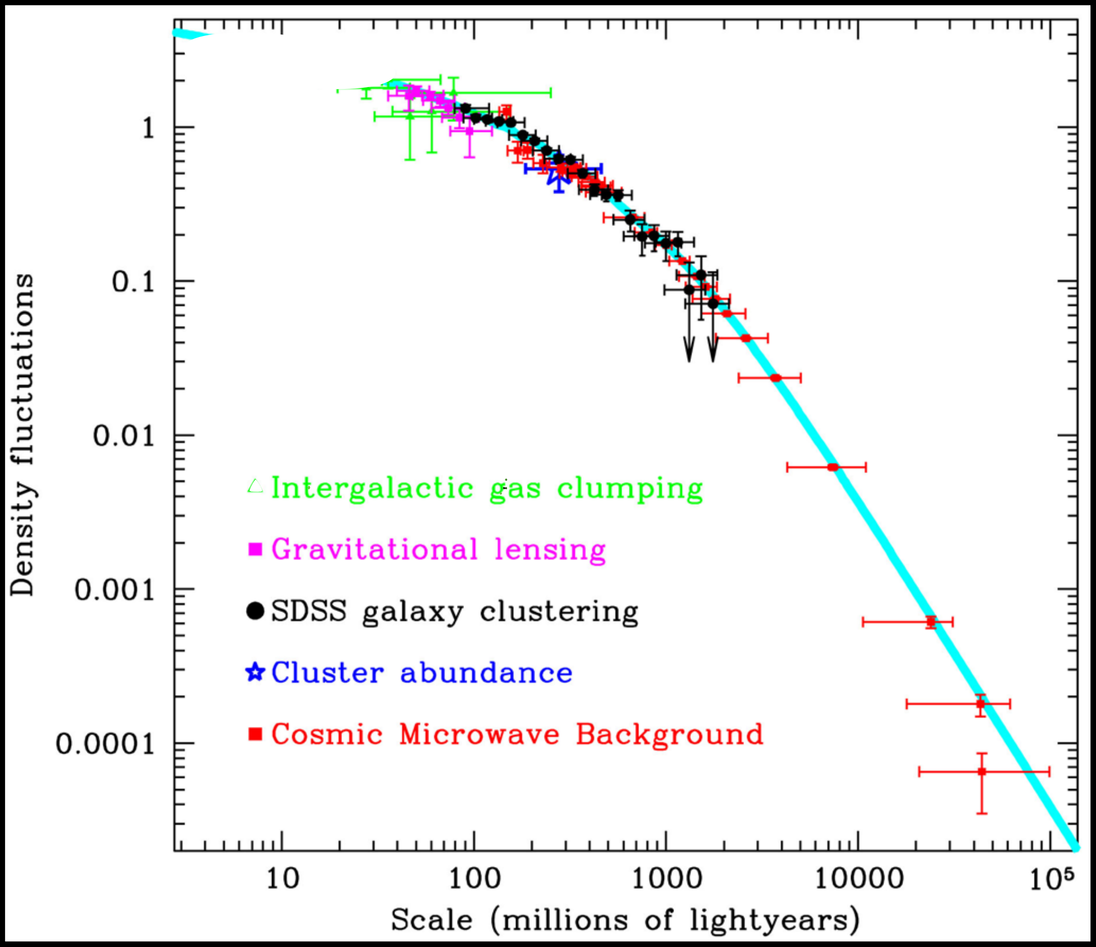

Dissipation, free-streaming scale

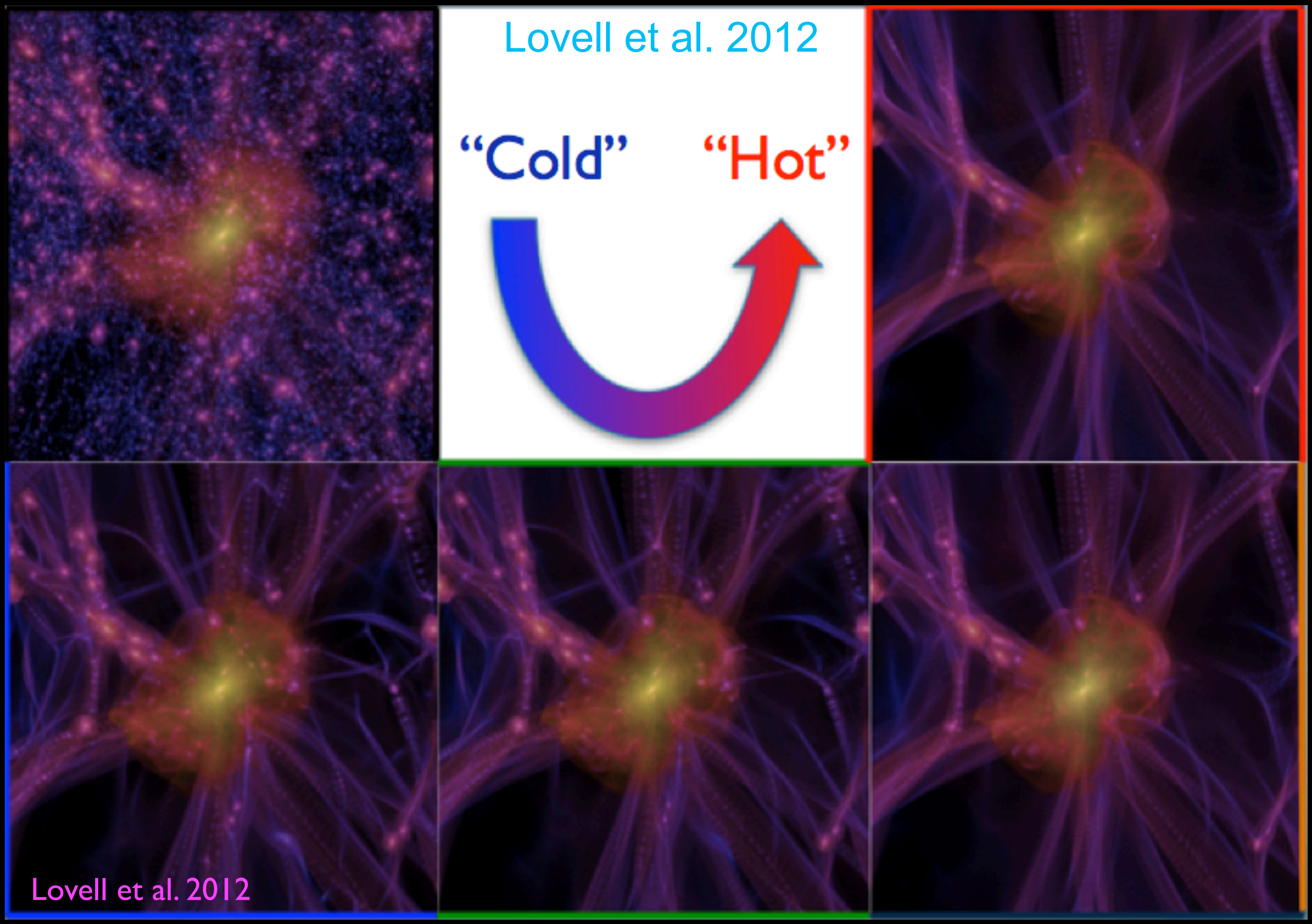

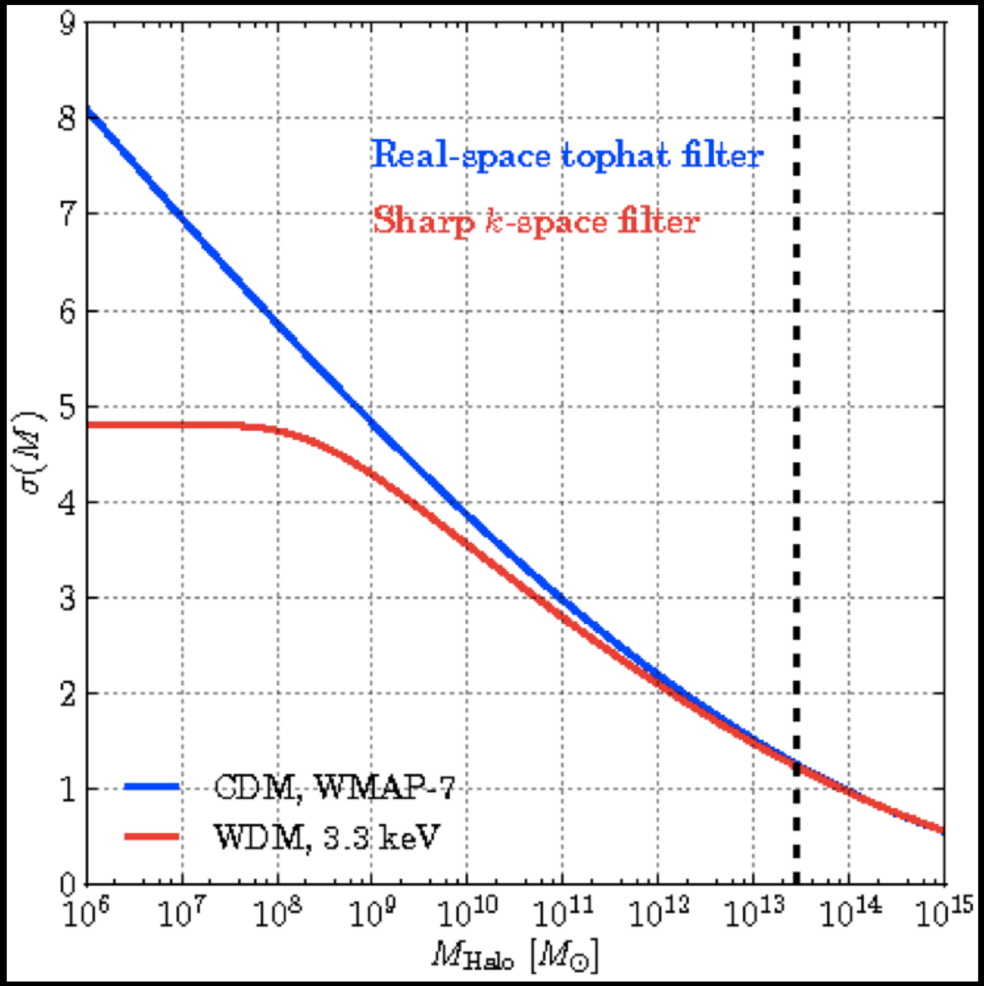

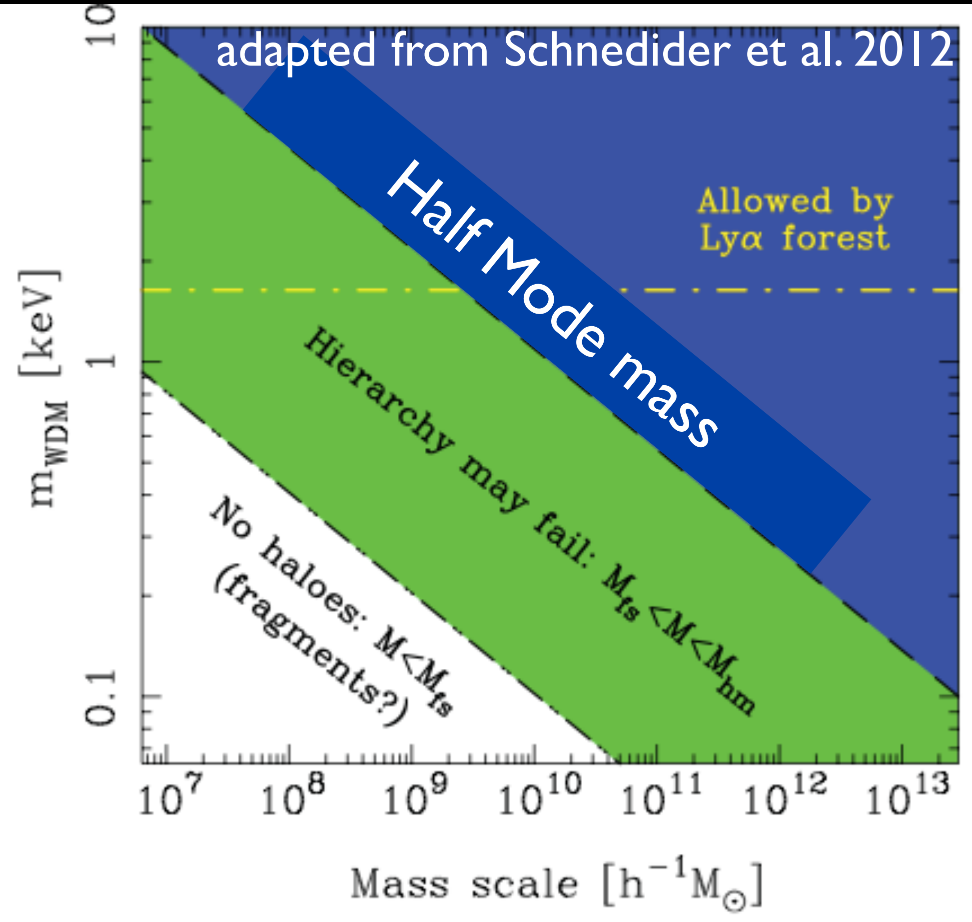

Dissipation, free-streaming scale

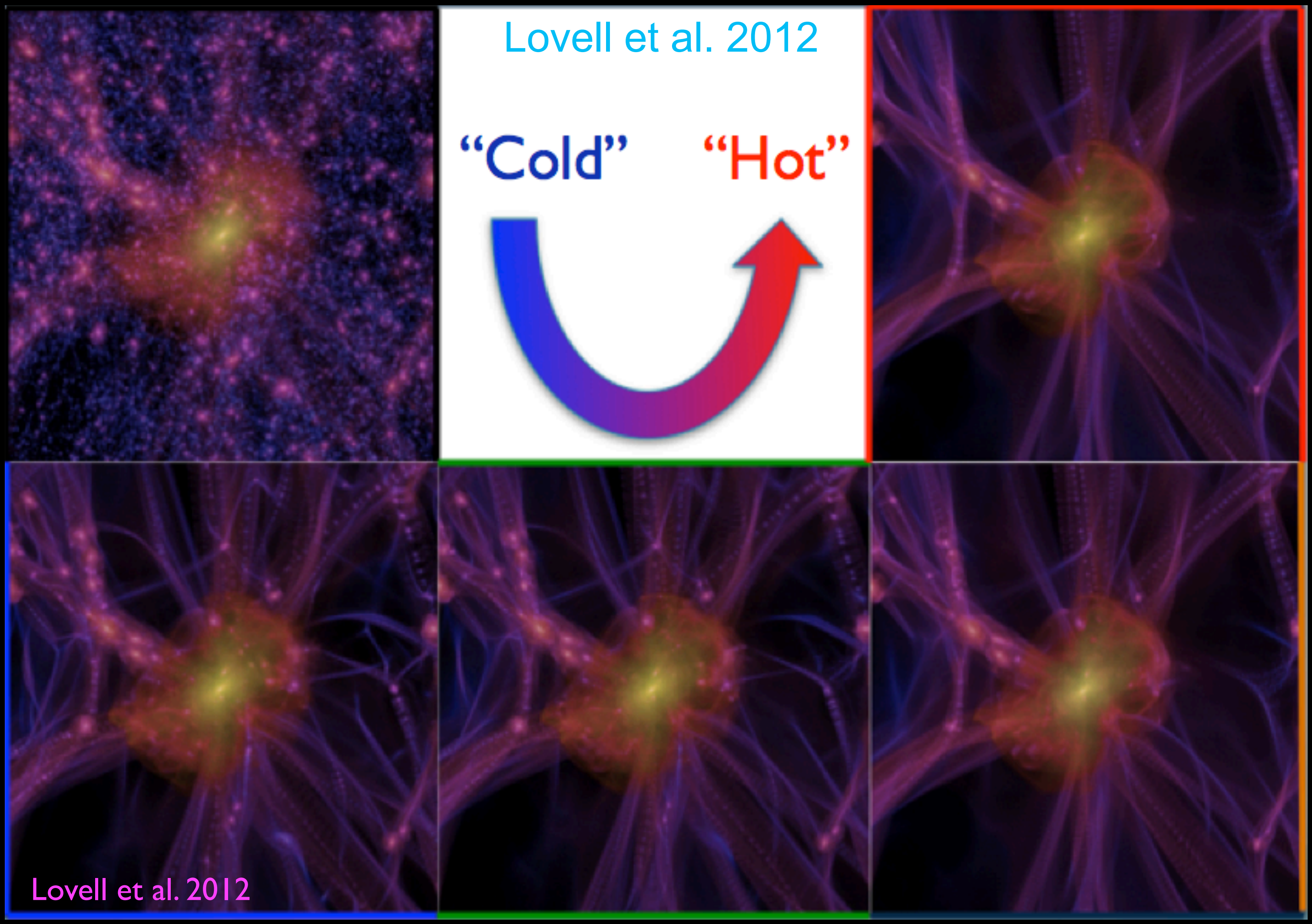

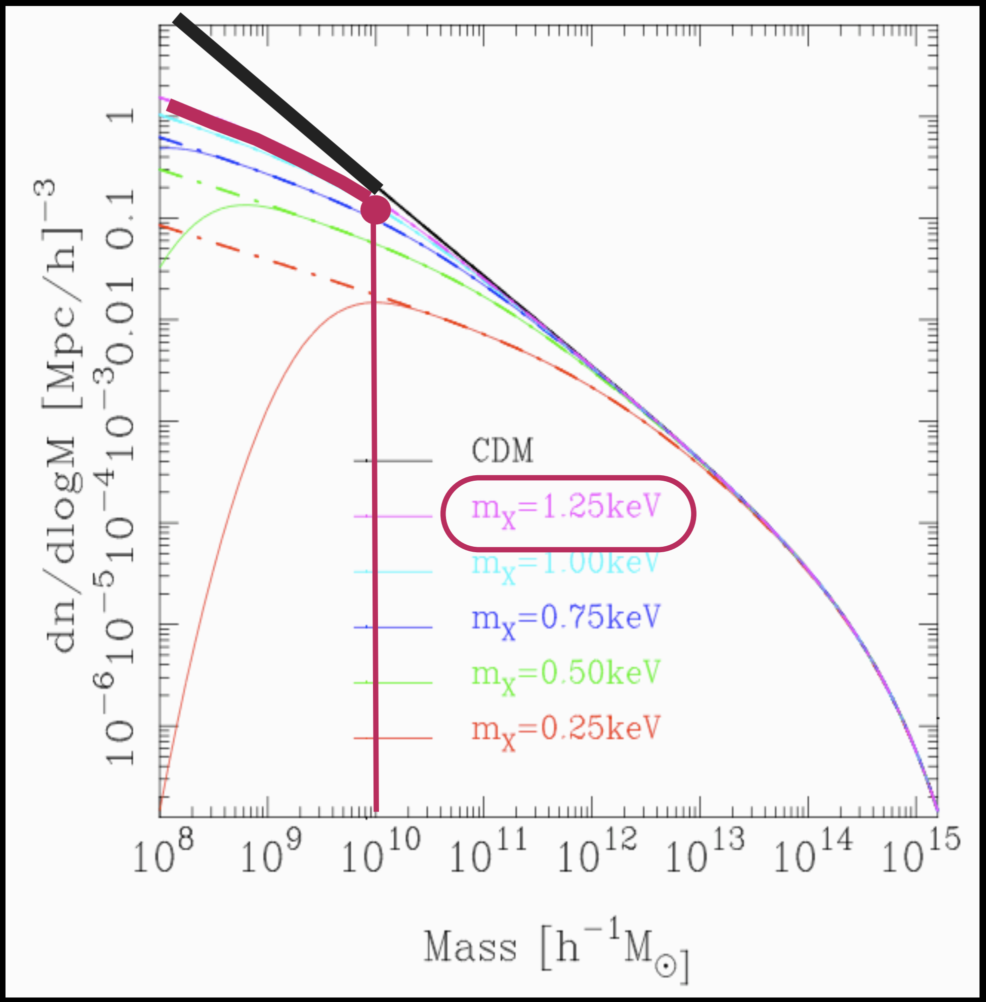

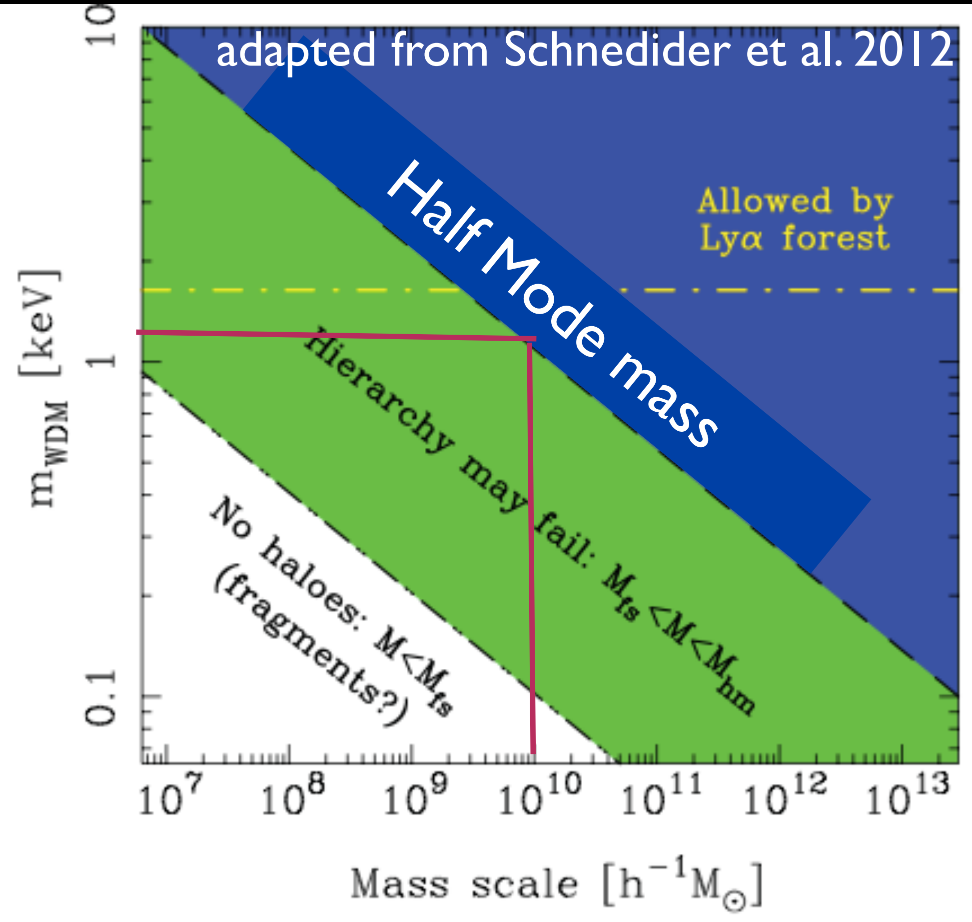

Compared to CDM, in WDM models the abundance of low-mass structures is suppressed below the half mode mass

Critical Issues
(concerning structure formation)

Overabundance of low-mass objects
i) abundance of faint galaxies
ii) abundance of satellite DM haloes
iii) density profiles
iv) the M_*-M_{halo} relation
v) star formation histories dwarfs

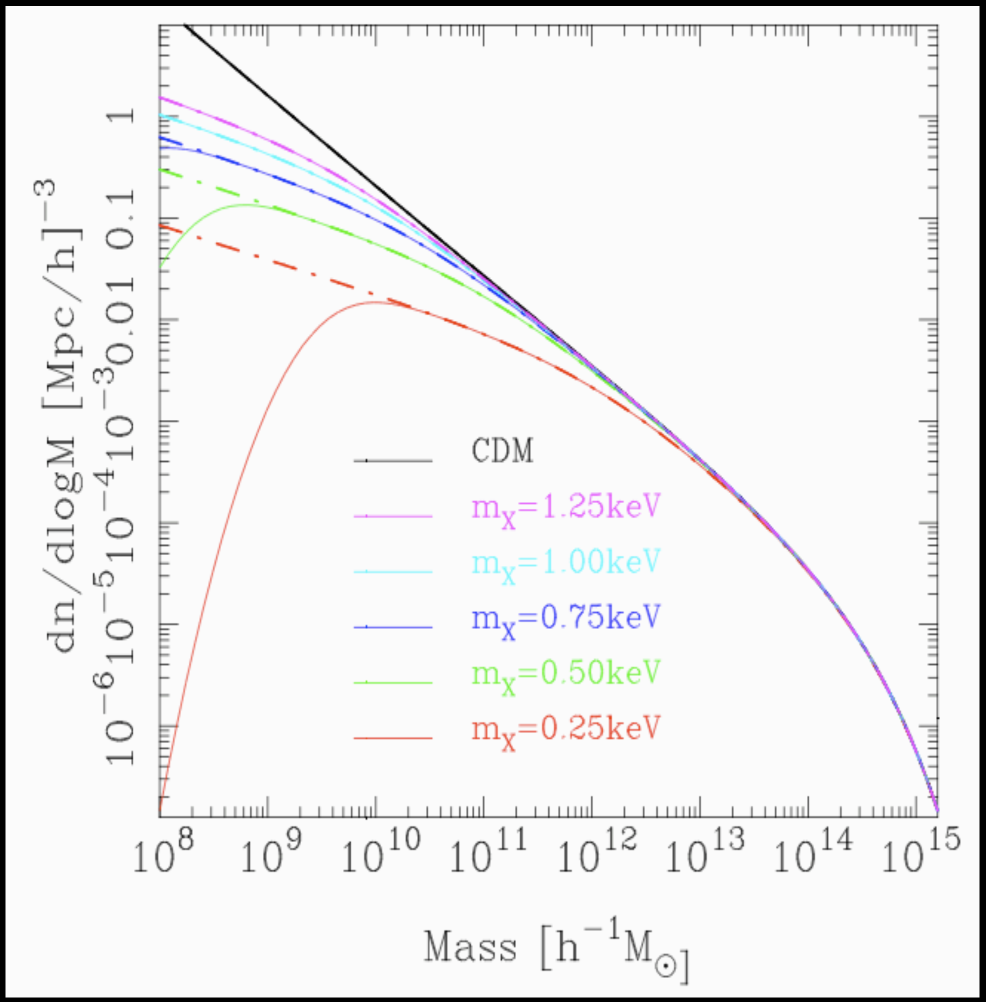

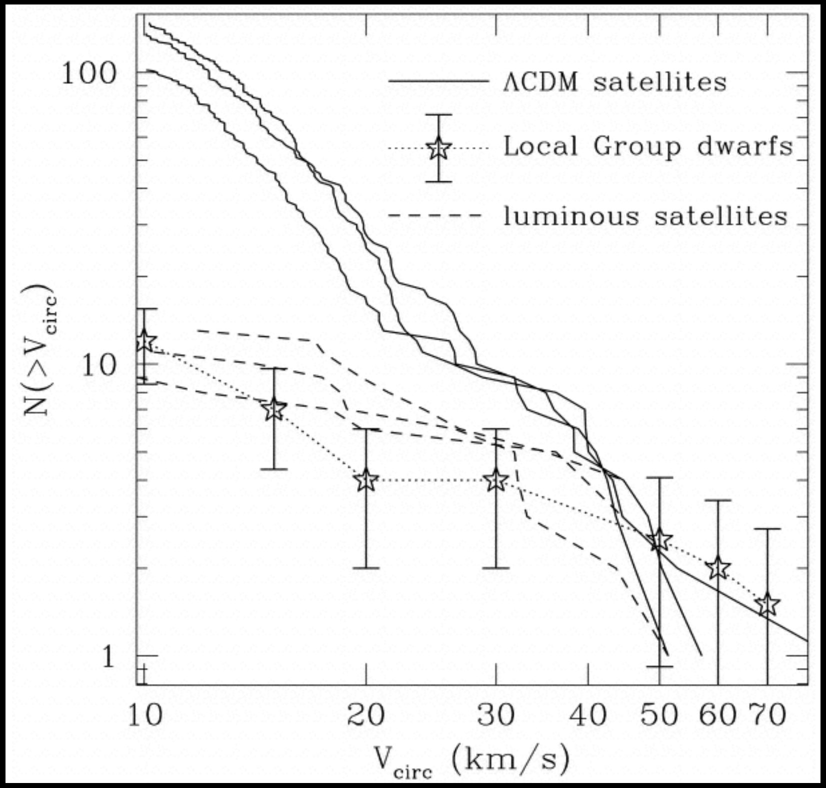

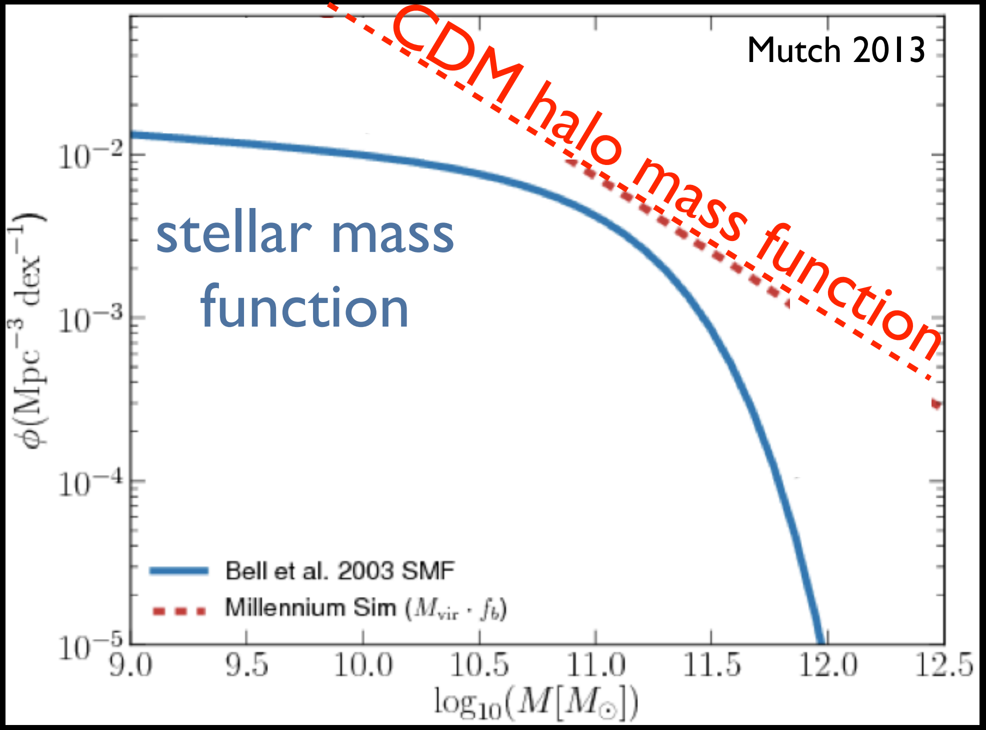

The DM-Feedback Degeneracy

The origin of the problem:
The CDM halo Mass function has a steep slope $N \sim M^{-1.8}$
The Observed Luminosity Function has a flatter slope $N \sim L^{-1.2}$

A Possible Solution:
Suppress luminosity (star formation) in low-mass haloes
$L/M \sim M^{\beta}$ $\beta = 1\text{-}3$

- Enhanced SN feedback
- UV background

Heat - Expell Gas from shallow potential wells

$$E_{SN} \approx 10^{51}\,\eta_0 \eta_{IMF}\,\Delta M_* erg/s$$

$$v_{SN} = \sqrt{E_{SN}/M_{gas}} \approx 100 \;\; km/s$$

At Z=0 the mass scale at which SN can effectively espell gas from DM potential wells

$$M_{SN} \sim 10^{10}\, M_\odot$$

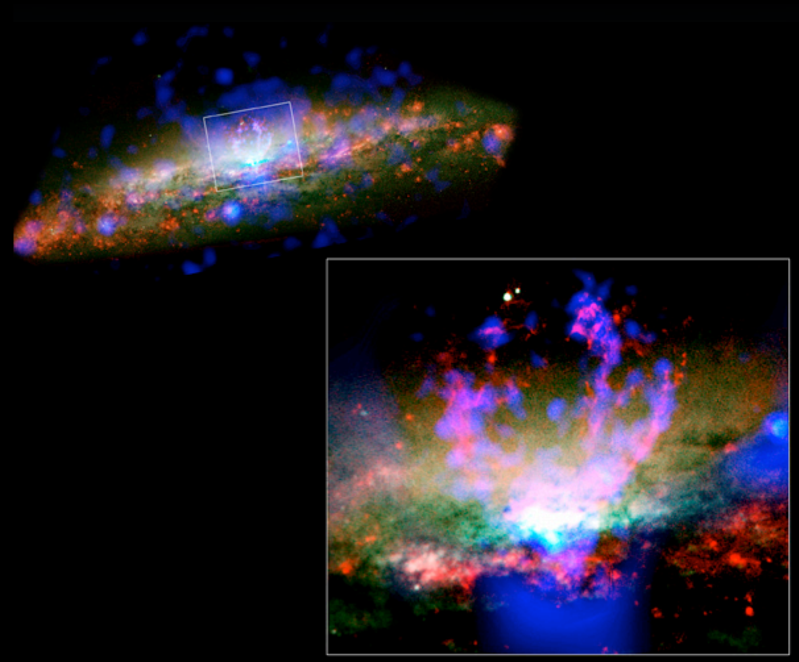

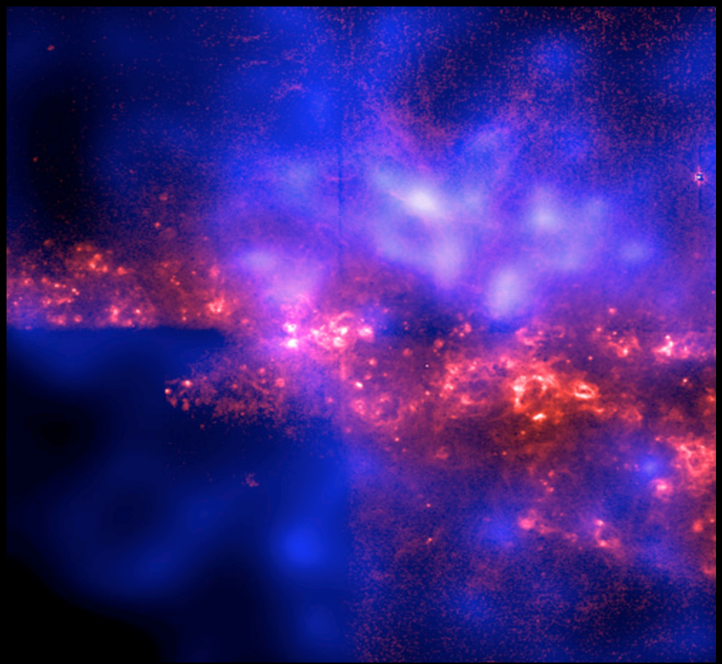

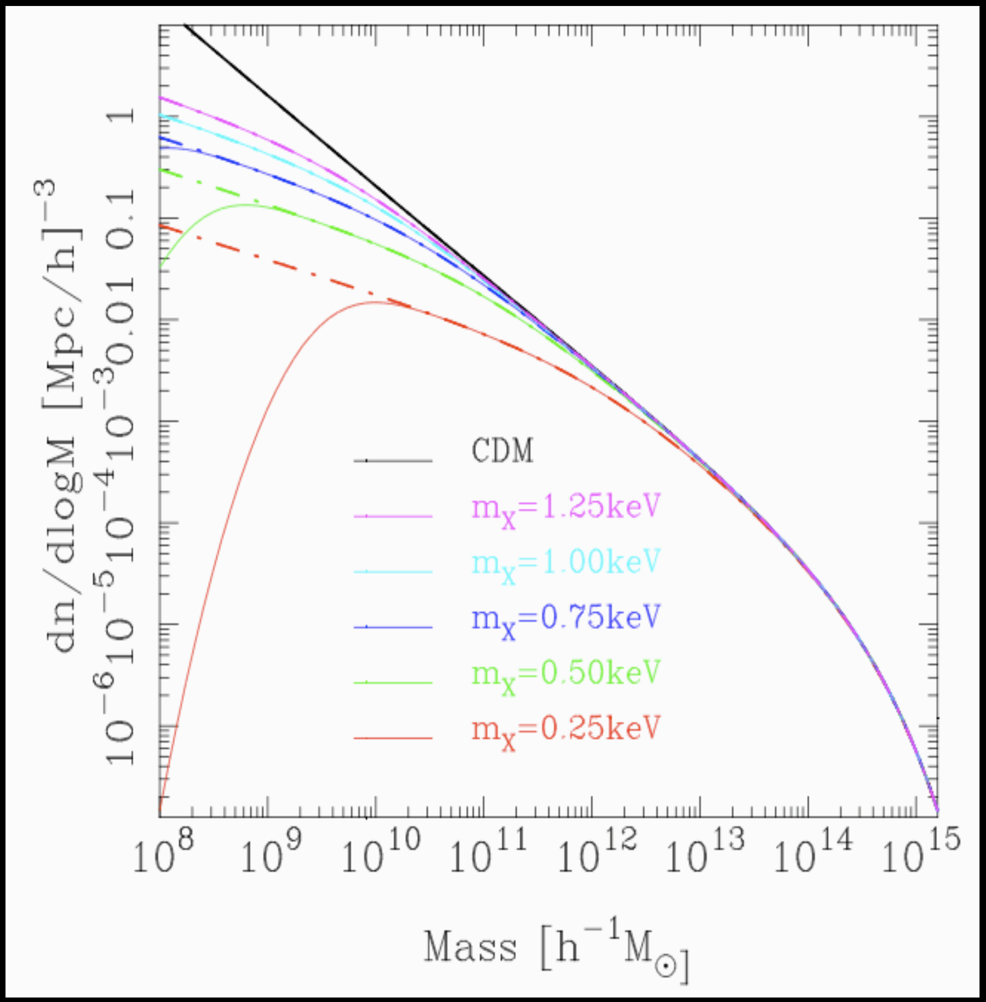

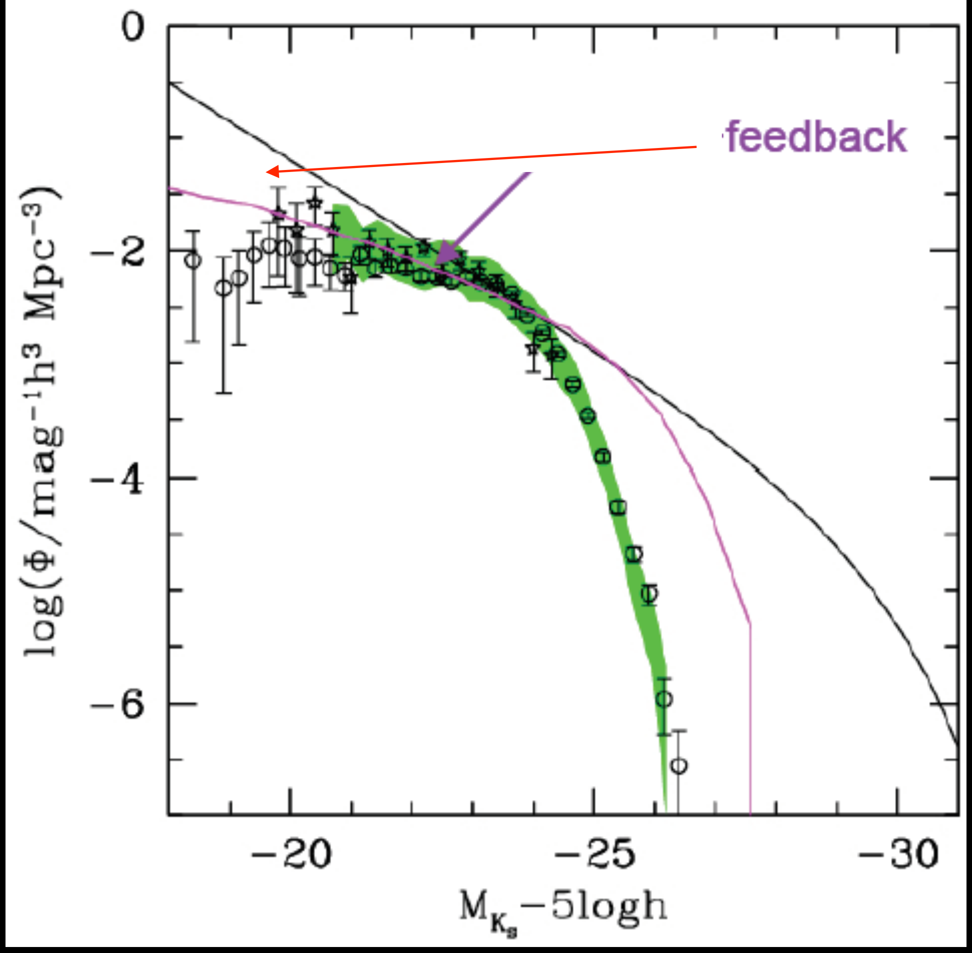

Galaxy Formation in a Cosmological Context

relating gas and star formation to the evolution of DM halos

Hydrodynamcal N-body simulations

Pros

include hydrodynamics of gas
contain spatial information

Cons

numerically expensive
(limited exploration of parameter space)
requires sub-grid physics

Semi-Analytic Models Monte-Carlo realization of collapse and merging histories

Pros

Physics of baryons linked to DM halos through scaling laws, allows a fast spanning of parameter space

Cons

Simplified description of gas physics
Do not contain spatial informations

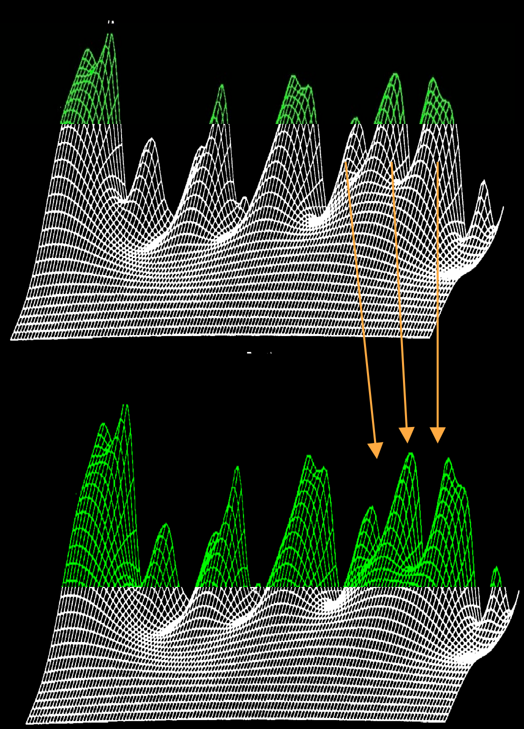

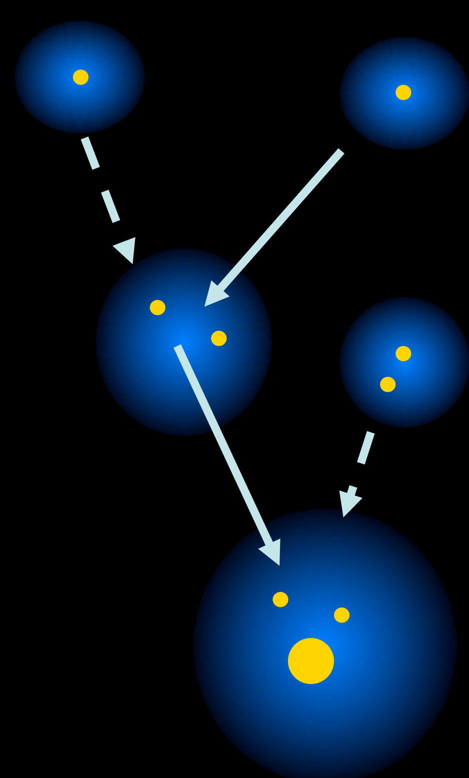

Sub-Halo dymanics:
dynamical friction, binary aggregation

Halo Properties
Density Profiles
Virial Temperature

Gas Properties
Profiles
Cooling - Heating Processes
Collapse, disk formation

Star Formation Rate

Gas Heating (feedback)
SNae
UV background

Evolution of stellar populations

Growth of Supermassive BHs
Evolution of AGNs

The DM-Feedback Degeneracy

Solutions from Feedback Processes

i) the abundance of satellite galaxies

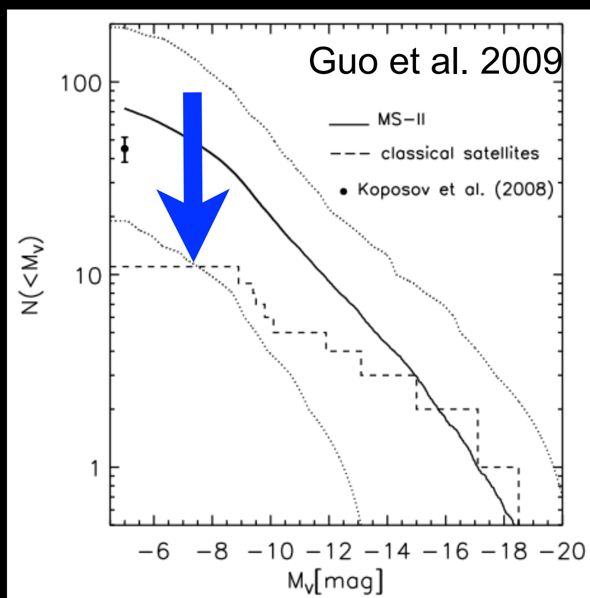

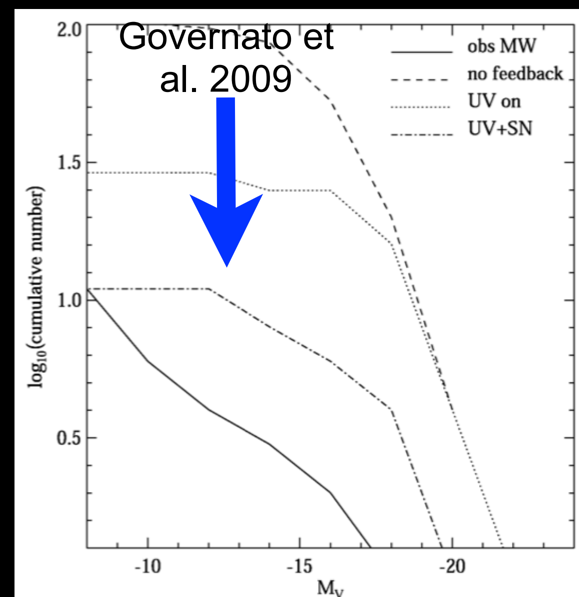

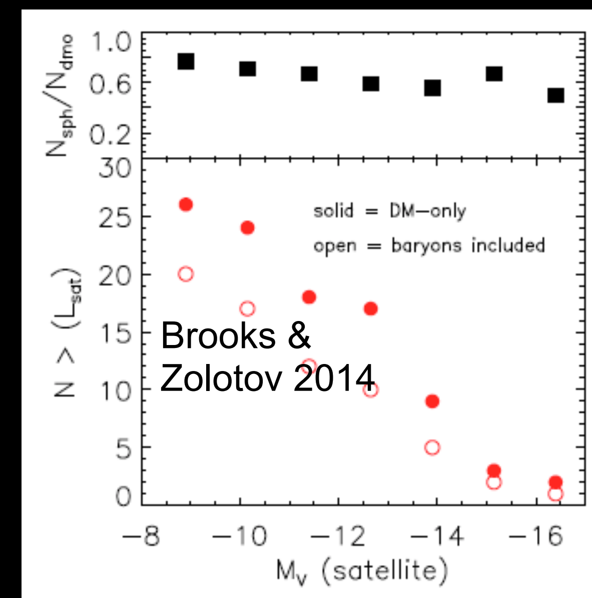

ii) the density profiles

A proposed solution at low redshift

"... The rapid fluctuations caused by episodic feedback progressively pump energy into the DM particle orbits, so that they no longer penetrate to the centre of the halo" (Weinberg et al. 2013, Governato et al. 2012)

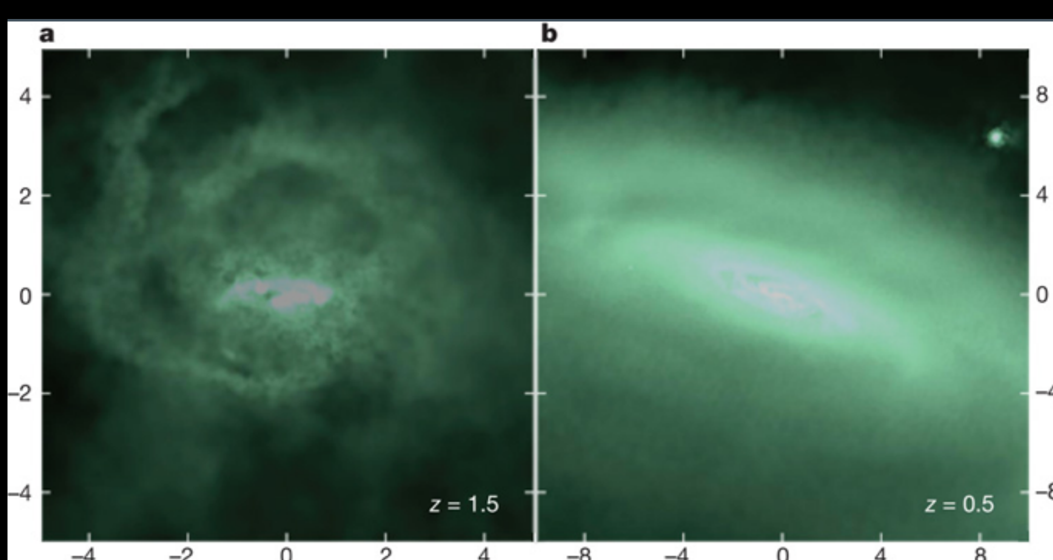

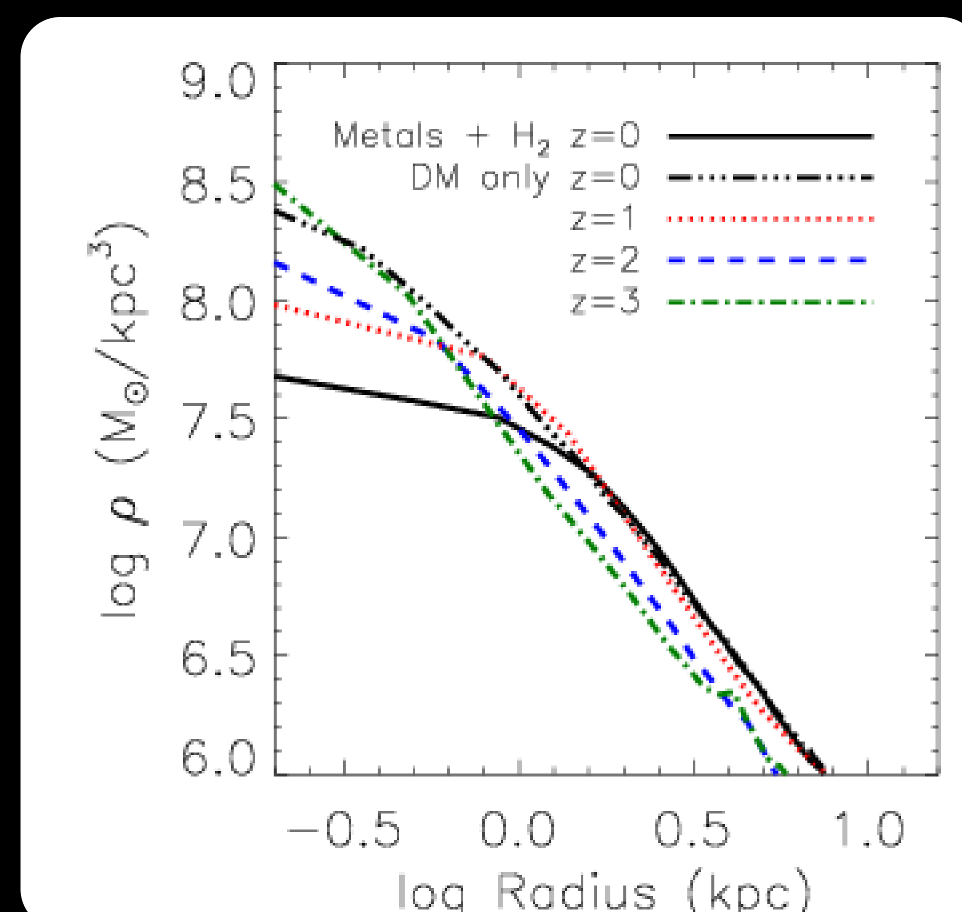

Breaking the DM-Feedback Degeneracy

1: Profiles and Abundances of low-mass galaxies at high redshifts

Velocities corresponding to Supernovae Feedback

$$v_{SN} = \sqrt{E_{SN}/M_{gas}} \approx 100 \quad km/s$$

$$M \approx (v_{esc}^2/G)\, r$$

$$r \propto (M/\rho)^{1/3}$$
$$\rho = 180\,\rho_u = 180\,\rho_u\,(1+z)^3$$
$$A \equiv \sqrt{3/G^3\,4\pi\,\rho_u}$$

$$M \approx A\,v_{esc}^3\,(1+z)^{-3/2}$$

$$v_{esc} = v_{SN}$$

Mass scale at which SN can effectively expel gas from DM halodecreases with redshift

$$M_{SN} \approx 10^{10}\,M_\odot\,(1+z)^{-3/2}$$

At high-z
larger densities imply larger escape velocity
even for low-mass galaxies:
feedback increasingly ineffective

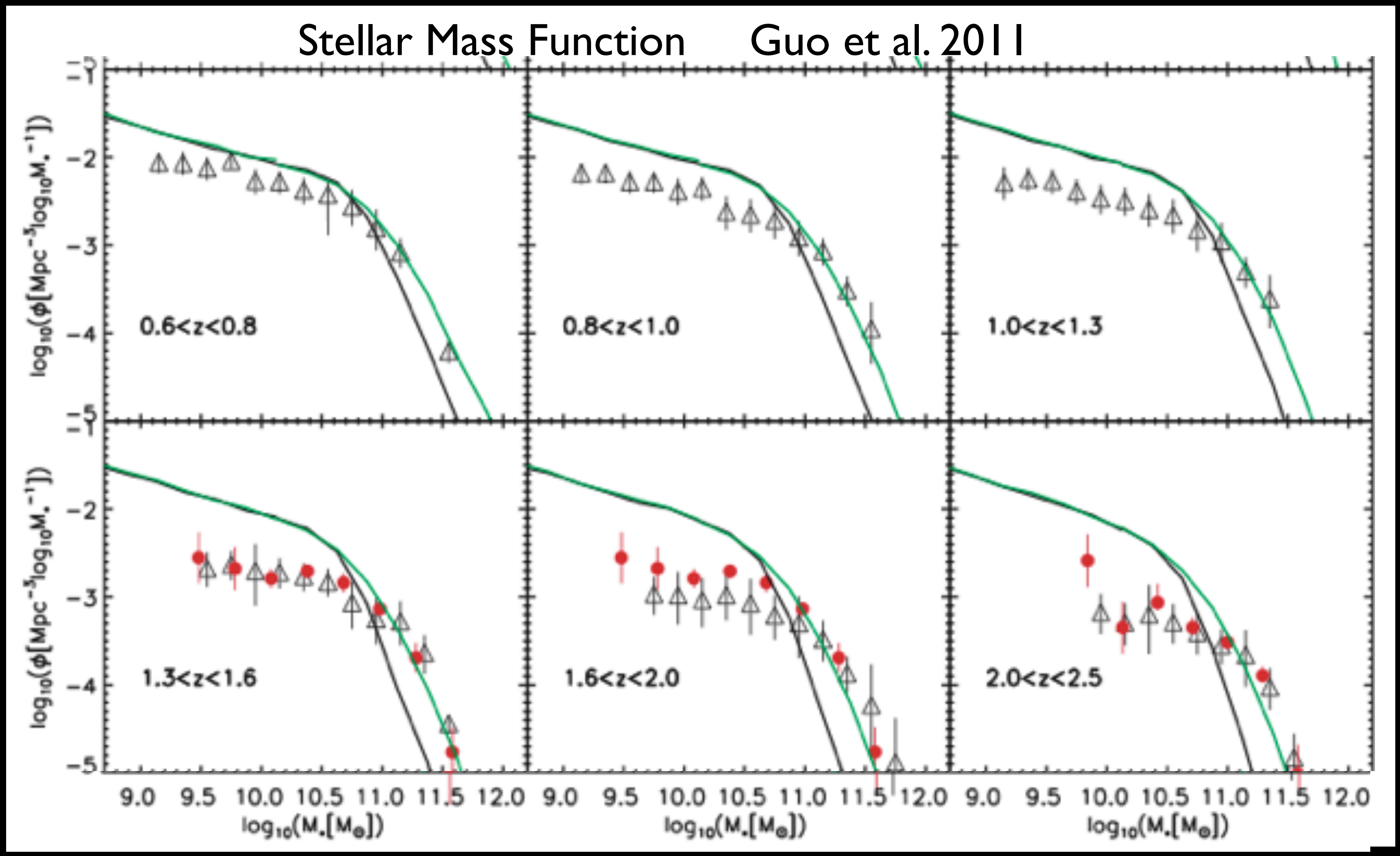

Breaking the DM-Feedback Degeneracy

II: The L/M ratio of low-mass galaxies

Enhancing the feedback results into inefficient star formation for given DM halo (suppress L/M).

This seems at variance with observed M_{star}-M relation

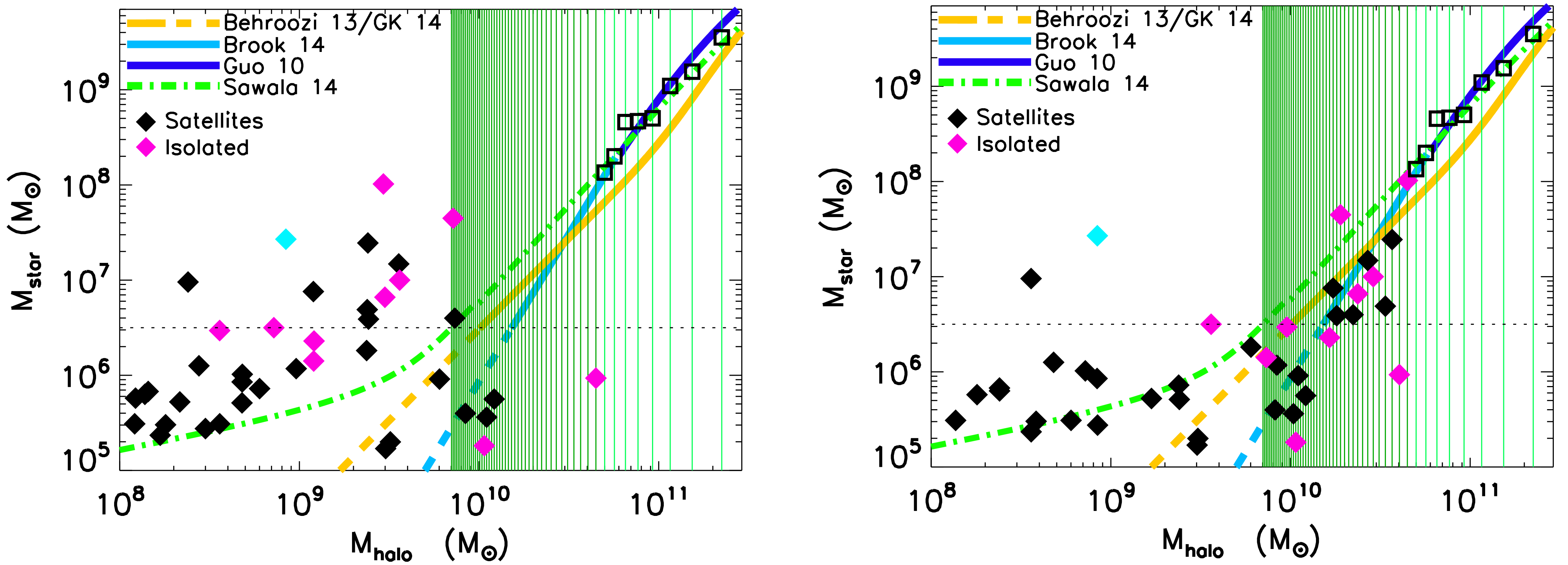

Figure 2. The relation between observed stellar mass and derived halo mass for LG galaxies. The halo mass has been found by fitting kinematical data and assuming two different halo profiles. The results for an NFW profile are shown in the left-hand panel, while the mass-dependent DC14 halo profile has been used in the right-hand panel. Satellites and isolated galaxies are shown in different colours, with Sagittarius dwarf irregular, highly affected by tides, shown in cyan. Several abundance matching predictions are indicated, in particular the Brook et al. (2014) one has been constrained using the LG mass function, and it is shown as dashed line below the observational completeness limit of the LG.

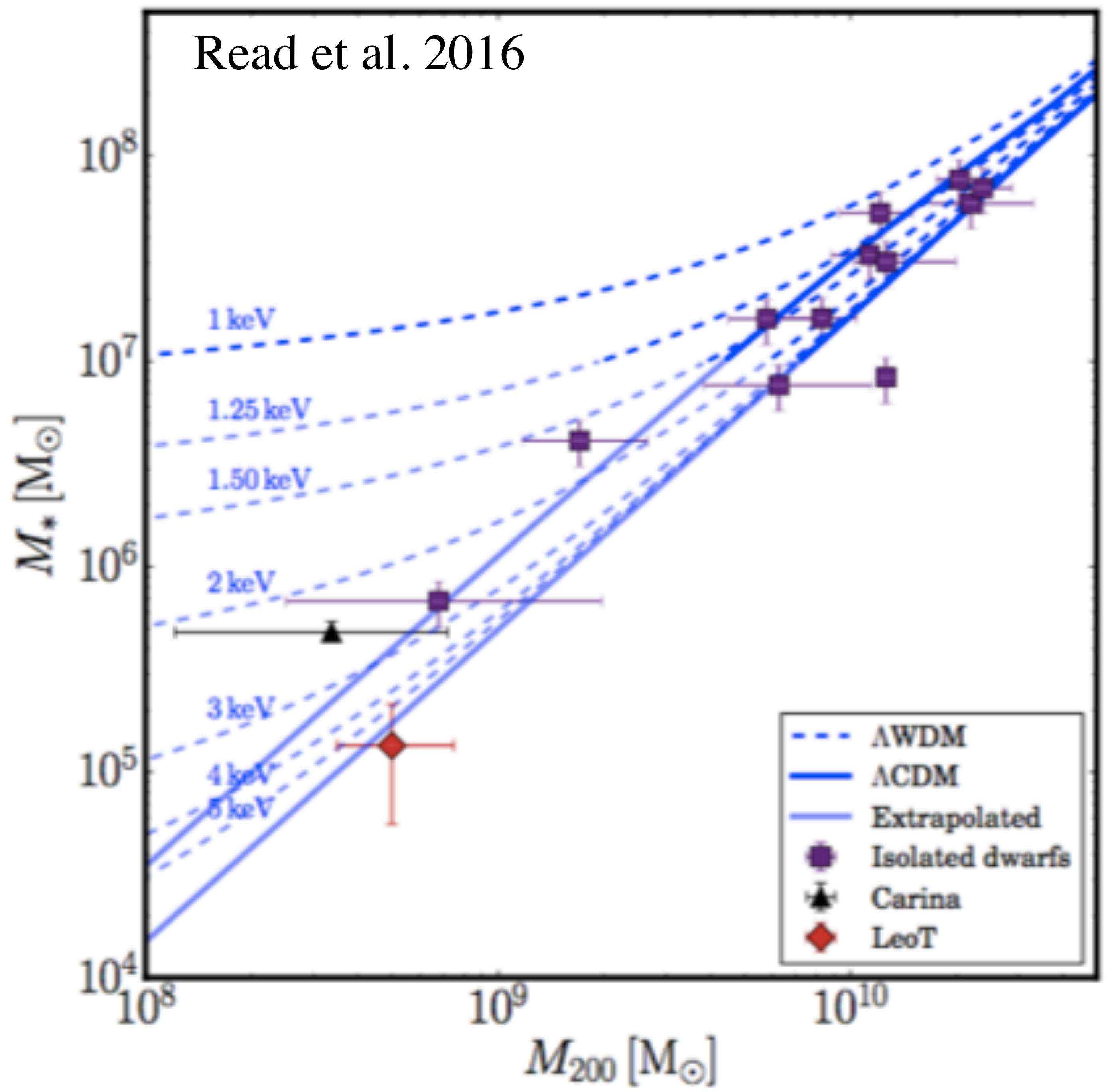

Figure 3. $M_* - M_{200}|_{\rm rot}$ (purple data points) as compared to $M_* - M_{200}|_{\rm abund}$ in ΛCDM (blue solid lines) and ΛWDM (blue dashed lines), using the SDSS field stellar mass function. The thermal relic mass $m_{\rm WDM}$ is marked on the curves in keV. The lines and symbols are as in Figure 2.

Implementing WDM power spectrum in the galaxy formation model

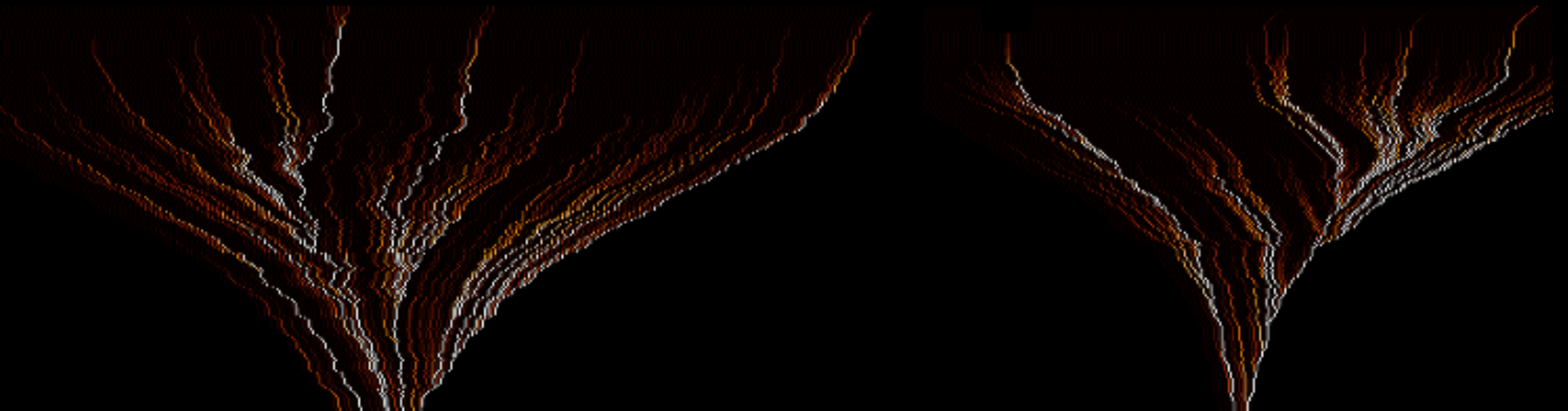

Halo Properties
Density Profiles
Virial Temperature

Gas Properties
Profiles
Cooling - Heating
Collapse
Disk formation

Star Formation

Gas Heating (feedback)
SNae
UV background

Evolution of stellar populations

WDM

Galaxy formation in WDM implies computing how modifications of the power spectrum propagate to the above processes

$$r_{fs} \approx 0.2 \left[\frac{\Omega_X\, h^2}{0.15}\right]^{1/3} \left[\frac{m_X}{rmkeV}\right]^{-4/3} \mathrm{Mpc} \qquad \frac{P_{WDM}(k)}{P_{CDM}(k)} = \left[1 + (\alpha\, k)^{2\,\mu}\right]^{-5\,\mu}$$

$$\alpha = 0.049 \left[\frac{\Omega_X}{0.25}\right]^{0.11} \left[\frac{m_X}{\mathrm{keV}}\right]^{-1.11} \left[\frac{h}{0.7}\right]^{1.22} h^{-1}\ \mathrm{Mpc}$$

From Thermal Relics to Sterile Neutrinos

The cutoff in the power spectrum is conventionally “labelled” according to the mass of “thermal relic” WDM particles

A similar cutoff can be achieved through WDM sterile neutrinos assuming different production mechanisms

correspondence between thermal relic mass m_X and sterile neutrino mass m_ν (yielding the same power spectrum) depends on the assumed production mechanism
E.g. for the Shi-Fuller mechanism $m_\nu \approx 2.5\ m_X$

In the following we shall show the results in terms of the equivalent thermal relic mass

Suppression with respect to CDM

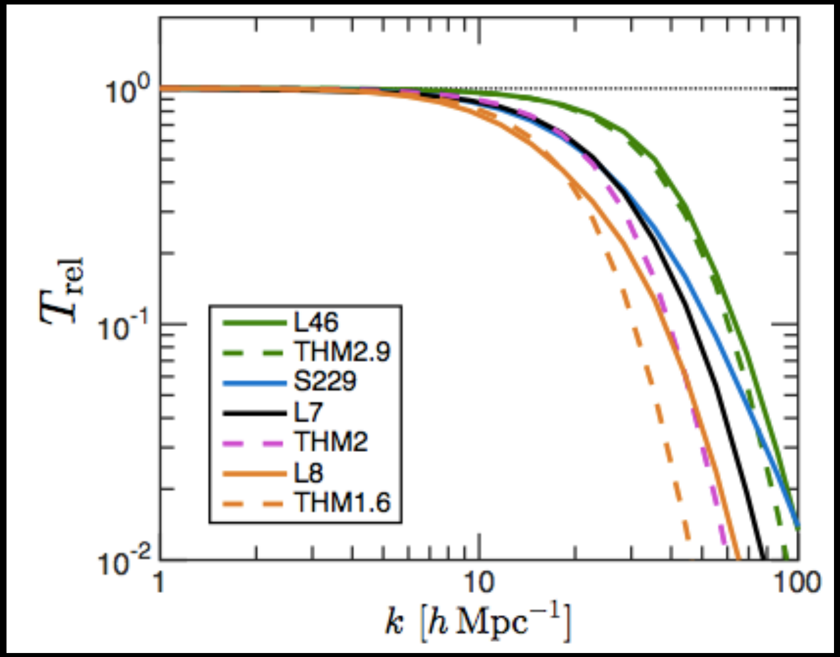

Bozek et al. 2015

Sterile Neutrinos

are produced in primordial plasma through

- off-resonance oscillations. Dodelson, Widrow; Abazajian, Fuller; Dolgov, Hansen;Asaka, Laine, Shaposhnikov et al.
- oscillations on resonance in presence of lepton asymmetry. Shi Fuller

- production mechanisms which do not involve oscillations
  – inflaton decays directly into sterile neutrinos Shaposhnikov, Tkachev
  – Higgs physics: both mass and production Petraki
  – decays of scalars in the early Universe Merle & Totzauer

From Thermal Relics to Sterile Neutrinos

The cutoff in the power spectrum is conventionally "labelled" according to the mass of "thermal relic" WDM particles

A similar cutoff can be achieved through WDM sterile neutrinos assuming different production mechanisms

correspondence between thermal relic mass m_X and sterile neutrino mass m_ν (yielding the same power spectrum) depends on the assumed production mechanism
E.g. for the Shi-Fuller mechanism $m_\nu \approx 2.5\, m_X$

In the following we shall show the results in terms of the equivalent thermal relic mass

Suppression with respect to CDM

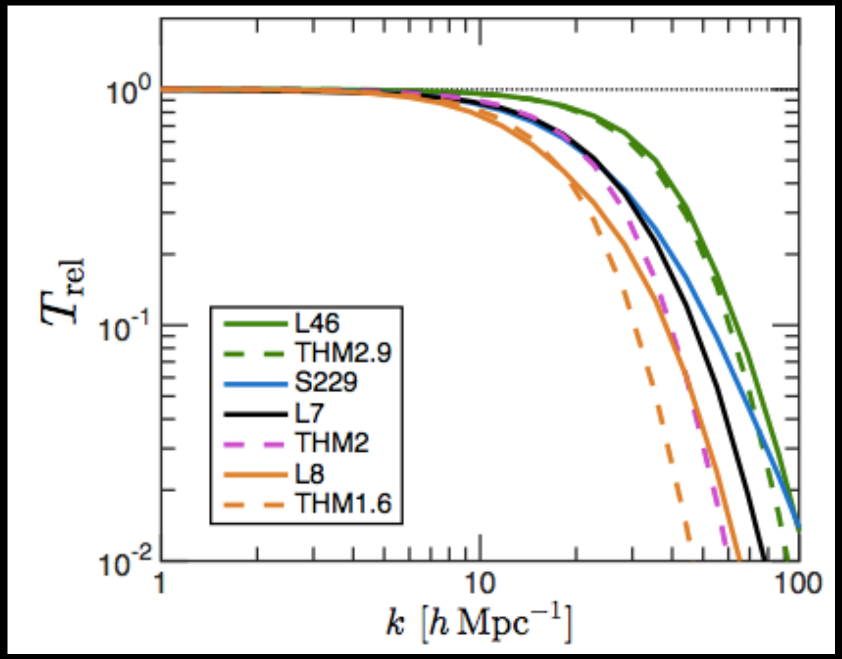

Bozek et al. 2015

Stacked XMM spectra (MOS and PN) of 73 bright galaxy clusters, blue-shifted to the same cluster rest frame

Searched for any unidentified emission lines in 2–10 keV band

Detected a very weak line at E = 3.55–3.57 keV rest-frame energy: IF due to WDM corresponds to the decay of

$m_\nu \approx 7$ keV $\rightarrow m_X \approx 2.5$ keV

X-ray line reported in stacked observations of X-ray clusters with the XMM-Newton X-ray Space telescope with both CCD instruments aboard the telescope, and the Perseus cluster with the Chandra X-ray Space Telescope (Bulbul et al. 2014; independent indications of a consistent line in XMM-Newton observations of M31 and the Perseus Cluster is reported in Boyarsky et al. 2014)

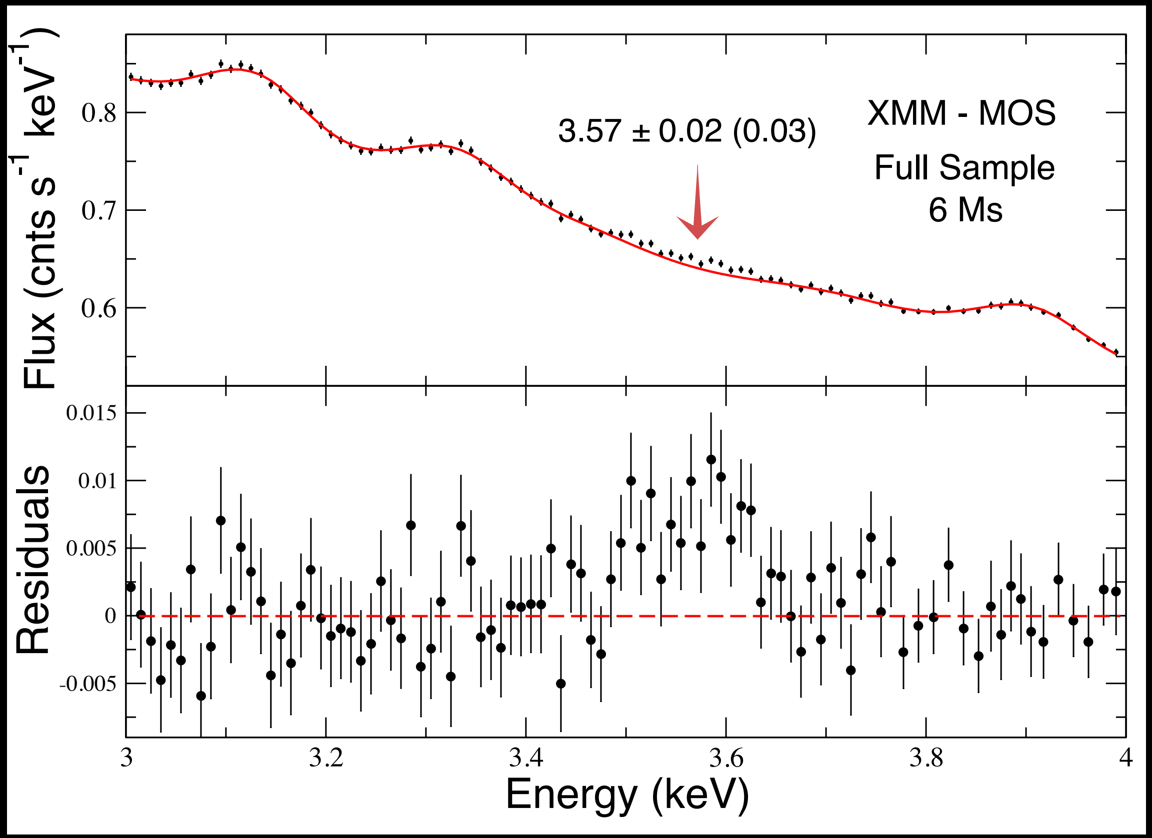

WDM models with m_X=1-4 can provide a solution to

Density profiles & Rotation curves in WDM

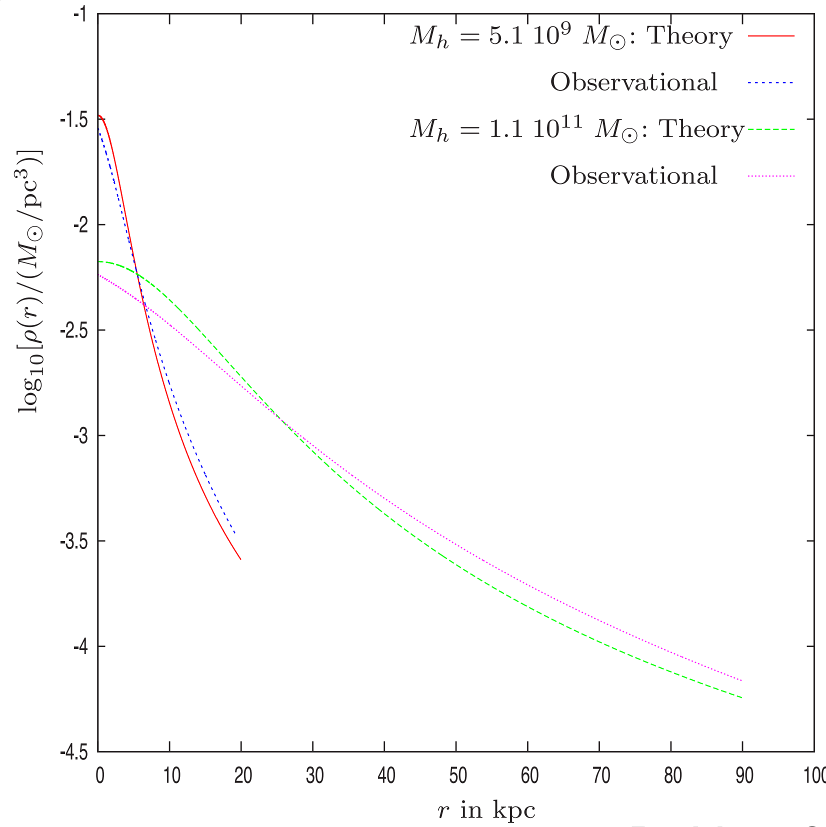

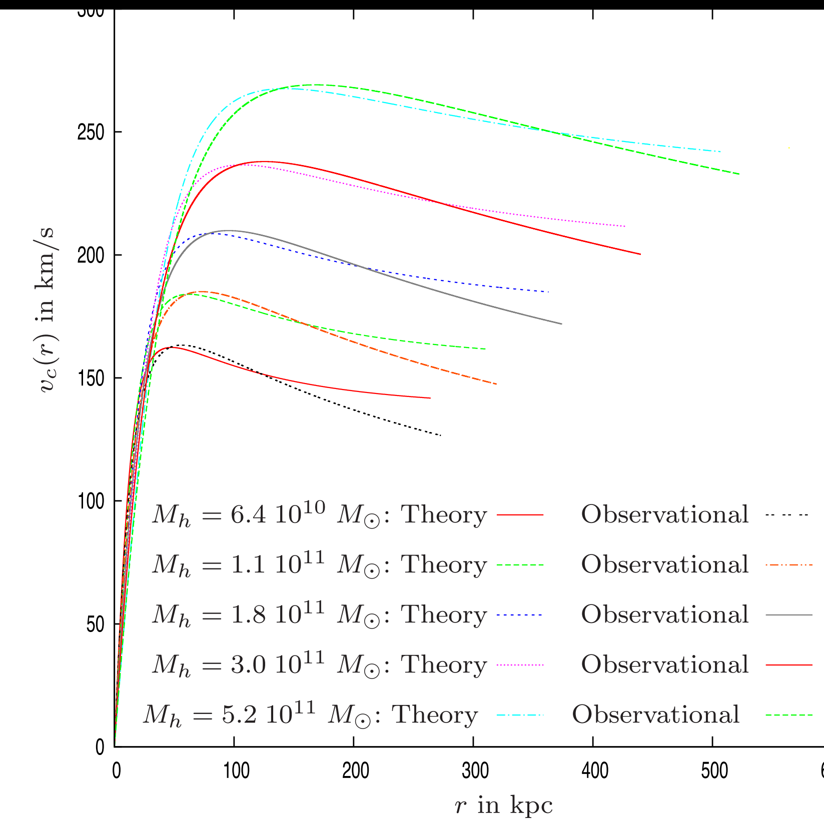

De Vega, Salucci, Sanchez 2014

Abundance of low-mass satellites

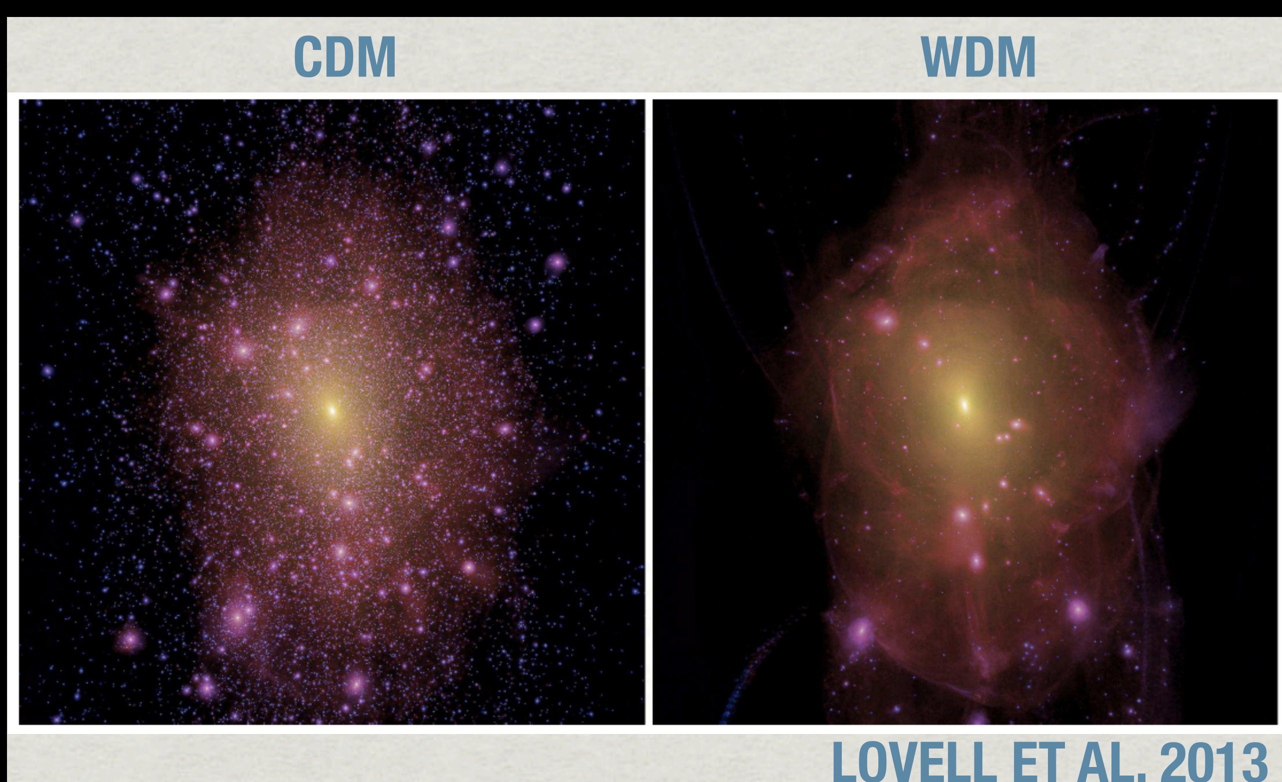

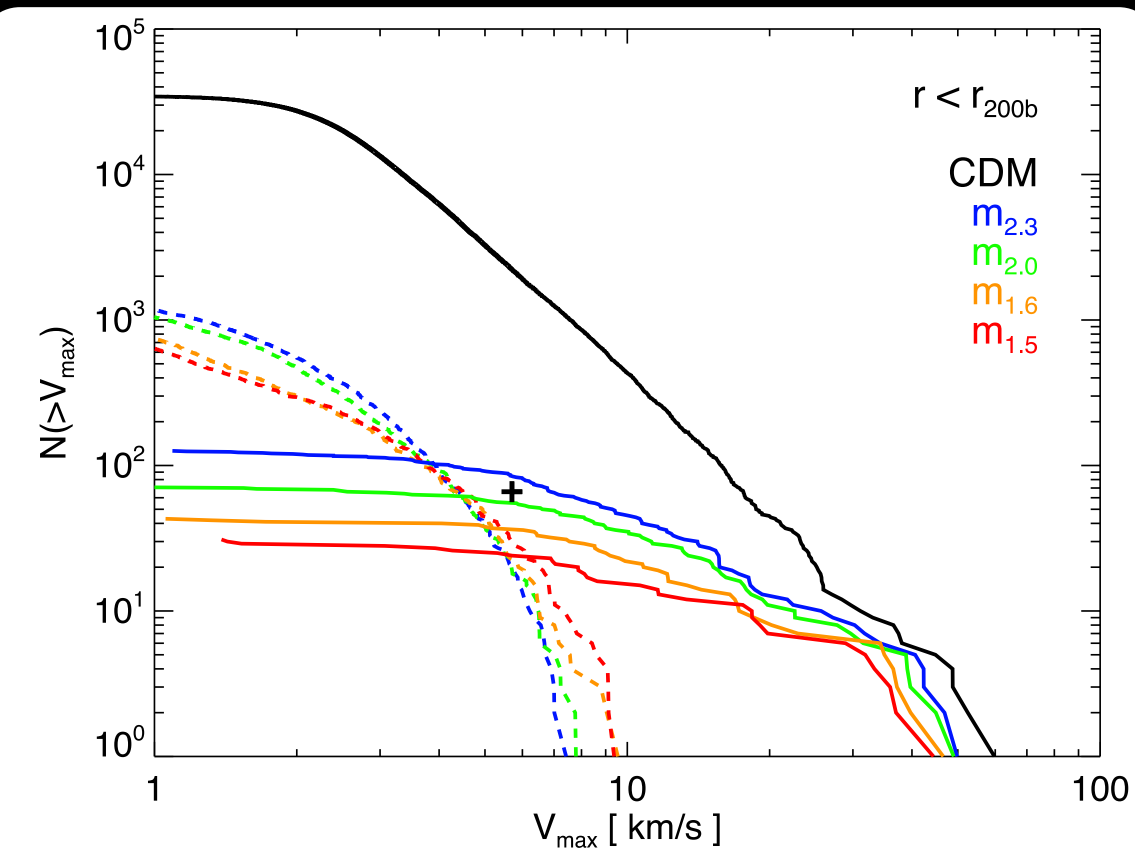

WDM models with m_X=1-4 constitutes a viable framework for galaxy formation

NM+2012

Are being investigated by several groups

Maccio et al. 2012, Benson et al. 2013,
Dayal, Mesinger, Pacucci 2014, Herpich et al.2014,
Governato et al. 2014, Kennedy et al. 2015
Bose et al. 2016, Chau, Mayer, Governato 2016

luminosity distributions at z=0

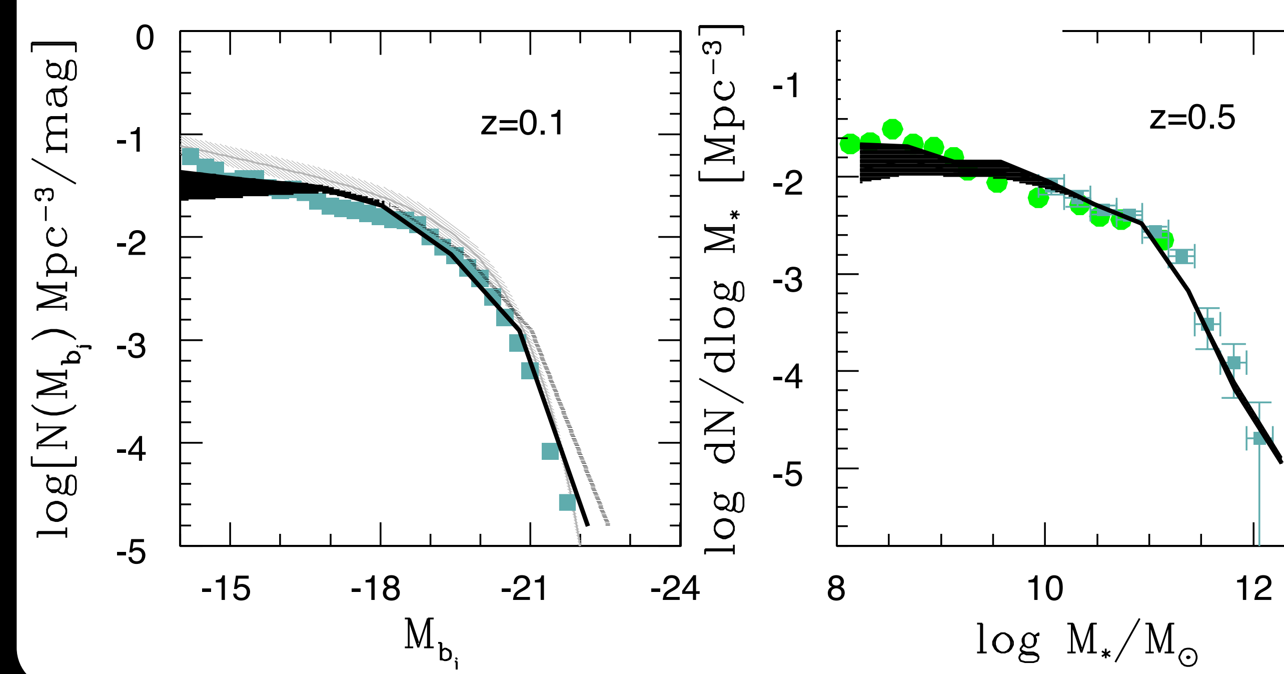

stellar mass distributions at z=1

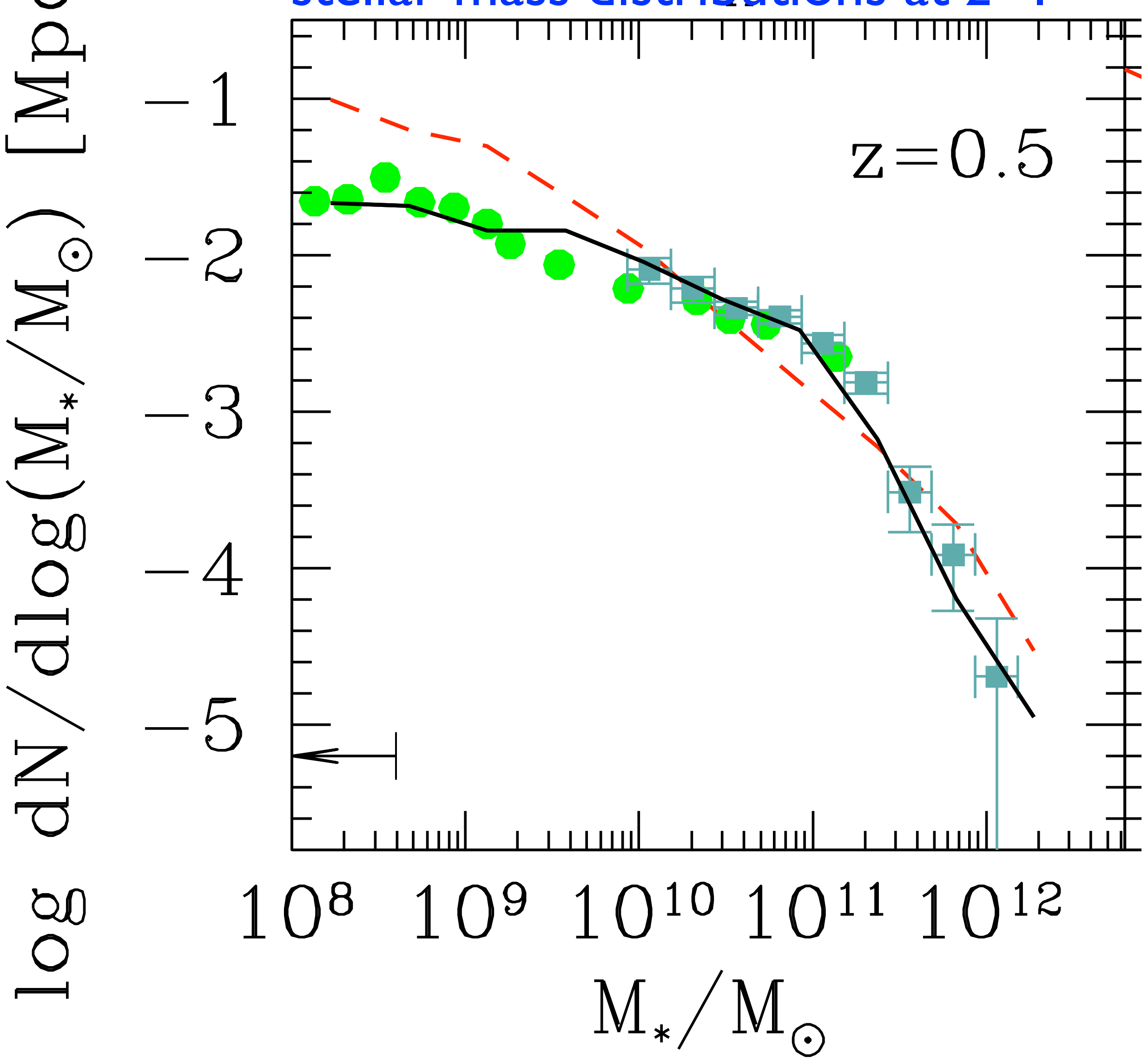

color distributions at z=0

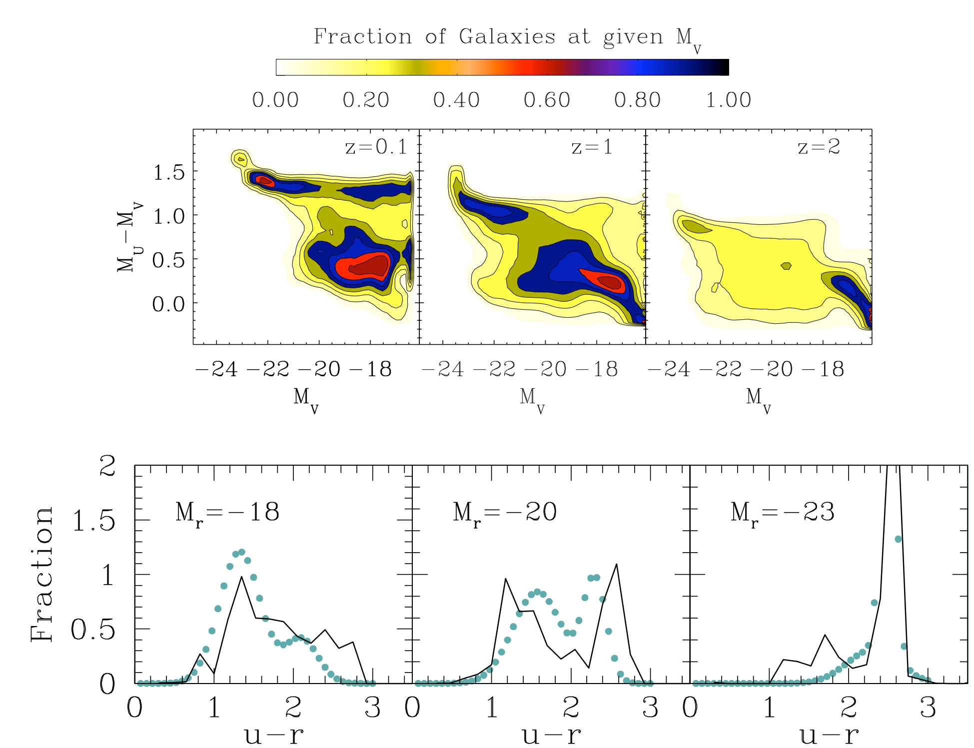

SOME PROPERTIES OF WDM GALAXY FORMATION

A Delayed Growth of Stellar Mass in WDM galaxy formation

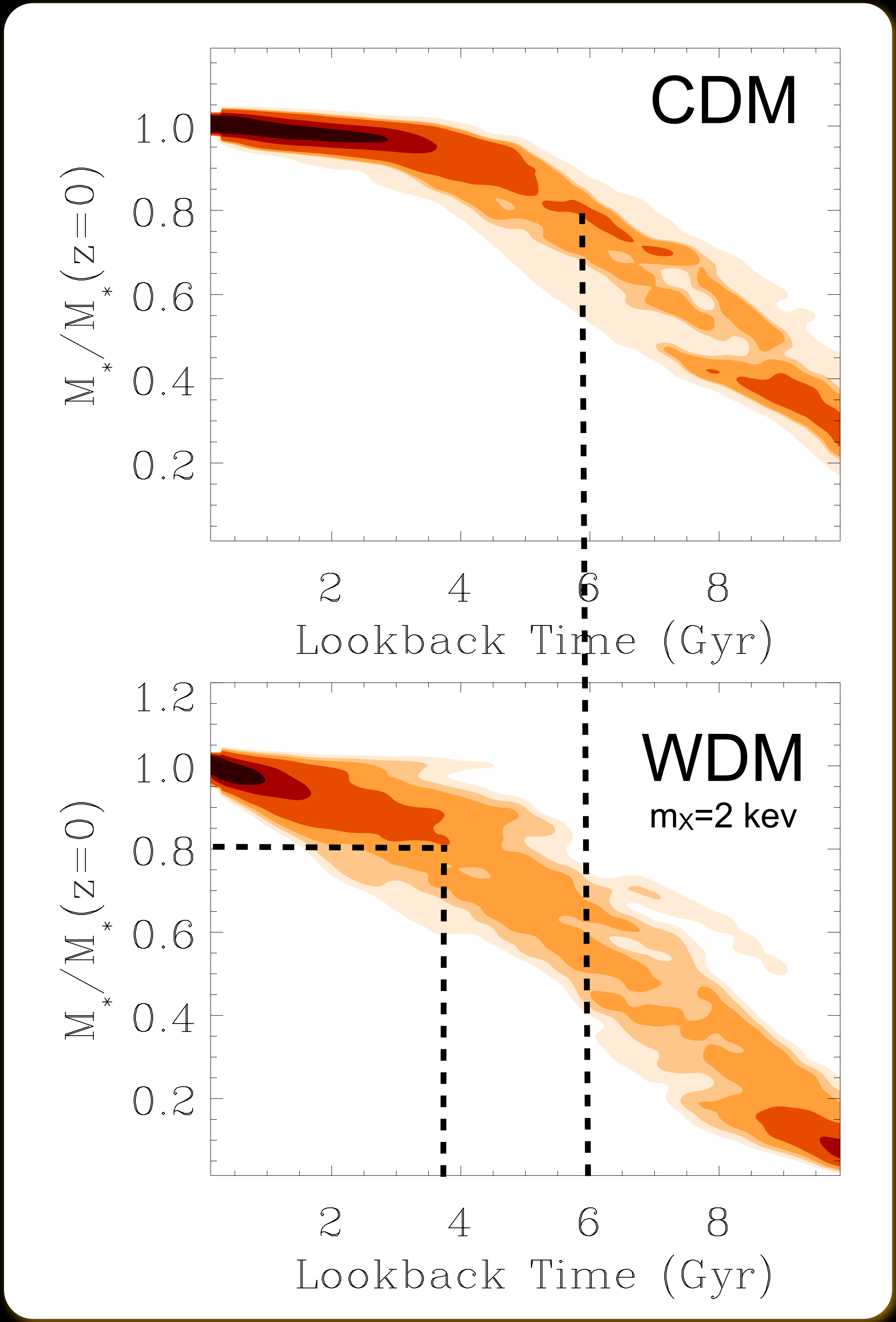

The suppression of progenitors of satellite galaxies with high SFR yields Slower growth of stellar mass in WDM

CDM: 80 % of mass formed 6 Gyr ago
WDM: 80 % of mass formed 4 Gyr ago

Approx. delay ~ 2 Gyr

Independent works based on hydro-Nbody simulations confirm such a result (Governato et al. 2014); see also A. Fialkov's talk

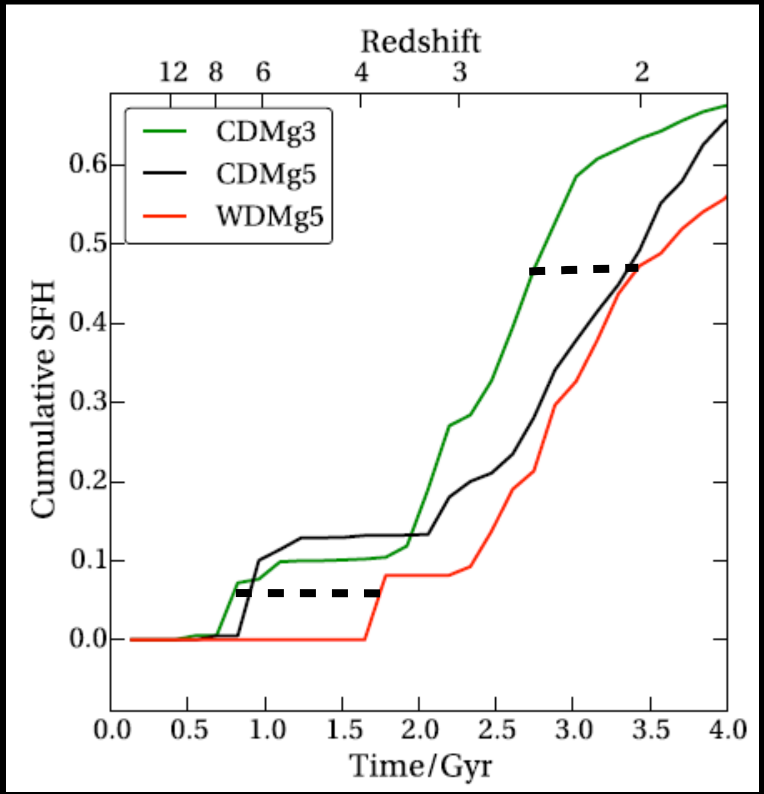

THE FRACTION OF QUIESCENT SATELLITE GALAXIES

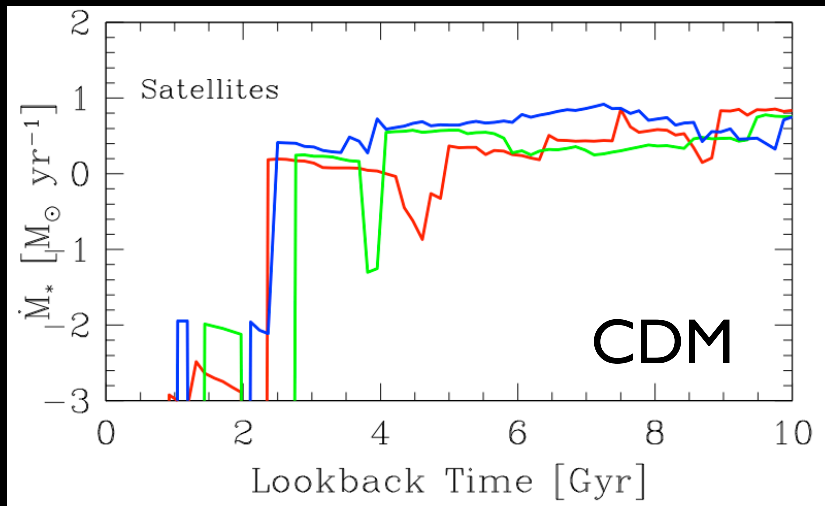

WDM delayed groth of
stellar mass
results into larger star formation
at low redshifts

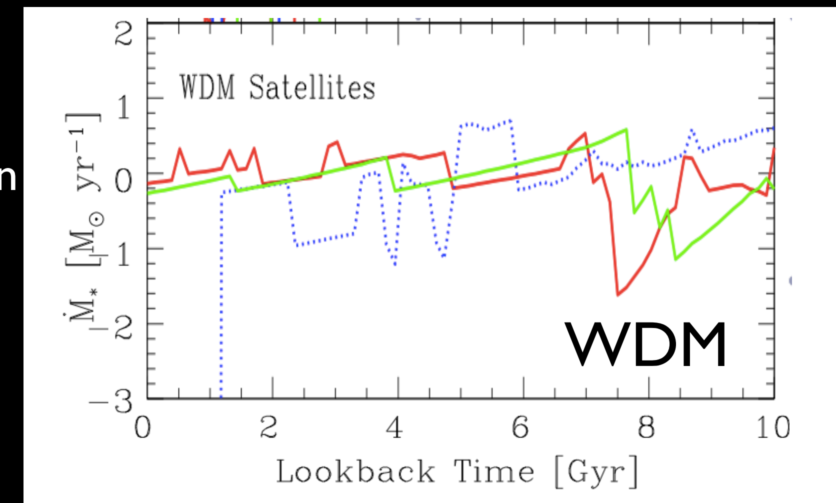

Specific Star Formation Rate $$SSFR = \dot{M}_*/M*$$

Quiescent Fraction = fraction of galaxies with SSFR<10^{-11} yrs^{-1}

corresponds to minimum in the SSFR distribution

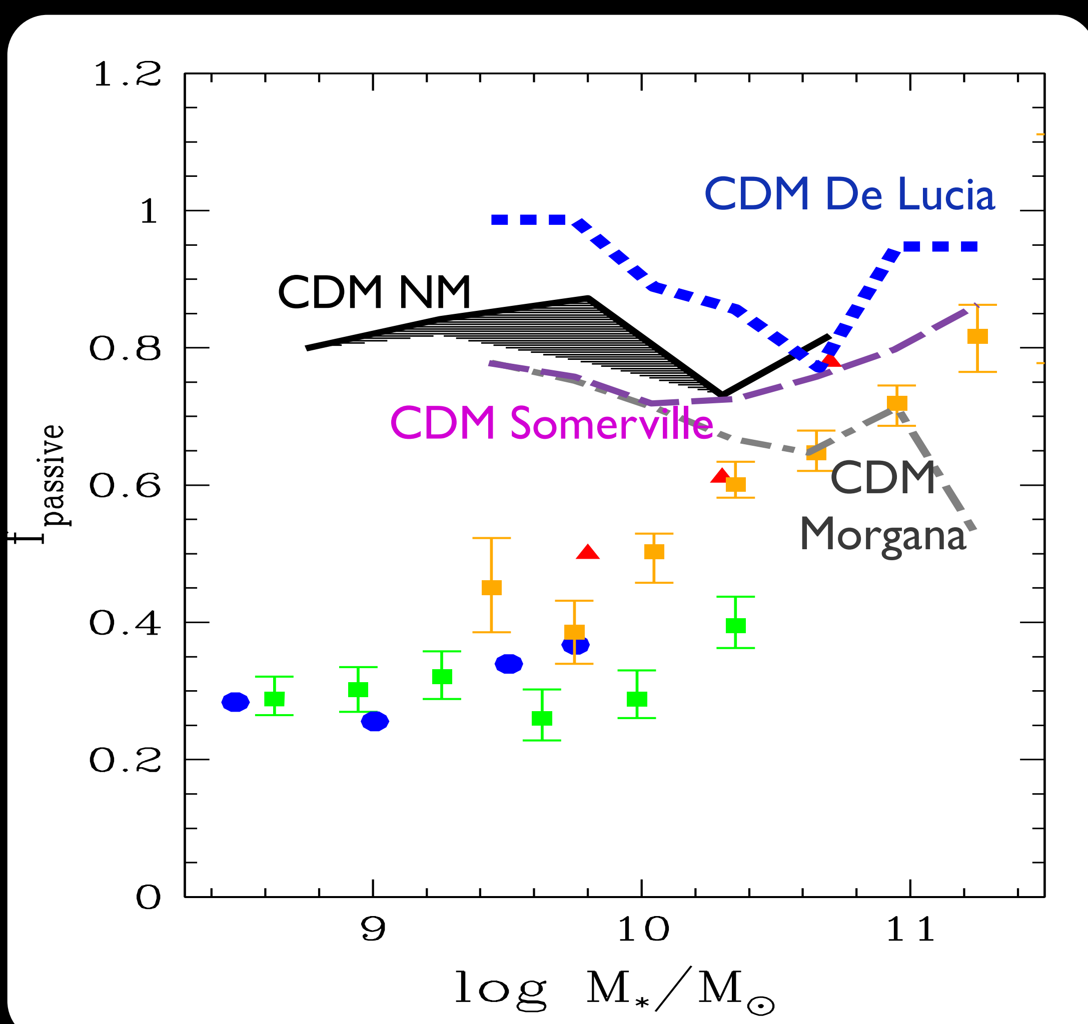

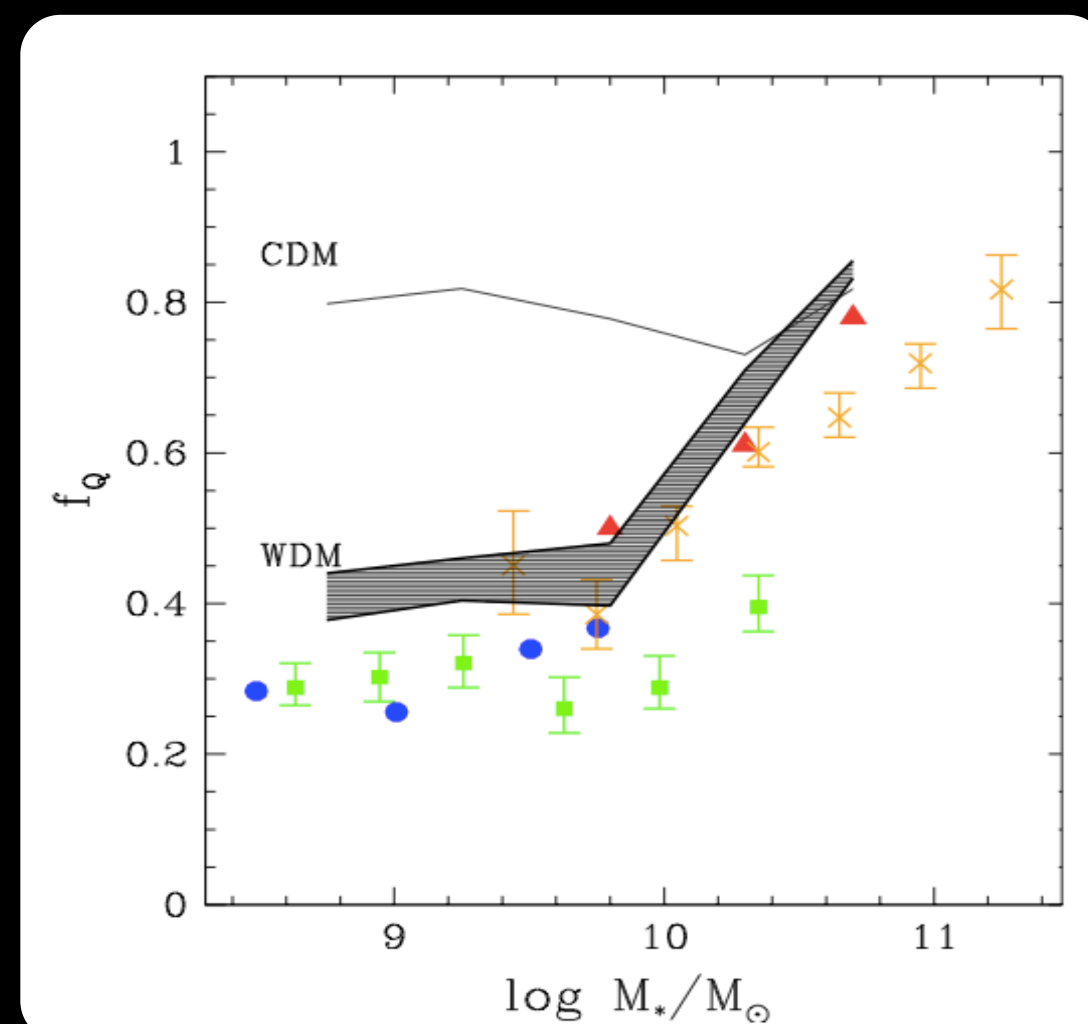

The M_*/M_h relation for low-mass galaxies

Enhancing the feedback results into inefficient star formation for given DM halo (suppress L/M).

This seems at variance with observed M_{star}-M relation

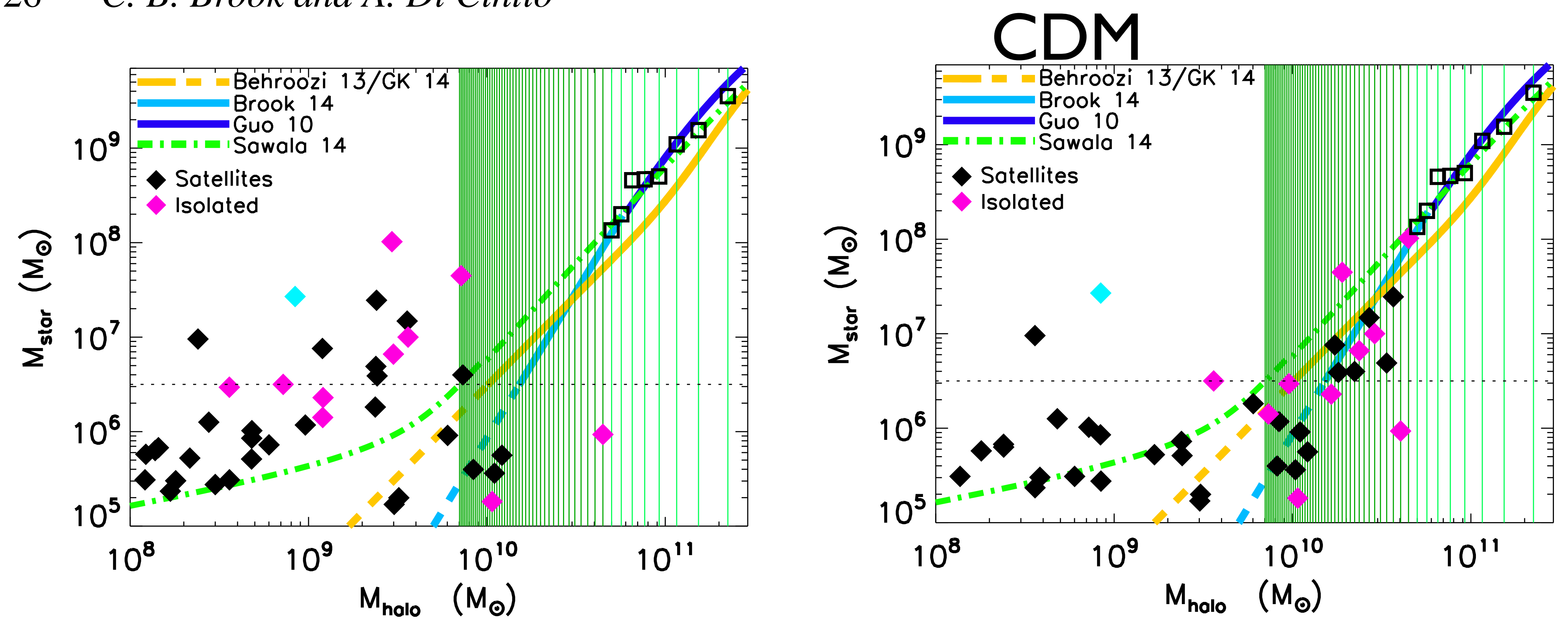

Figure 2. The relation between observed stellar mass and derived halo mass for LG galaxies. The halo mass has been found by fitting kinematical data and assuming two different halo profiles. The results for an NFW profile are shown in the left-hand panel, while the mass-dependent DC14 halo profile has been used in the right-hand panel. Satellites and isolated galaxies are shown in different colours, with Sagittarius dwarf irregular, highly affected by tides, shown in cyan. Several abundance matching predictions are indicated, in particular the Brook et al. (2014) one has been constrained using the LG mass function, and it is shown as dashed line below the observational completeness limit of the LG.

The M_*/M_h relation for low-mass galaxies

Enhancing the feedback results into inefficient star formation for given DM halo (suppress L/M).

In WDM the flatter shape of the LF allows for larger L/M ratios

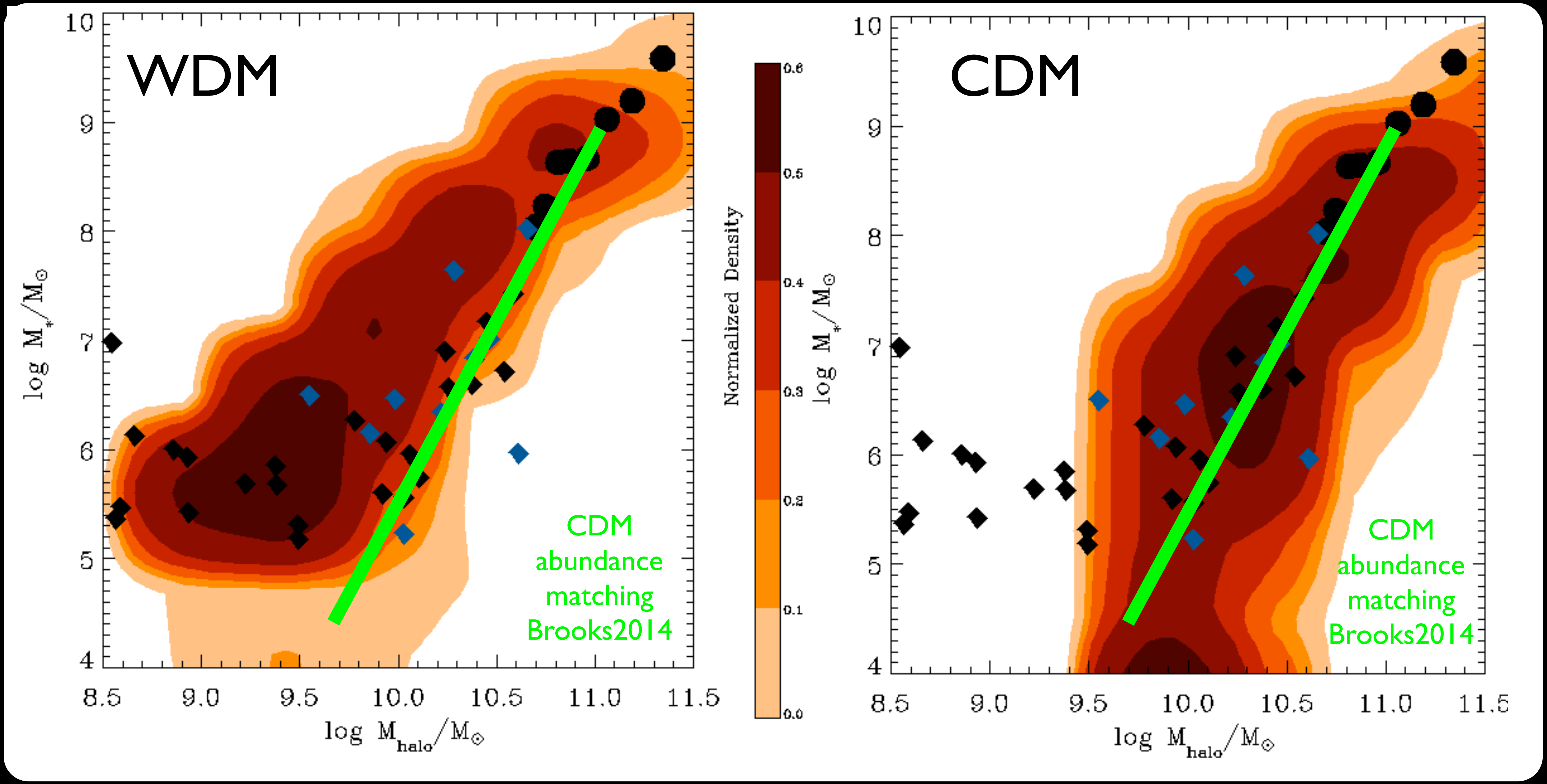

CONSTRAINING THE WDM PARTICLE MASS

In terms of thermal relic mass m_X
(conversion to sterile neutrino masses depends on production mechanism)

E.g.
Dodelson-Widrow mechanism $m_\nu \approx 2.9\ m_X$
Shi-Fuller mechanism $m_\nu \approx 2.5\ m_X$

$m_X > 4$ keV is indistinguishable from CDM from the point of view of galaxy formation

WDM particle mass: limits from the Ly-α forest vs. Hydro-Simulations

Viel et al. 2005-2013

$m_{WDM}>3.3$ keV	Thermal relics WDM
$m_\nu>12$ keV	Sterile ν WDM (DW) Dodelson-Widrow

Results subject to further investigations

Still affected by the difficult-to-characterize physics of intergalactic gas. Degeneracy between WDM effects and Jeans and Doppler broadening of the absorption lines. These are affected by the IGM temperature

WDM particles are 10^{68} times heavier (10^5 $M_\odot$) than the real WDM particles. This makes difficult to infer the initial velocity distribution of the effective particles from the known initial velocity distribution of the real WDM particles (Lovell et al. 2012, 2014; Maccio` et al. 2012; Viel et al. 2013).

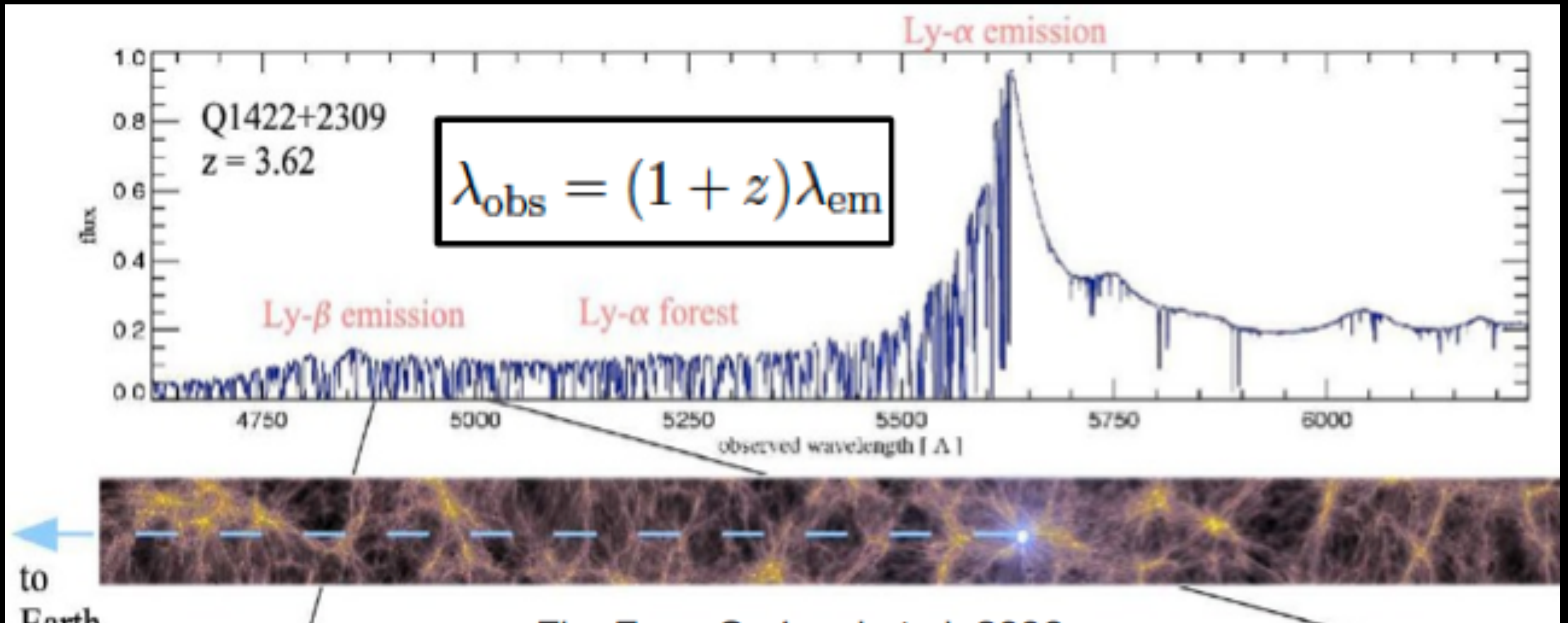

Fig. From Springel et al. 2006

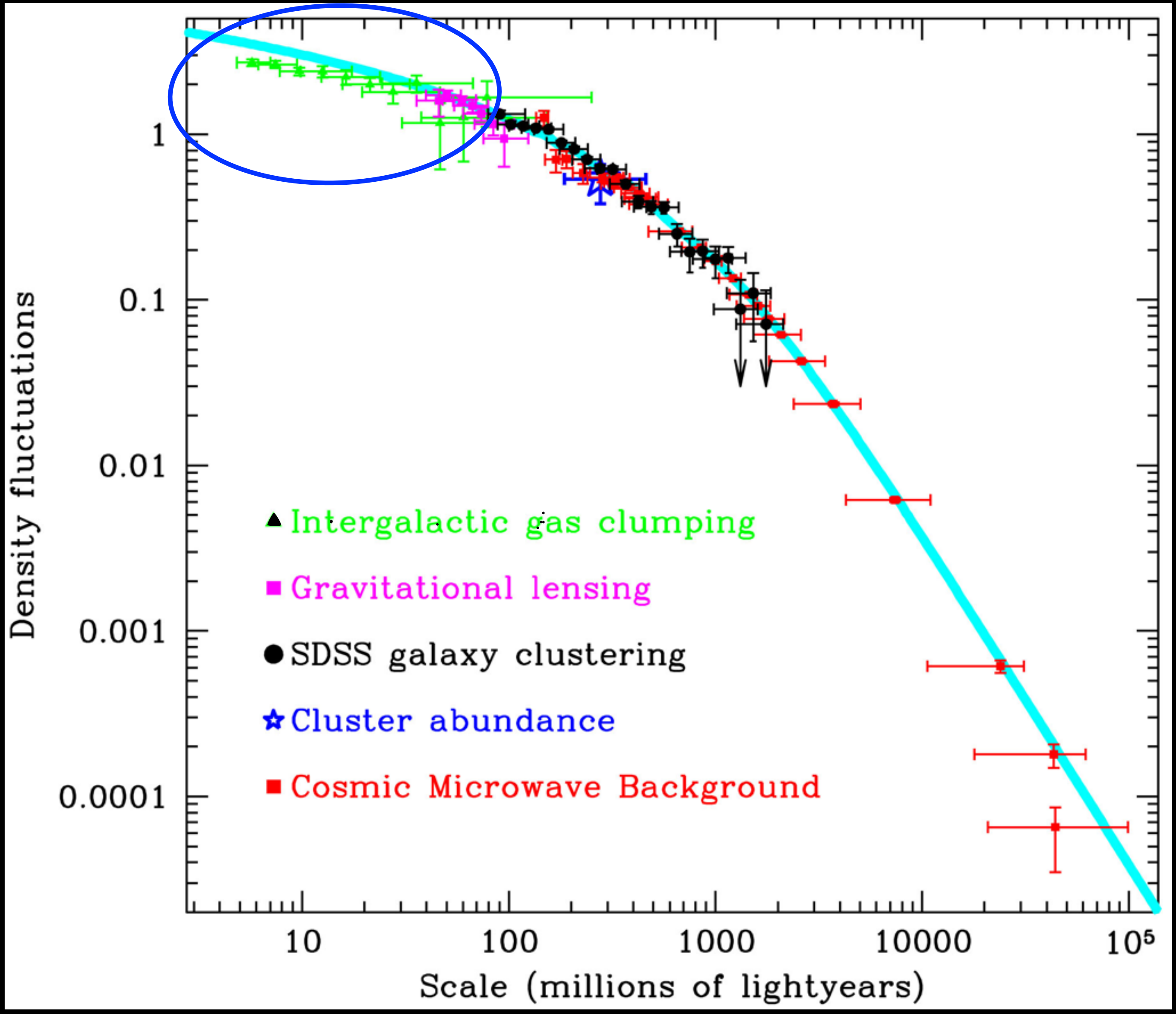

Constraining the WDM candidate mass through the abundance of low-mass galaxies

Structure formation in WDM models suppressed on small mass scales.

Small mass galaxies are the first to form.

The most powerful for probe for these scenarios is the abundance of high-redshift galaxies

Constraining the WDM candidate mass through the abundance of low-mass galaxies

Schultz et al. 2014 (see also Lapi & Danese 2015, Pacucci 2013)
Compare predicted abundance of low-mass DM halos at z>6 with observed abundance of faint galaxies in the HUDF
Delicate issue: relate UV luminsity of observed galaxies to the mass of the host DM halo

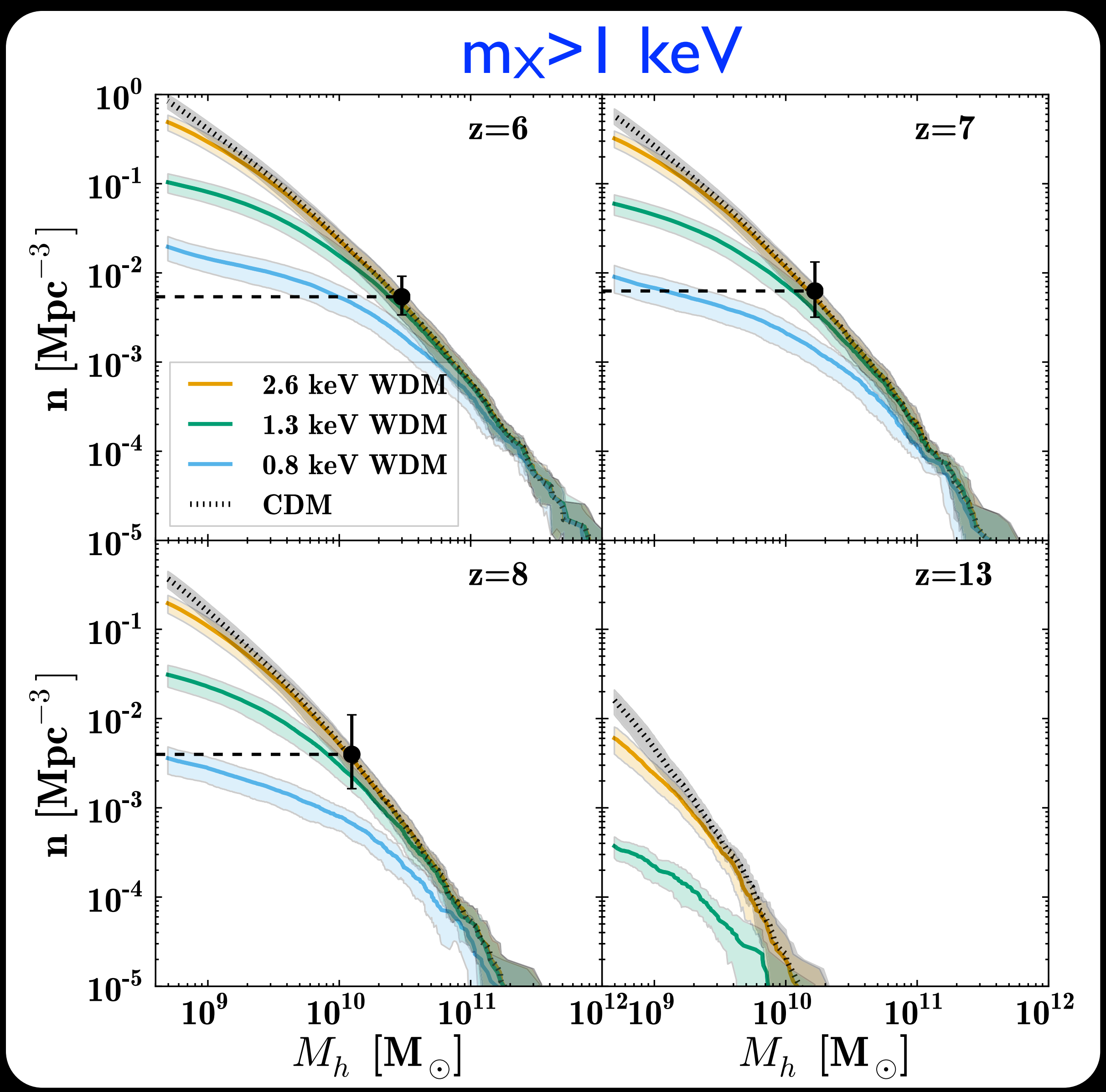

Magnitude limit mag=30
at z=6 this corresponds to M_{UV}=-18

Constraints on m_X from the abundance of low-mass galaxies: getting rid of degeneracy with astrophysics of gas and stars

At masses close to the Half-Mode mass WDM mass functions exhibit a down turn.
Observed galaxy densities larger than the maximum predicted abundance of a given WDM model would rule out the corresponding WDM particle mass <u>independently of L/M relation</u>

m_X>1 keV

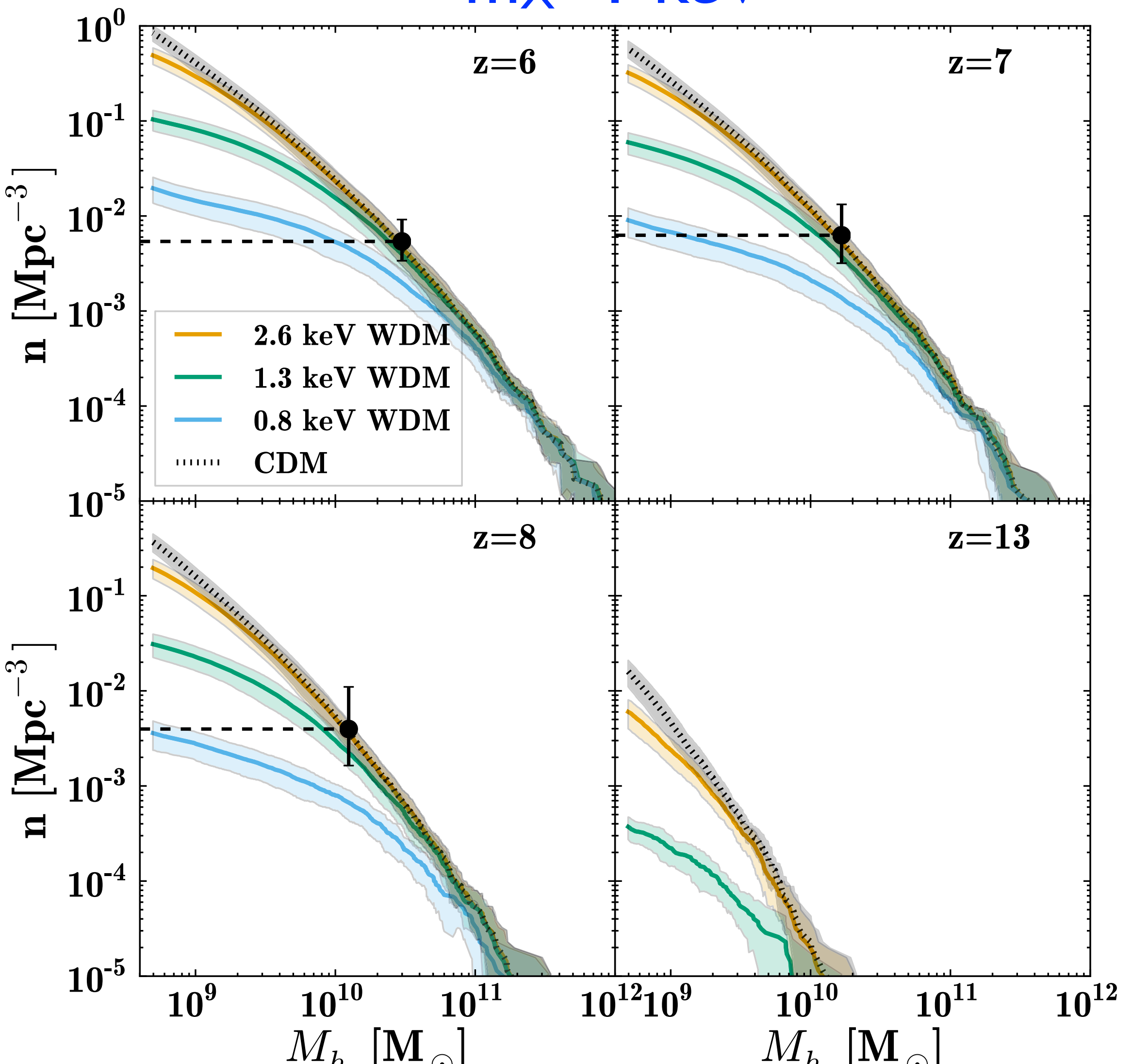

Probing the Half-mode mass of ~ 2 keV WDM models requires reaching $M_{UV} \approx$ -13

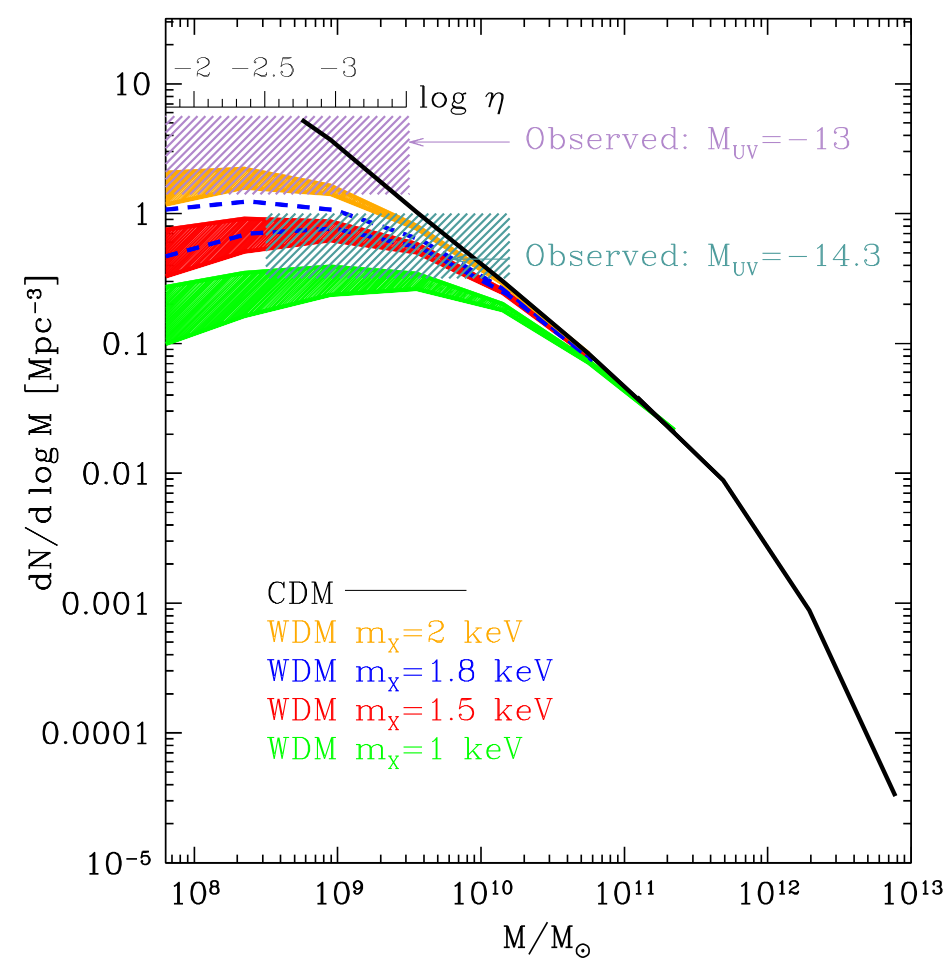

Constraints on m_X from the abundance of low-mass galaxies: getting rid of degeneracy with astrophysics of gas and stars

At masses close to the Half-Mode mass WDM mass functions exhibit a down turn.
Observed galaxy densities larger than the maximum predicted abundance of a given WDM model would rule out the corresponding WDM particle mass <u>independently of L/M relation</u>

m_X>1 keV

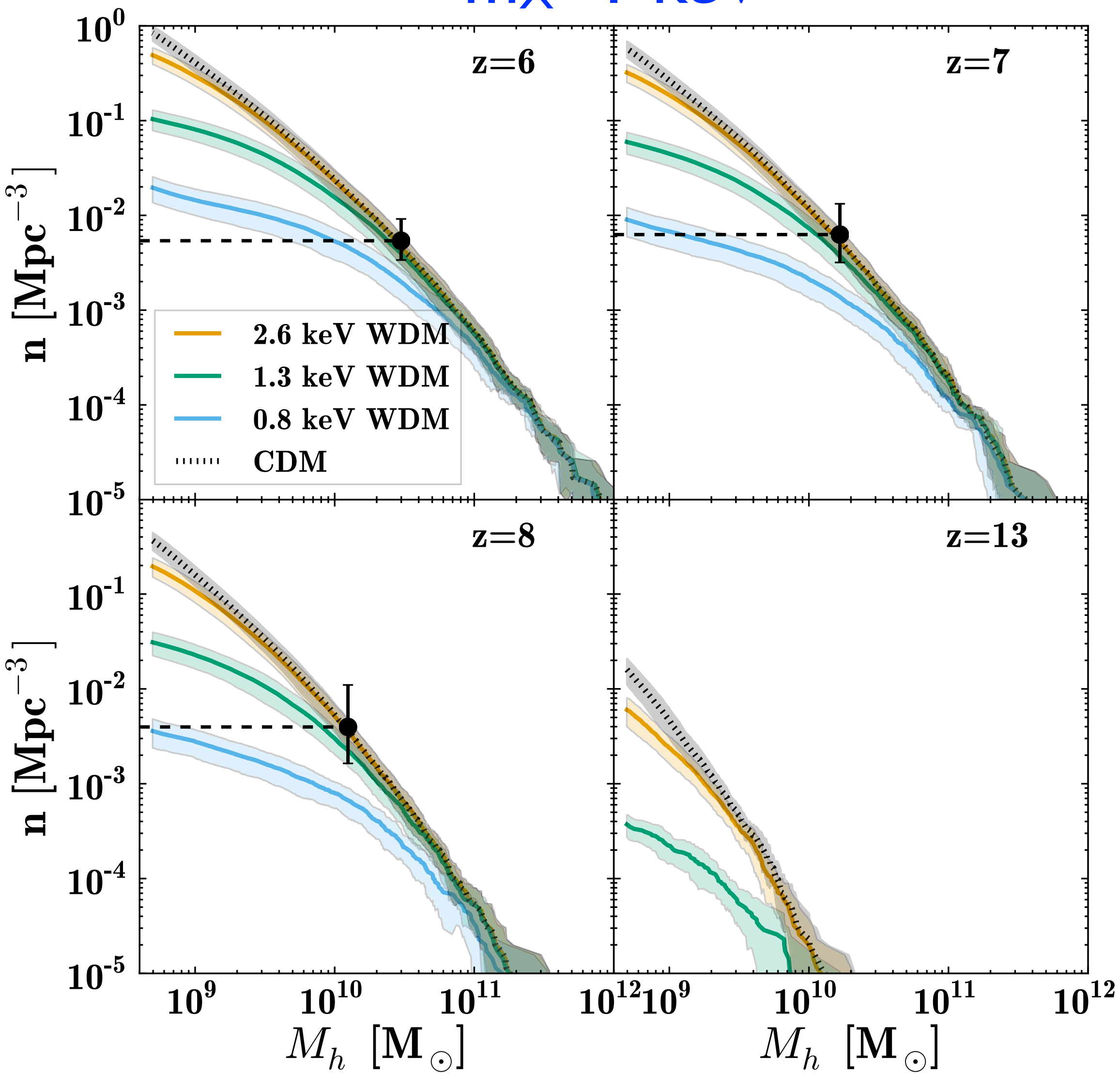

Probing the Half-mode mass of ~ 2 keV WDM models requires reaching $M_{UV}\approx$ -13
much, much deeper than present limit of HST

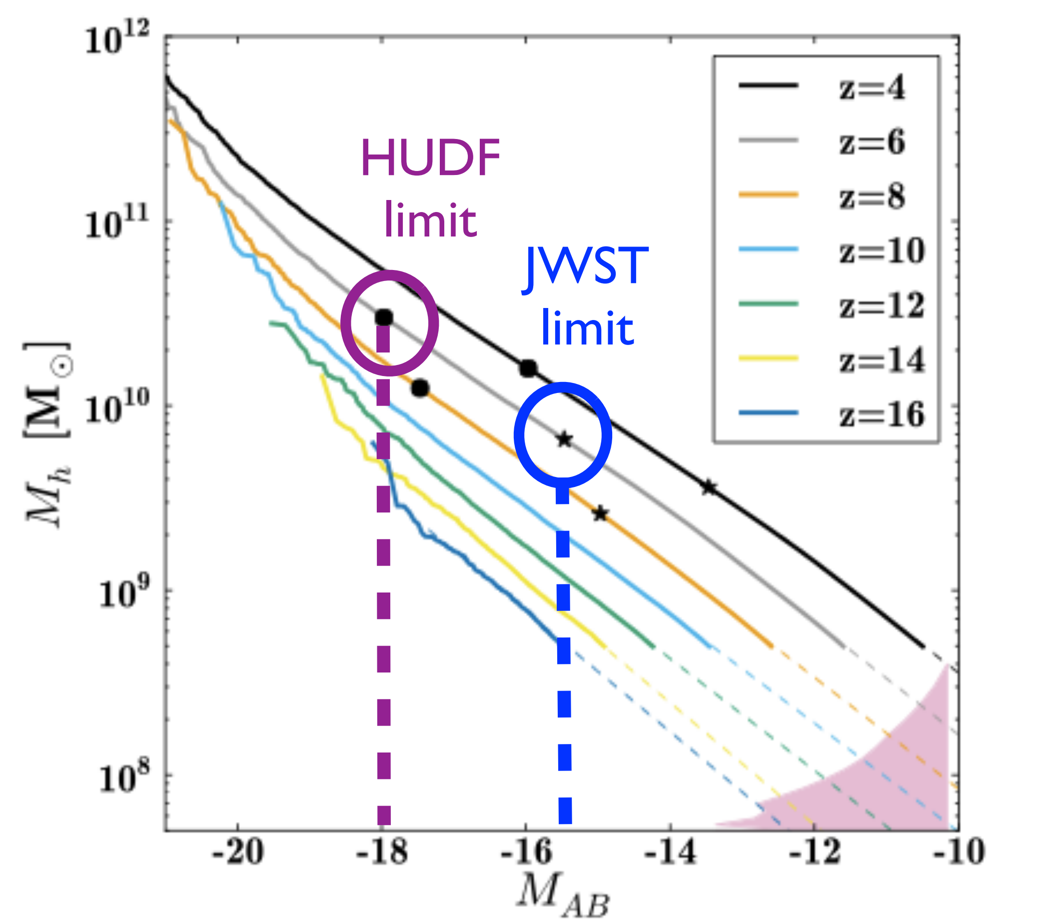

Hubble Frontier Field

The Frontier Fields Goals

Using Director's Discretionary (DD) observing time, HST is undertaking a revolutionary deep field observing program to peer deeper into the Universe than ever before and provide a first glimpse of JWST's universe.

These Frontier Fields will combine the power of HST with the natural gravitational telescopes of high-magnification clusters of galaxies. Using both the Wide Field Camera 3 and Advanced Camera for Surveys in parallel, HST will produce the deepest observations of clusters and their lensed galaxies ever obtained, and the second-deepest observations of blank fields (located near the clusters). These images will reveal distant galaxy populations ~10-100 times fainter than any previously observed, improve our statistical understanding of galaxies during the epoch of reionization, and provide unprecedented measurements of the dark matter within massive clusters.

This program is based upon the 2012 recommendations from the Hubble Deep Fields Initiative Science Working group: SWG Report 2012

Six Frontier Fields

Cluster Name	z	Cluster		Parallel Field	
		RA	Dec	RA	Dec
Year 1:					
Abell 2744	0.308	00:14:21.2	-30:23:50.1	00:13:53.6	-30:22:54.3
MACSJ0416.1-2403	0.396	04:16:08.9	-24:04:28.7	04:16:33.1	-24:06:48.7
Year 2:					
MACSJ0717.5+3745	0.545	07:17:34.0	+37:44:49.0	07:17:17.0	+37:49:47.3
MACSJ1149.5+2223	0.543	11:49:36.3	+22:23:58.1	11:49:40.5	+22:18:02.3
Year 3:					
Abell S1063 (RXCJ2248.7-4431)	0.348	22:48:44.4	-44:31:48.5	22:49:17.7	-44:32:43.8
Abell 370	0.375	02:39:52.9	-01:34:36.5	02:40:13.4	-01:37:32.8

Abell 2744 Cluster

Clusters as lensing telescopes

slide by Jennifer Lotz

slide by Jennifer Lotz

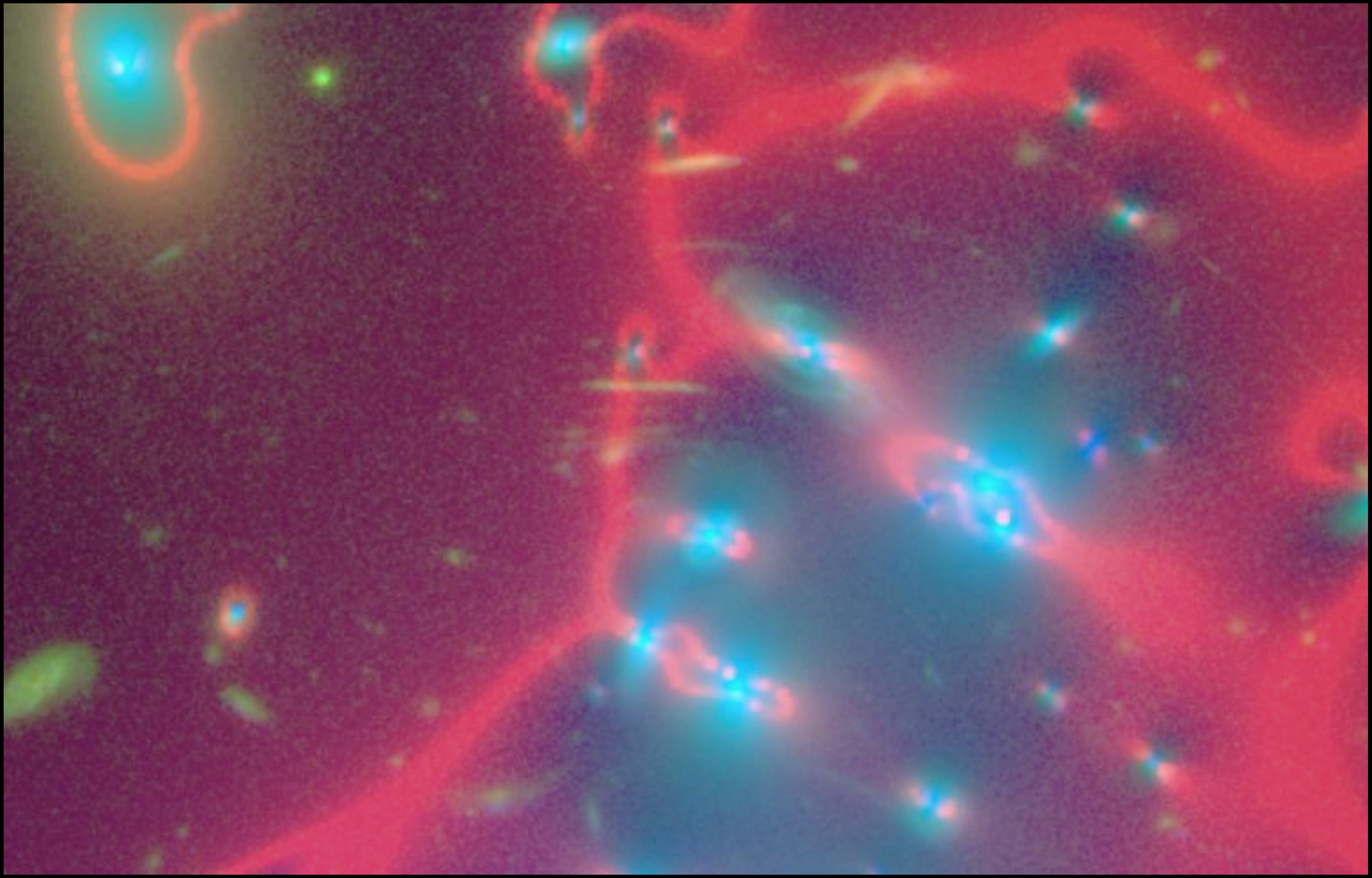

background galaxies are magnified by factors up to ~10-20,
providing the deepest yet view of the universe

slide by Jennifer Lotz

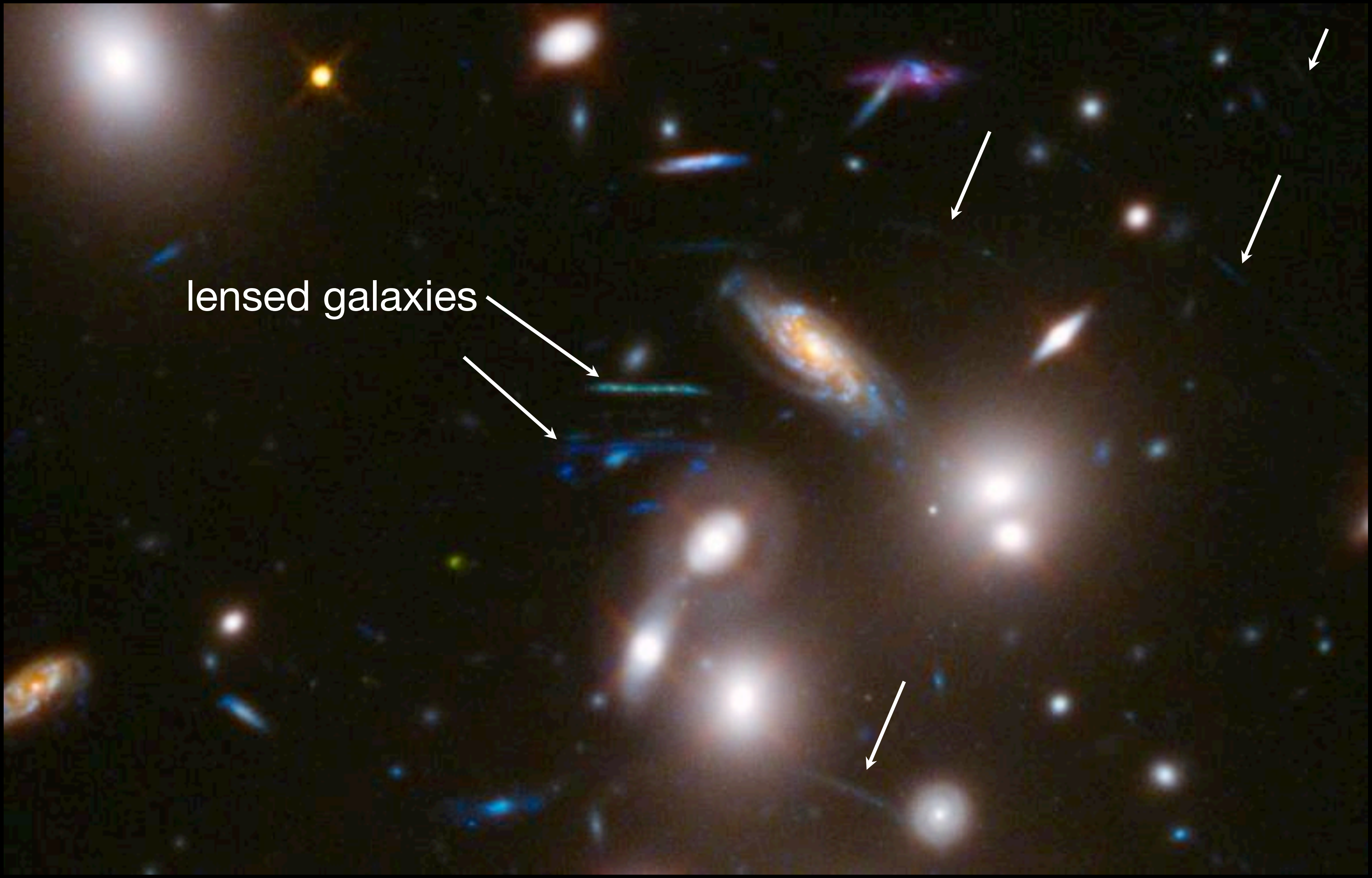

background galaxies are magnified by factors up to ~10-20, providing the deepest yet view of the universe

slide by Jennifer Lotz

Deepest view yet into the distant universe:

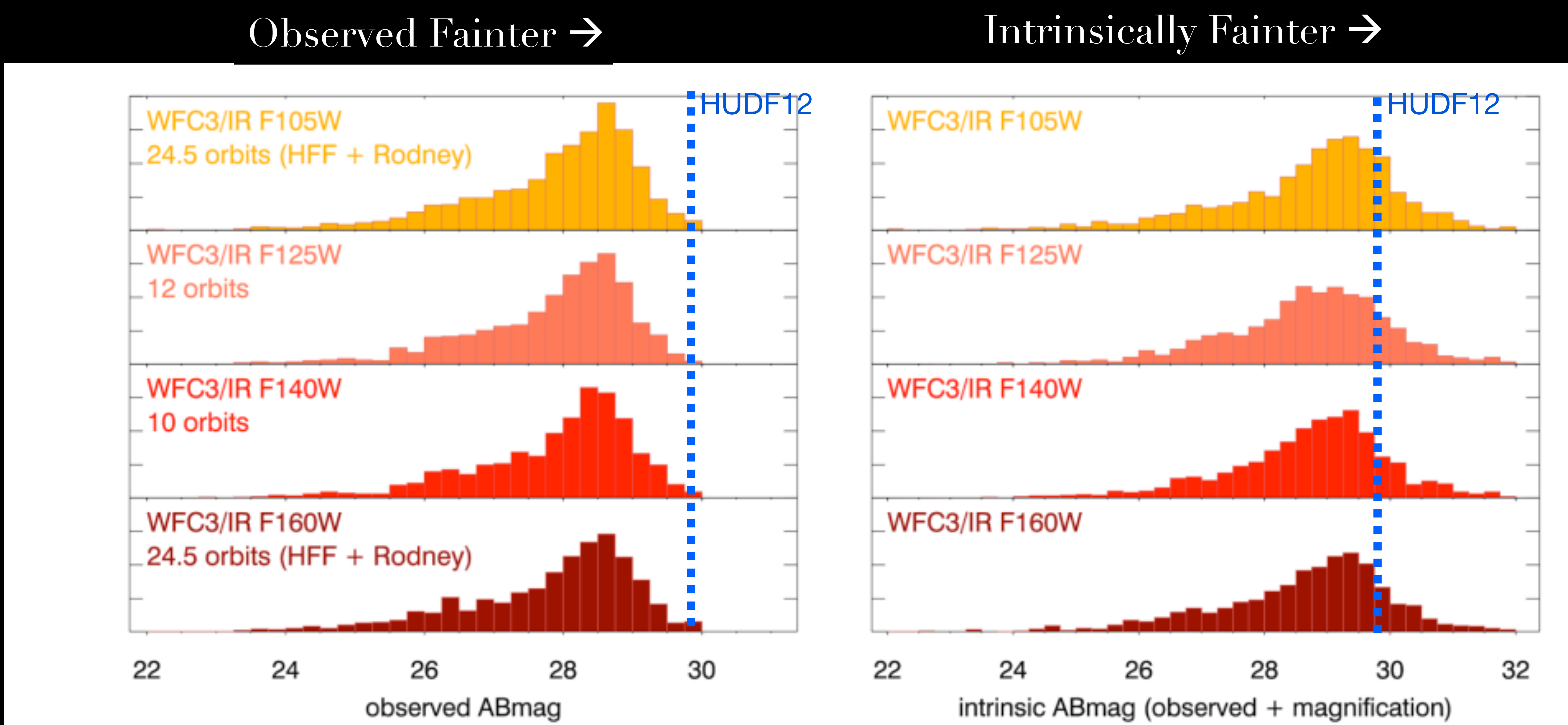

Take observed fluxes x lensing magnifications (average ~1.8x, max ~80x)

⇒ intrinsically faintest Frontier Fields galaxies ~2.5 magnitudes (10x) fainter than Ultra Deep Field (blue dashed line)

slide by Jennifer Lotz

A single cluster lens provided m_X>1.8 keV (thermal relic mass)

NM, Sanchez, Grazian, Castellano 2015

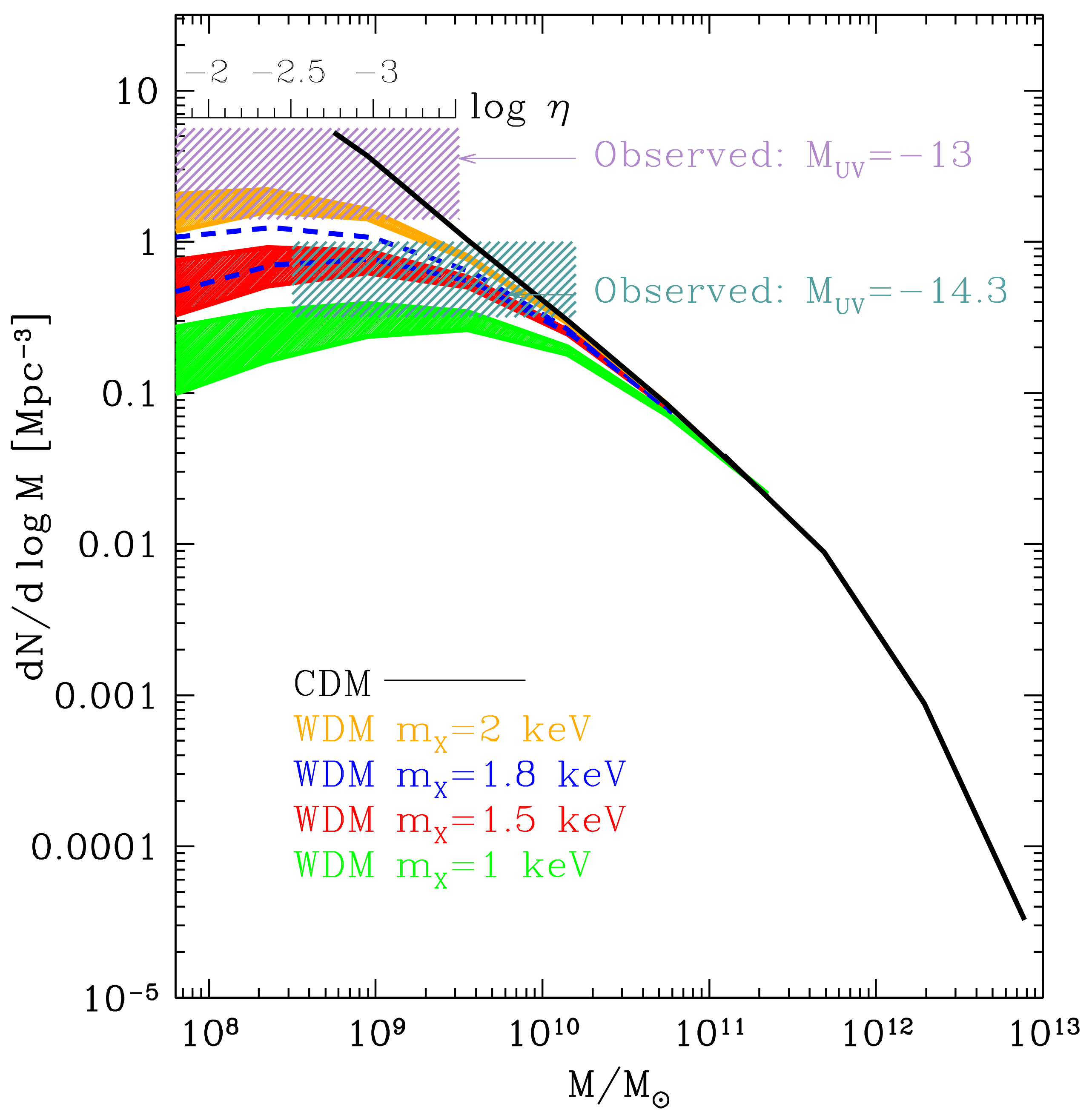

lower m_X do not provide the observed abundance. Note: baryonic processes can make the LF flatter but not steeper !

The result is robust with respect to

The effect of baryonic processes included in η. Observations probe the mass function in the mass range around the half-mode mass where the DM mass functions are characterized by a maximum value.

The modeling of residual DM dispersion velocities. Their would yield a sharper decrease of the mass function at small masses (see, e.g., Benson et al. 2013), thus yielding tighter constraints.

The collapse threshold: conservatively assume spherical collapse model. elliptical collapse yields even stronger limits

Recently Livermore, Finkelstein, Lotz 2016 obtained LFs of z=6 galaxies down to M_{UV}=-12.5

Based on 2 HFF lensing clusters Abell 2744 and MACS 0416

164 galaxies at z>6

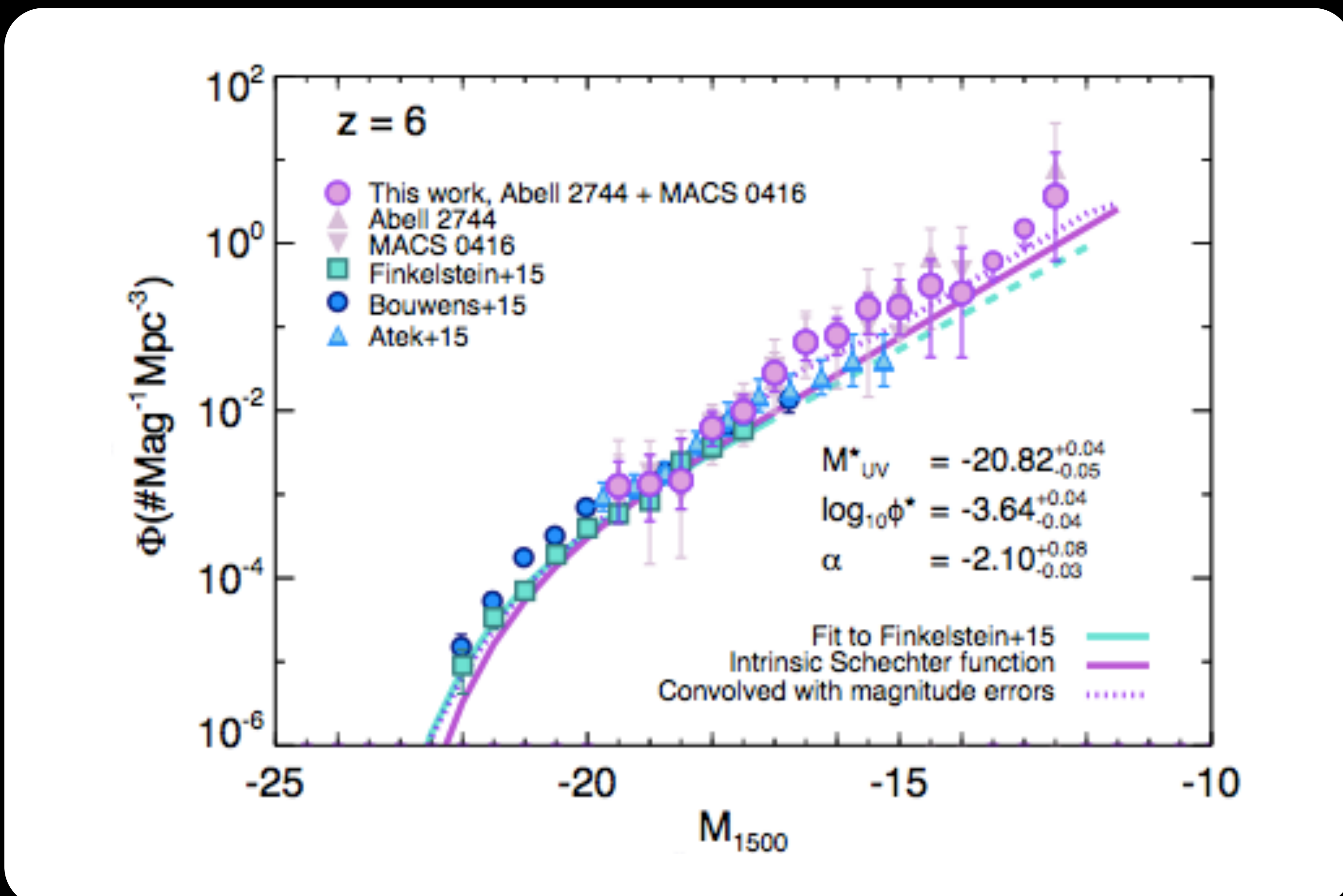

Lensing magnifications >50X

Magnifications have been derived by adopting the full range of possible lens models produced for the HFF by seven independent groups who used different assumptions and methodologies.

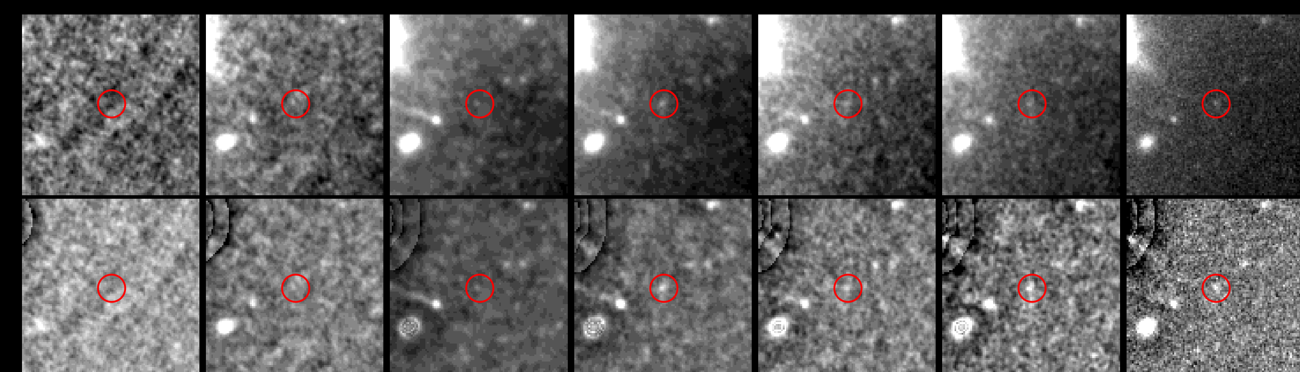

Postage stamp image of a2744 z6 3341, from the z ~ 6 sample detected in the Abell 2744 cluster field. The circle shows a 0.4" aperture. This galaxy is magnified by a factor ~ 20×, giving it an intrinsic UV magnitude of MUV = −14.54, but was not detected in previous studies due to the bright foreground object close to the line of sight (top row). It is easily detected in the wavelet-subtracted images (lower row

Such measurements have been shown to provide important constraints on the contribution to reionization, and on the star formation and feedback processes of primeval galaxies.

Recently Livermore, Finkelstein, Lotz 2016 obtained LFs of z=6 galaxies down to M_{UV}=-12.5

Based on 2 HFF lensing clusters Abell 2744 and MACS 0416

164 galaxies at z>6

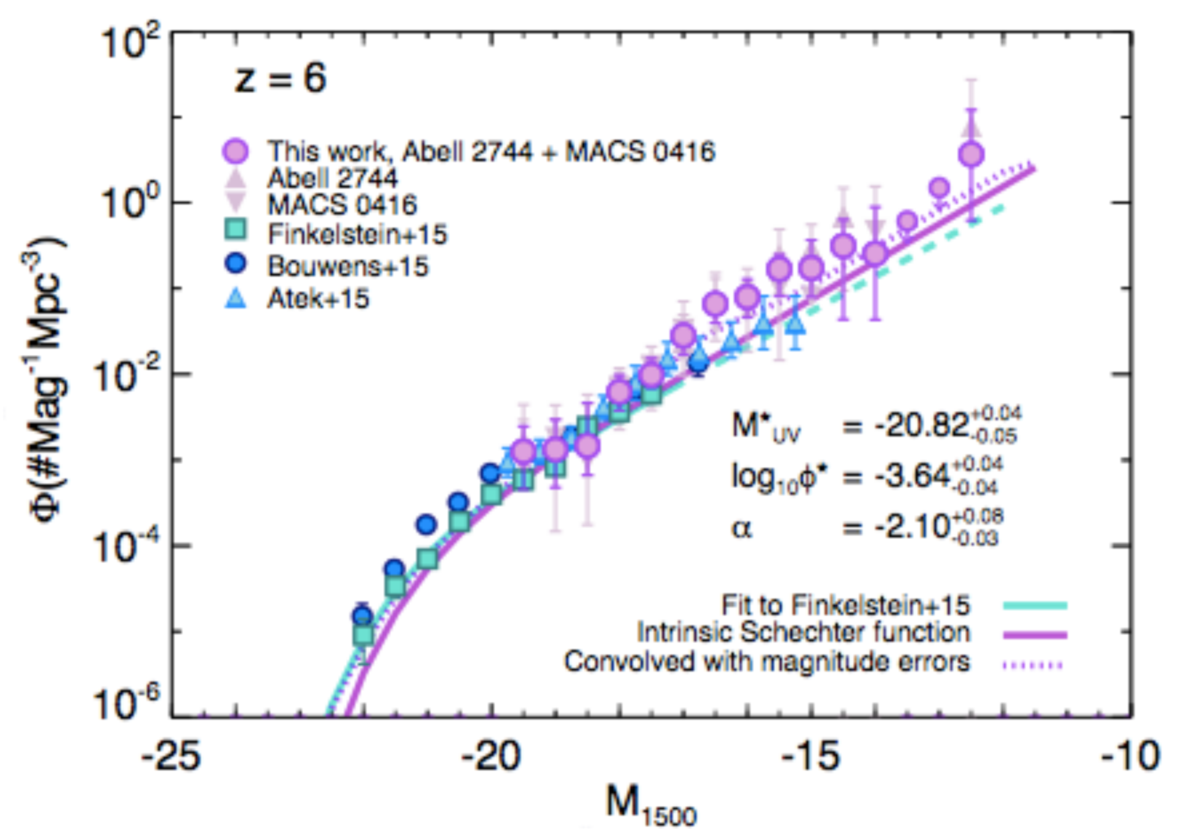

NM, Grazian Castellano Sanchez 2016

1. Starting from observed luminosity function, we run 10^7 Monte Carlo extractions of galaxies according to the observed distribution and with an uncertainty provided by the observed error bars.

2. Compute the total nuber density of galaxies down to the faintest magn bin:
# of galaxies/Mpc^3
at different confidence levels:

Best fit	$\log \Phi_{obs}/Mpc^3 = 0.54$
1σ	$\log \Phi_{obs}/Mpc^3 = 0.26$
2σ	$\log \Phi_{obs}/Mpc^3 = 0.01$
3σ	$\log \Phi_{obs}/Mpc^3 = -0.36$

Recently Livermore, Finkelstein, Lotz 2016 obtained LFs of z=6 galaxies down to M_{UV}=-12.5

Based on 2 HFF lensing clusters Abell 2744 and MACS 0416

NM, Grazian Castellano Sanchez 2016

1. Starting from observed luminosity function, we run 10^7 Monte Carlo extractions of galaxies according to the observed distribution and with an uncertainty provided by the observed error bars.

2. Compute the total nuber density of galaxies down to the faintest magn bin: # of galaxies/Mpc^3 at different confidence levels:

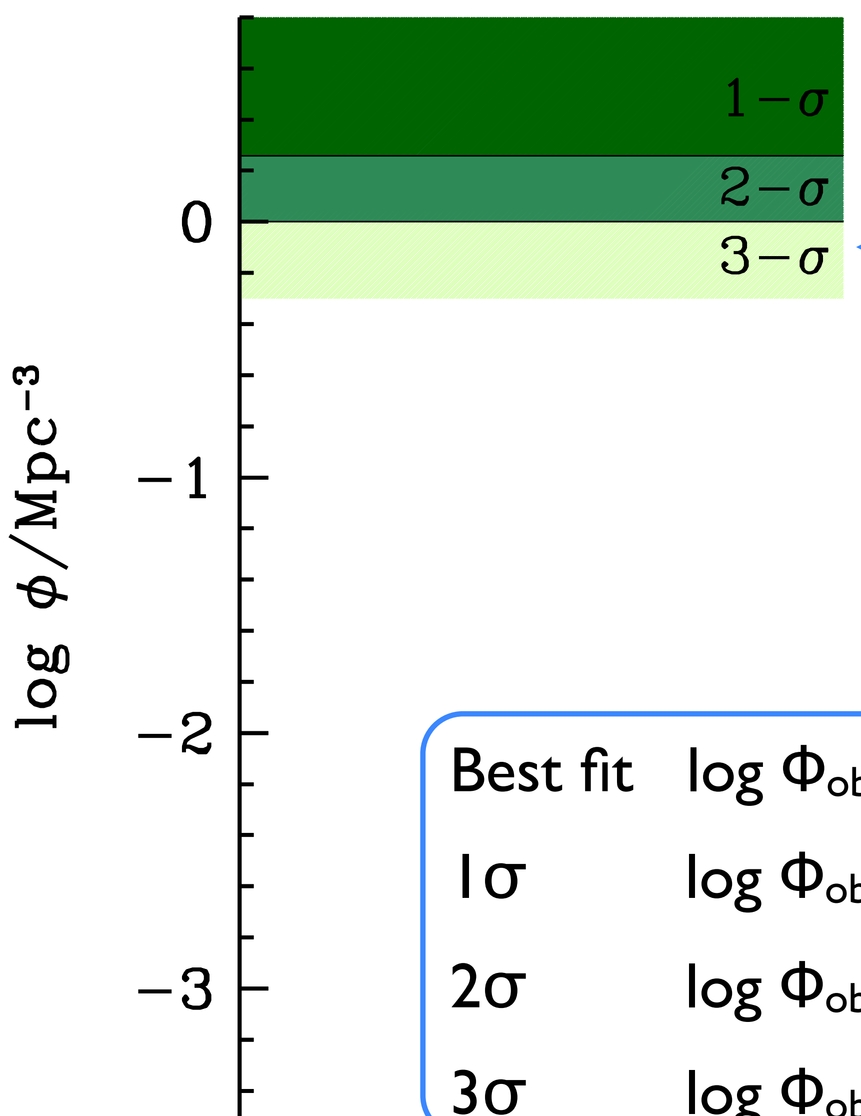

Best fit	$\log \Phi_{obs}/Mpc^3 = 0.54$
1σ	$\log \Phi_{obs}/Mpc^3 = 0.26$
2σ	$\log \Phi_{obs}/Mpc^3 = 0.01$
3σ	$\log \Phi_{obs}/Mpc^3 = -0.36$

Recently Livermore, Finkelstein, Lotz 2016 obtained LFs of z=6 galaxies down to M_{UV}=-12.5

Based on 2 HFF lensing clusters Abell 2744 and MACS 0416

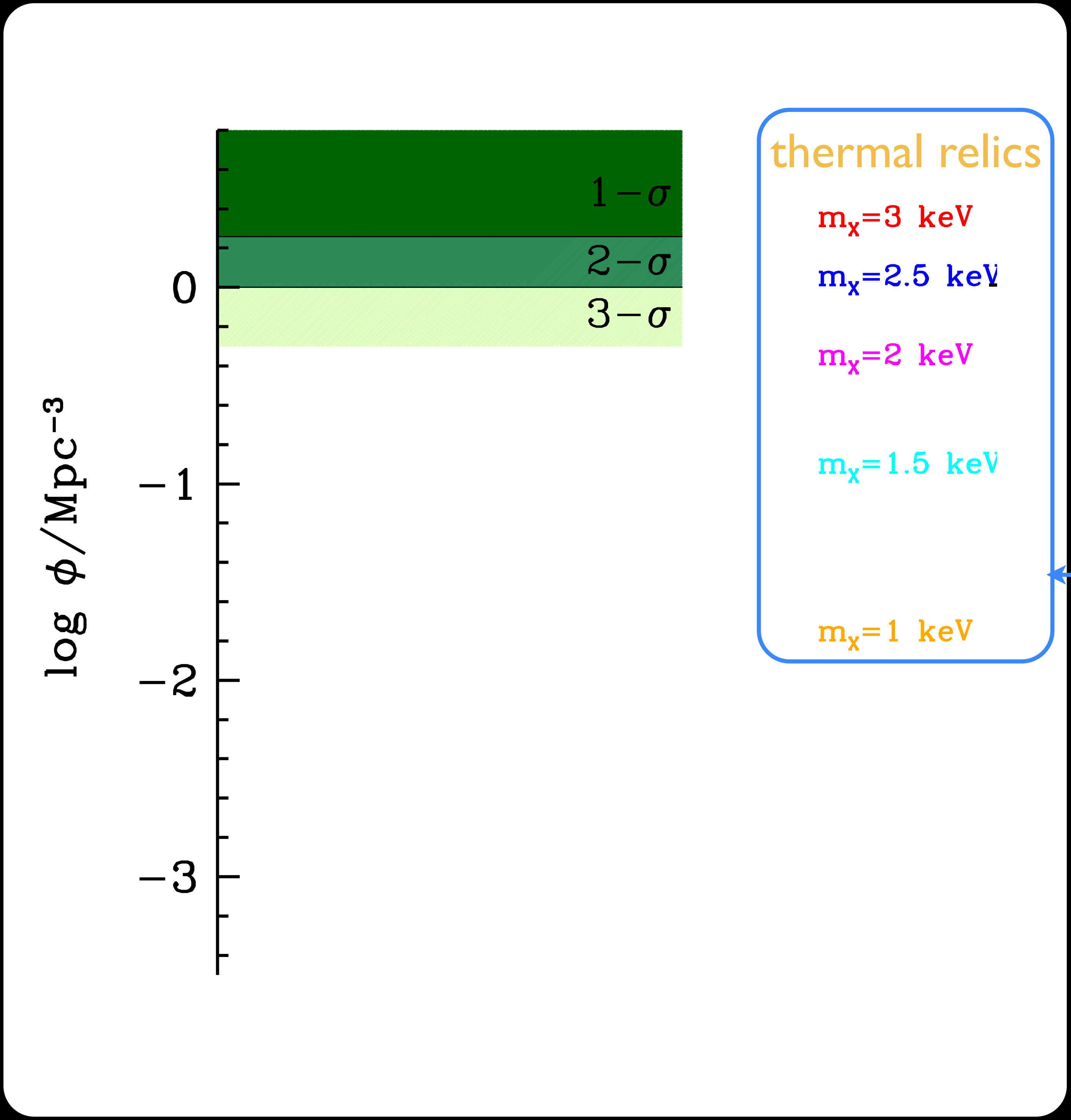

NM, Grazian Castellano Sanchez 2016

1. Starting from observed luminosity function, we run 10^7 Monte Carlo extractions of galaxies according to the observed distribution and with an uncertainty provided by the observed error bars.

2. Compute the total nuber density of galaxies down to the faintest magn bin:
\# of galaxies/Mpc^3
at different confidence levels:

3. Assume a Power Spectrum
P(m_X, production model)

Recently Livermore, Finkelstein, Lotz 2016 obtained LFs of z=6 galaxies down to M_{UV}=-12.5

Based on 2 HFF lensing clusters Abell 2744 and MACS 0416

thermal relics

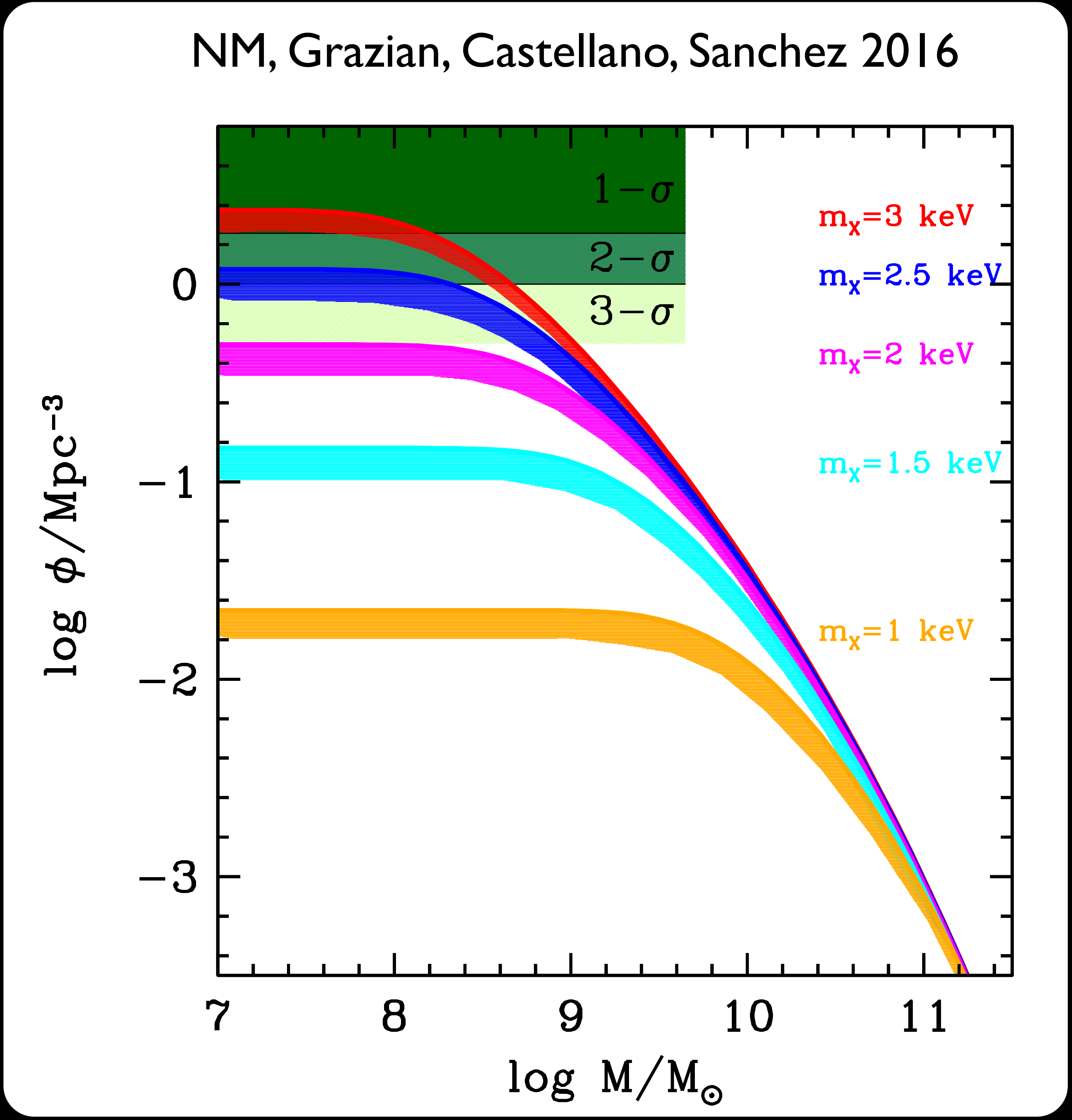

NM, Grazian Castellano Sanchez 2016

1. Starting from observed luminosity function, we run 10^7 Monte Carlo extractions of galaxies according to the observed distribution and with an uncertainty provided by the observed error bars.

2. Compute the total nuber density of galaxies down to the faintest magn bin: # of galaxies/Mpc^3 at different confidence levels:

3. Assume a Power Spectrum P(m_X, production model)

4. Compute the associated WDM cumulative mass function and the corresponding maximum number density $\tilde{\Phi}$ (m_X, production model)

5. Allowed WDM models are those with $\Phi_{obs} \leq \tilde{\Phi}$ (m_X, production model)
observed galaxies cannot outnumber the DM halos

Recently Livermore, Finkelstein, Lotz 2016 obtained LFs of z=6 galaxies down to M_{UV}=-12.5

When compared with maximum number density of DM halos in WDM models

we find a limit m_X>3 keV (1σ), m_X>2.4 keV (2σ) thermal relics

The tighter limits on mX derived so far independently of astrophysical processes

NM, Grazian, Castellano, Sanchez 2016

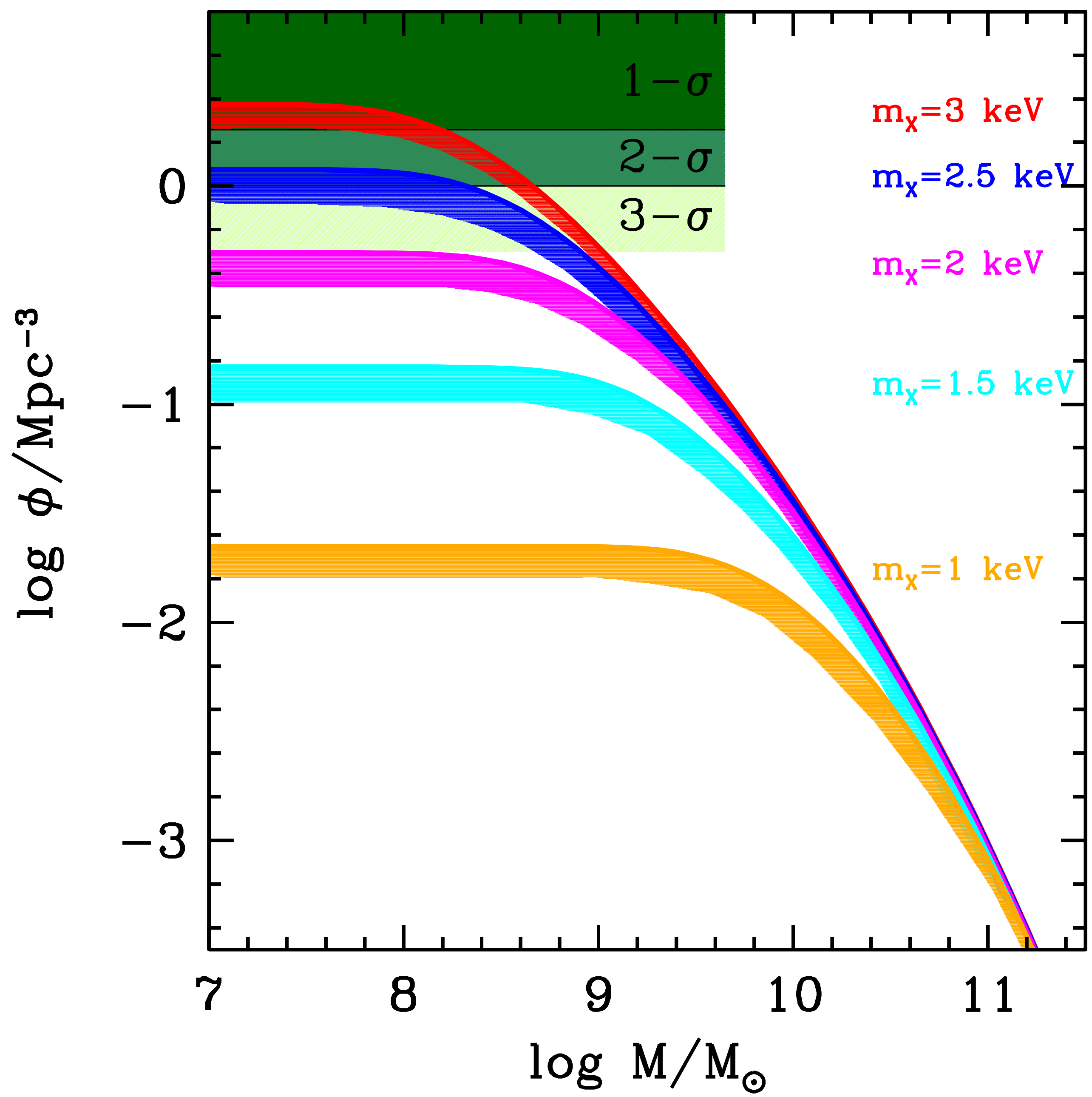

No matter what are the gas and star formation processes involved in galaxy formation visible galaxies cannot outnumber their host DM haloes

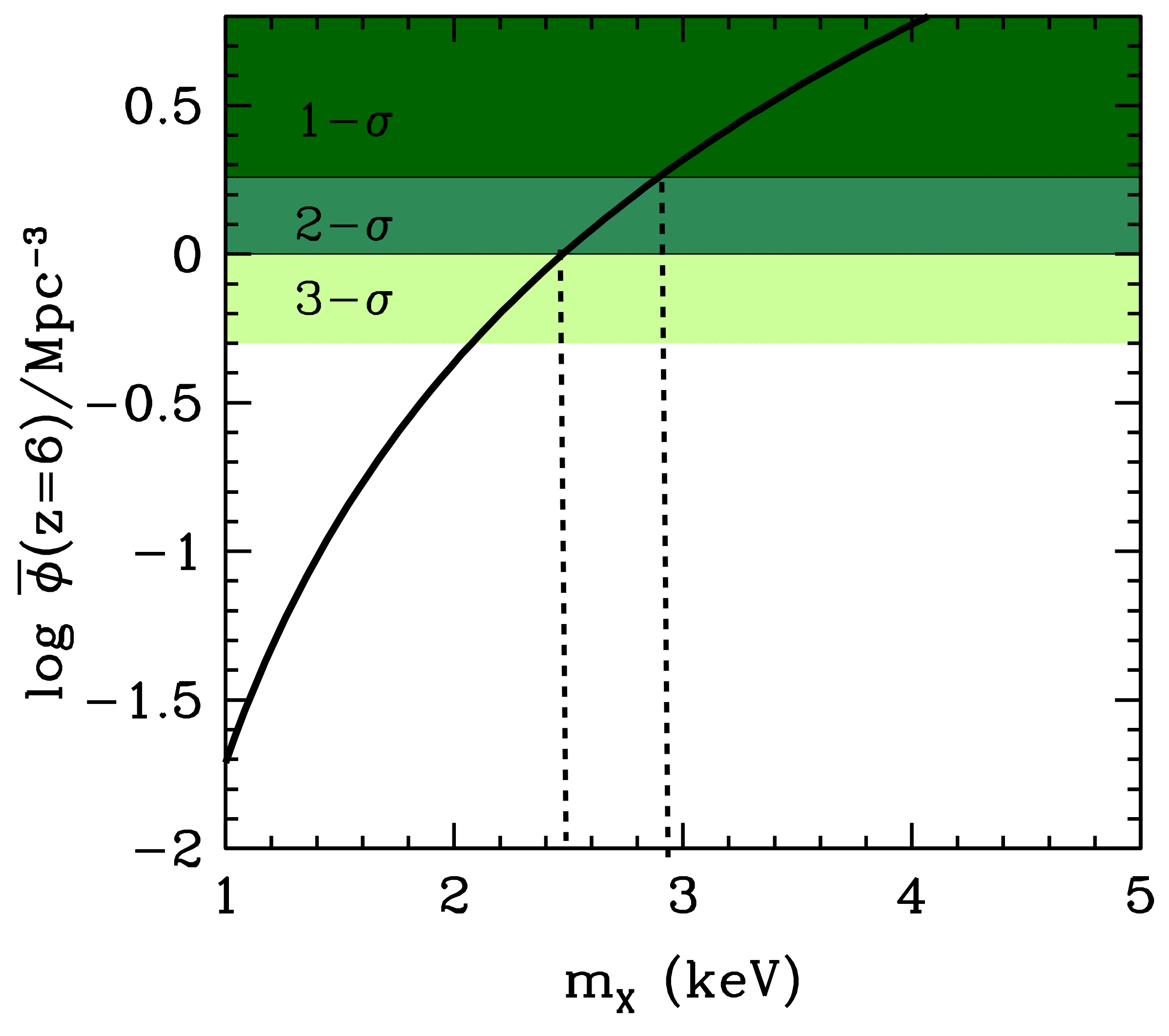

Comparison with previous limits based on galaxy abundances

NM+2016

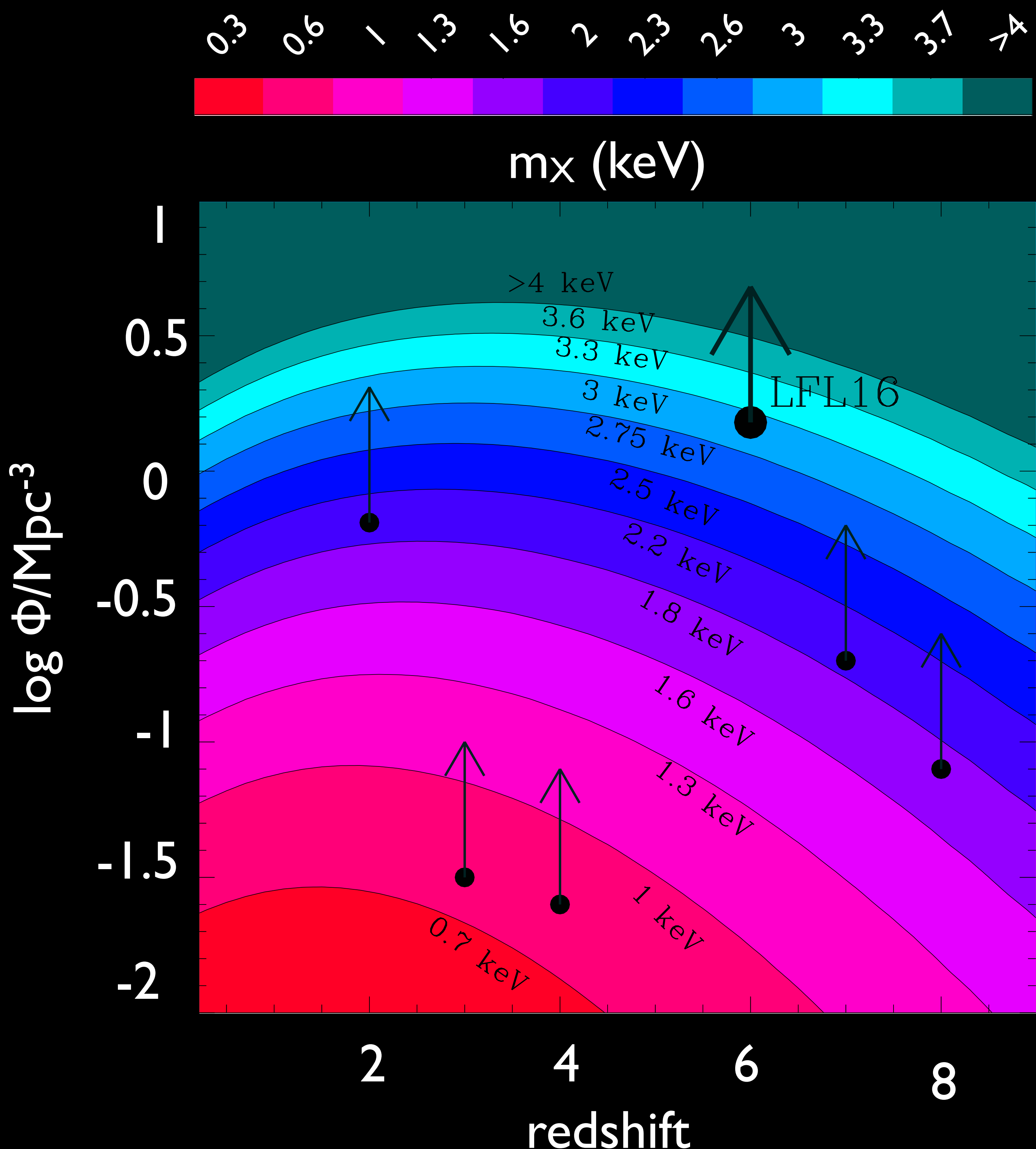

Data from

Alavi et al. 2015 z=2

Parsa et al. 2015 z=3-4

Livermore et al. 2016 z>6

The ultra-deep LF at z=6 constitute an extremely powerful probe

courtesy A. Merle

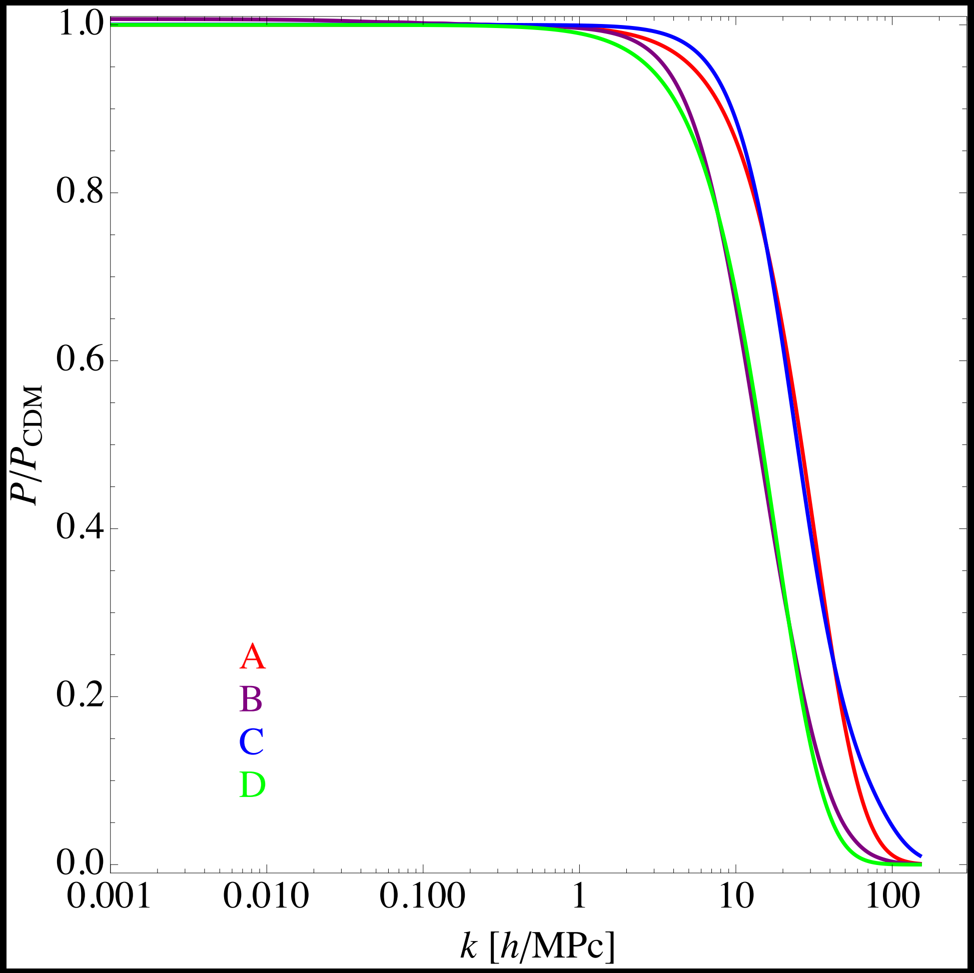

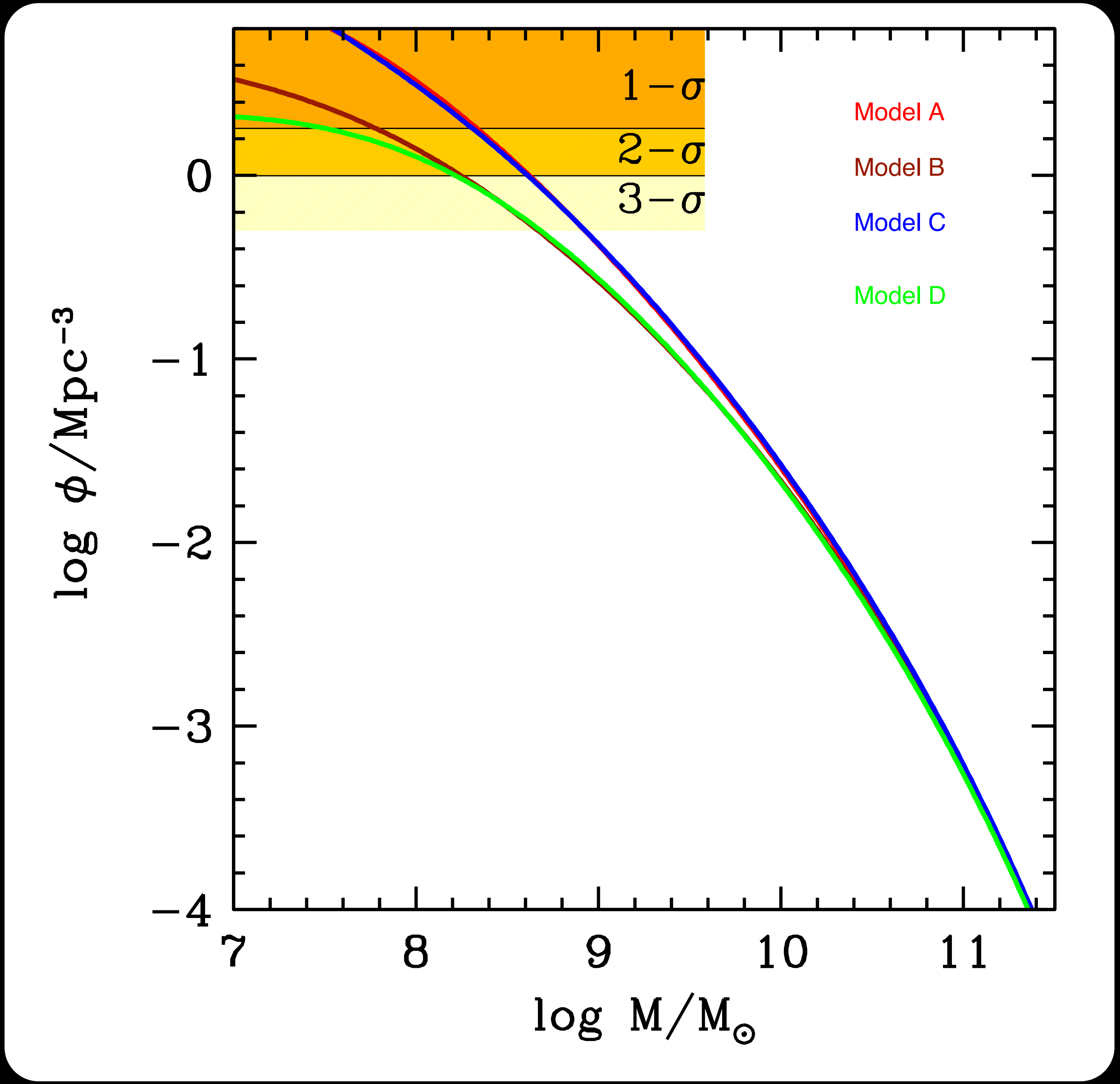

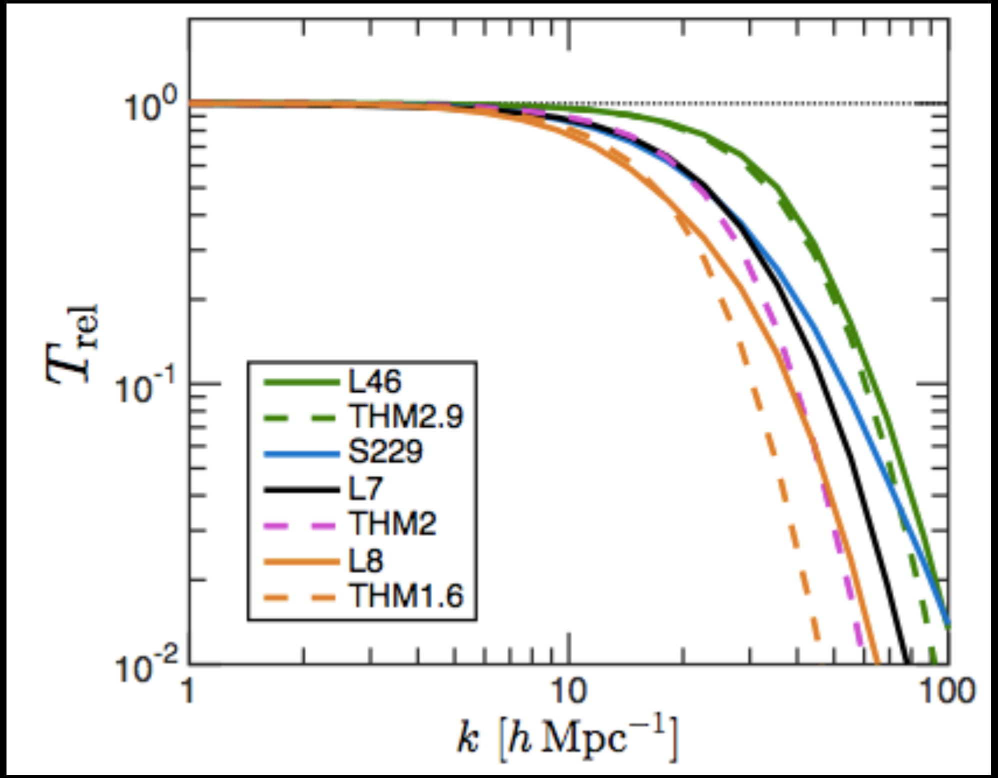

Bozek et al. 2015

Non-Thermal Relics: Resonant Production of sterile neutrinos (Shi Fuller 1999)

NM, Merle Schneider, Toutzer, Sanchez Cstellano, Grazian in progress

Off resonance with negligible lepton asymmetry: Dodelson Widrow scenario: mixing angles too large (conflicts with bounds from X-ray observations)

Sterile neutrinos could be produced from neutrino oscillations: for a
a given lepton asymmetry, oscillations on Mikheev–Smirnov–Wolfenstein (MSW) resonance generate a
relic sterile neutrinos with a lower average momentum than in the DW case.

Lepton asymmetry related to mixing angle to reproduce observed DM density

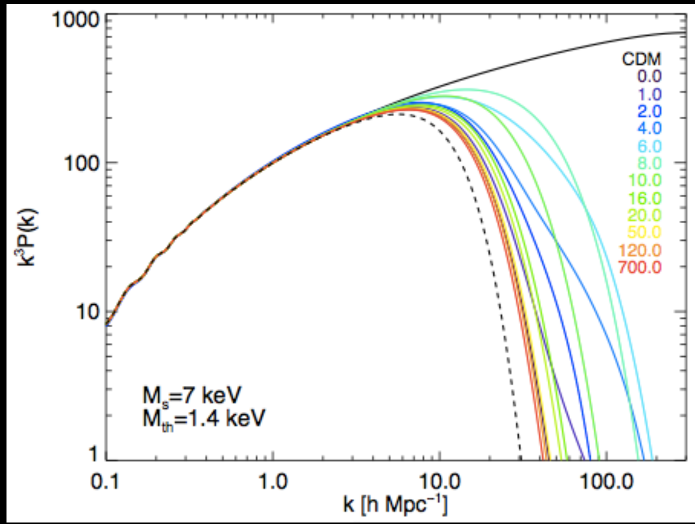

Lovell et al. 2015

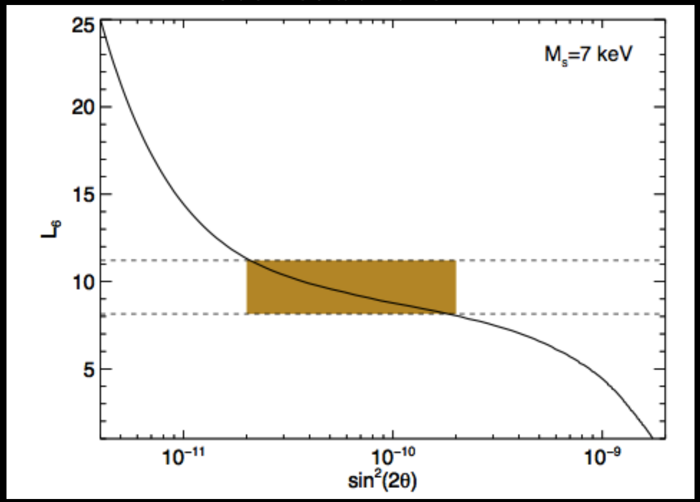

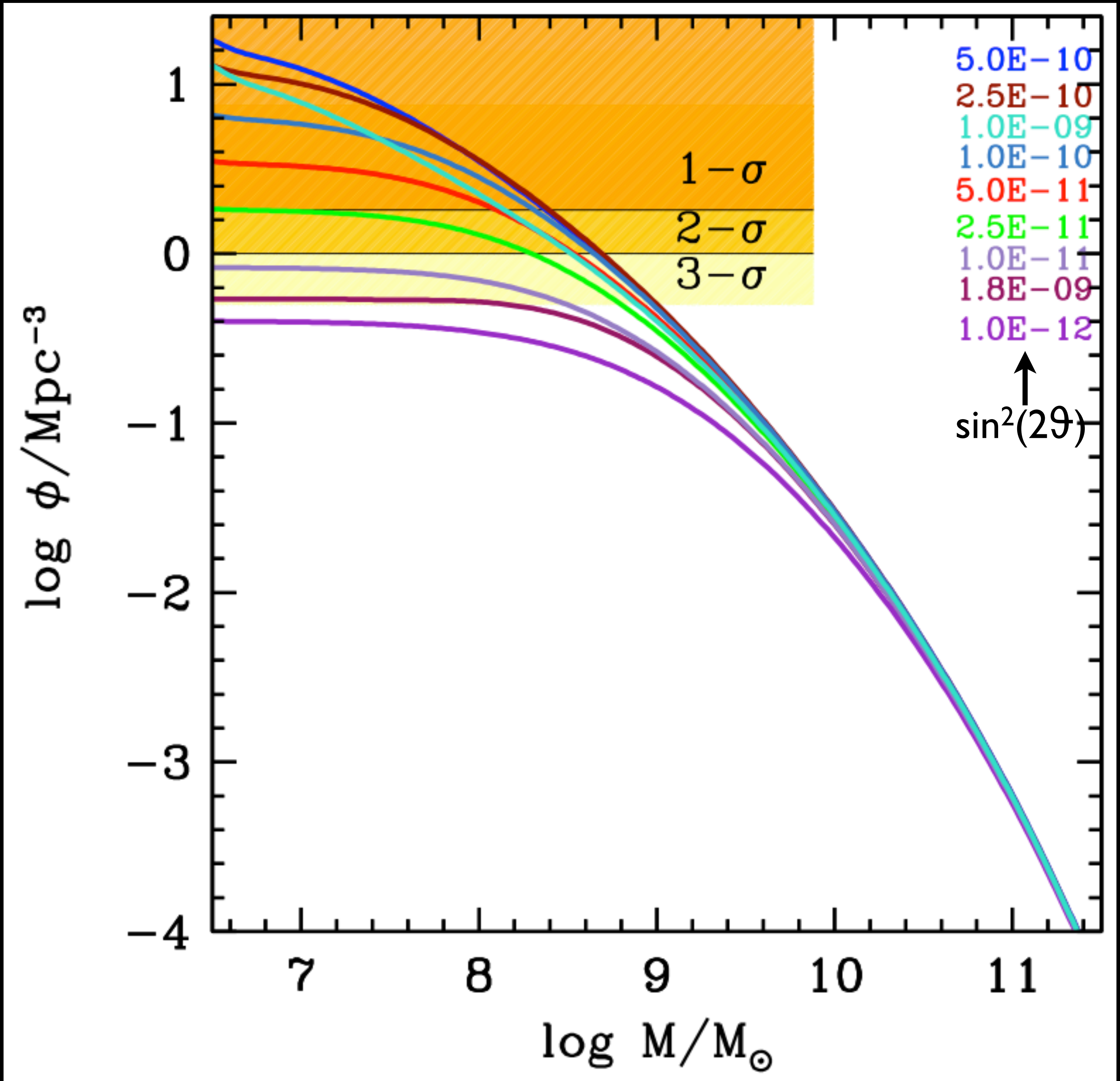

Resonant Production of sterile neutrinos: constraints on the $\sin^2(2\vartheta)$-$m_{sterile}$ plane

X-ray Bounds

$$\Gamma_{\nu_s \to \gamma\nu} \simeq 1.38 \times 10^{-22} \sin^2 2\theta \left(\frac{m_{\rm sn}}{\rm keV}\right)^5 s^{-1}$$

$$F_\gamma = \frac{\Gamma_{\nu_s \to \gamma\nu}\,\Omega_{\rm fov}}{8\pi} \int_{\rm los} dx\, \rho_{\rm DM}(x)$$

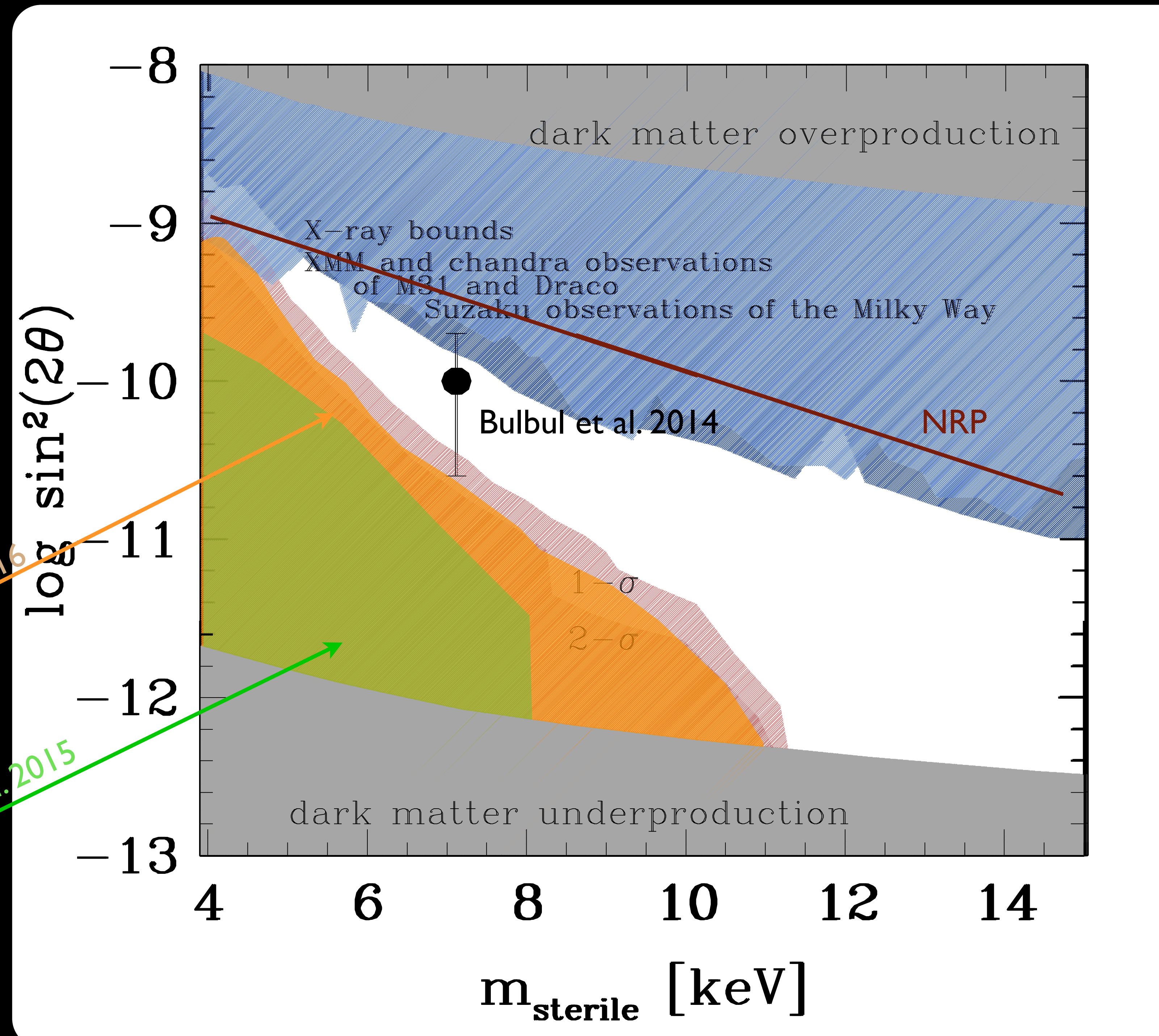

Limits from Milky Way satellites: depend on

- assumed upper limit for MW mass
- assumed lower limit for satellite masses
- assumed isotropic distribution to correct SDSS observations for limited sky coverage
- assumed halo-to-halo variance

Sterile neutrinos from scalar decay (Merle et al. 2013)

Scalar field S coupled to the right-handed neutrino fields N. The most generic coupling is a Yukawa term with coupling strength y which, if the scalar develops a non-zero vacuum expectation value $\langle S \rangle$, leads to a Majorana mass $m_N = y\langle S \rangle$. IF $\langle S \rangle \approx$ GeV – TeV → y ~ 10^{-9}–10^{-5} in order for the mass of the sterile neutrino to be in the keV-range.

y determines the decay time of the scalar.

NM, Merle Schneider, Toutzer, Sanchez Cstellano, Grazian 2016

For a given sterile neutrino mass, matching the observed DM density leaves y as the only free parameter (for small Higgs portal coupling $\lambda \ll 10^{-6}$).

$y>10^{-8}$ at 2-σ level

for $m_{sterile}$=7 keV

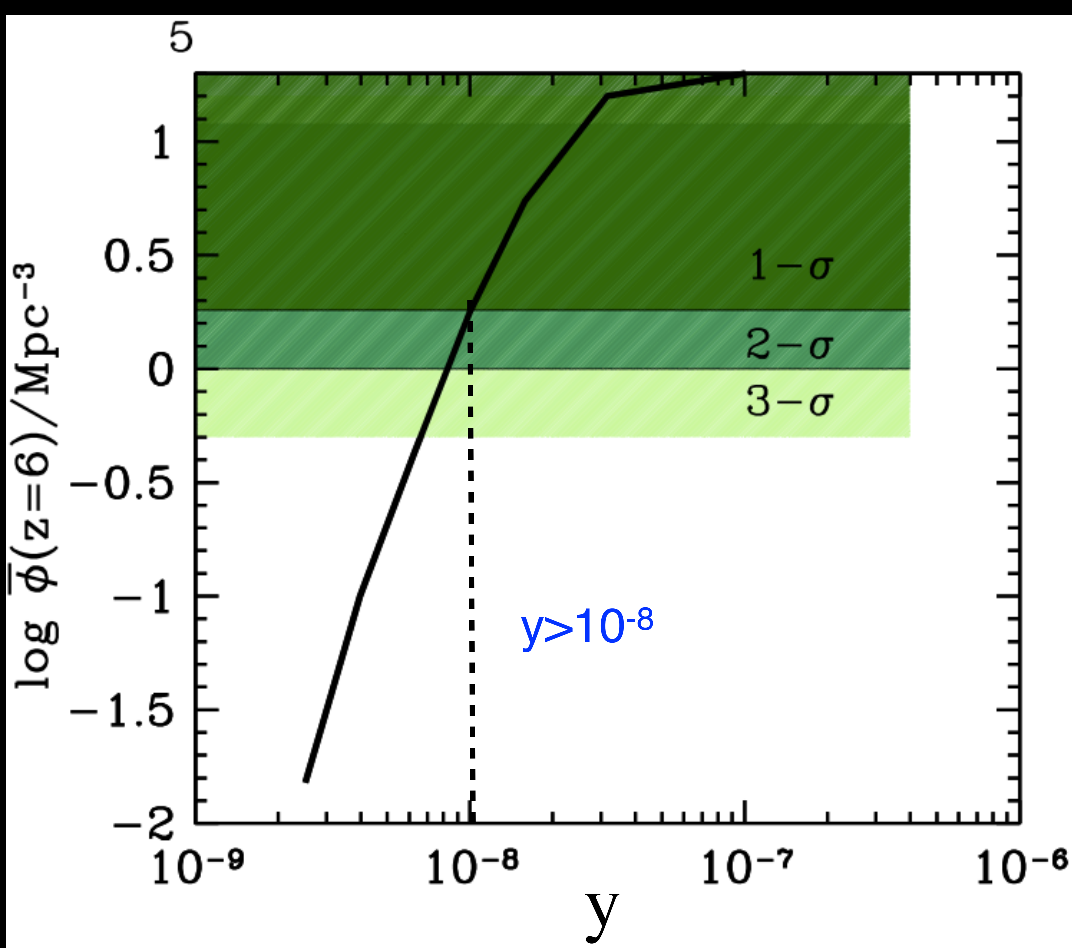

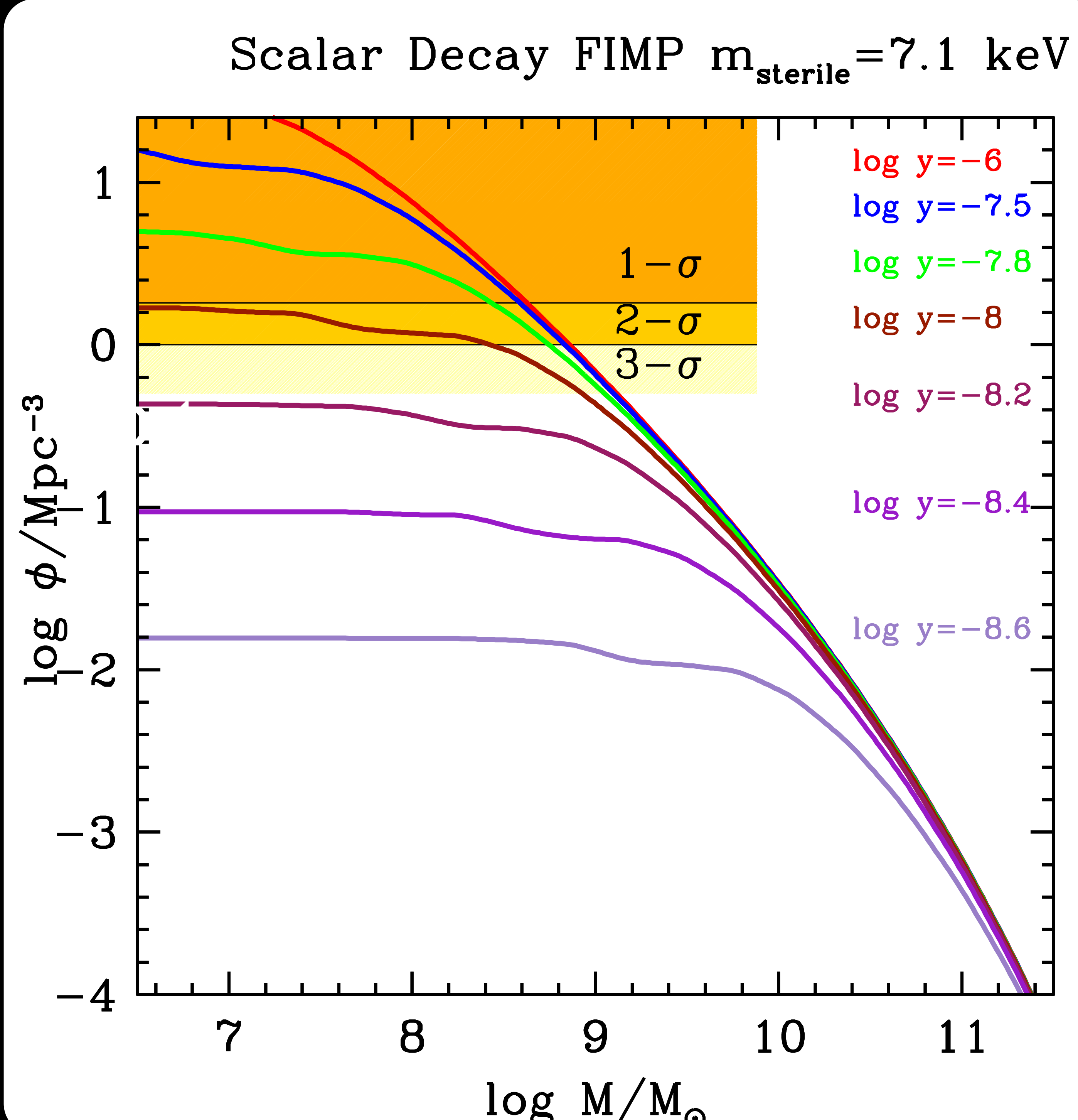

Wave DM - Fuzzy Dm: Bose condensate of ultra-light axion $m_X \sim 10^{-22}$ ev.

wavelike dark matter composed of a non-relativistic Bose-Einstein condensate,
so the uncertainty principle counters gravity below a Jeans scale (see Hu et al. 2000)

coulping Schrodinger's equation to gravity via Poisson's equation: a new form of stress tensor from quantum uncertainty, giving rise to a comoving Jeans length $\lambda_J \propto (1 + z)^{1/4} m_B^{-1/2}$

A distinct gravitationally self-bound solitonic core is found at the center of every halo, with a profile quite different from cores modeled in the warm or self-interacting dark matter scenarios.

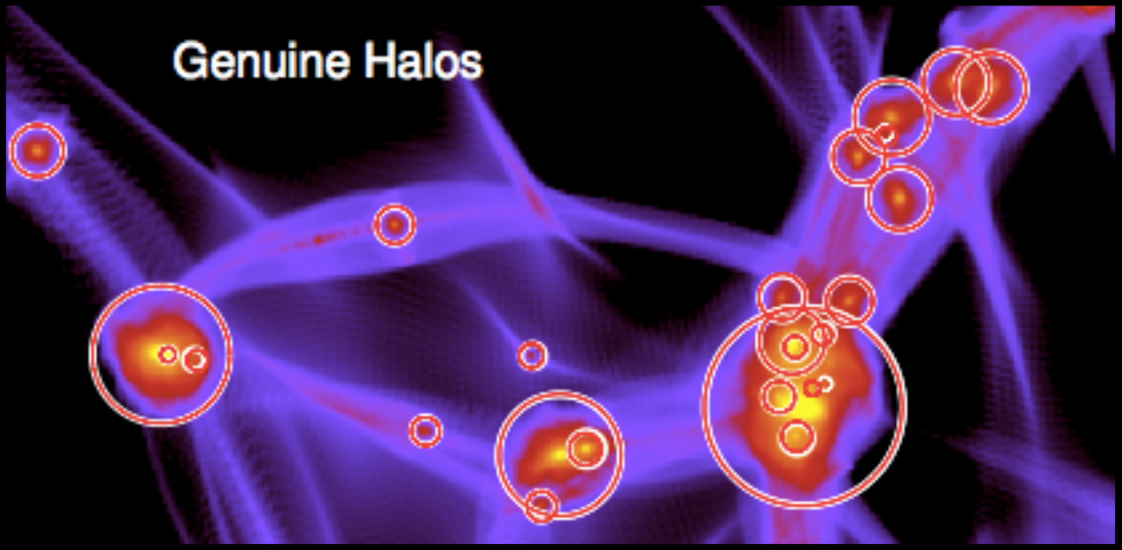

Schive, Chiueh, Broadhurst 2014

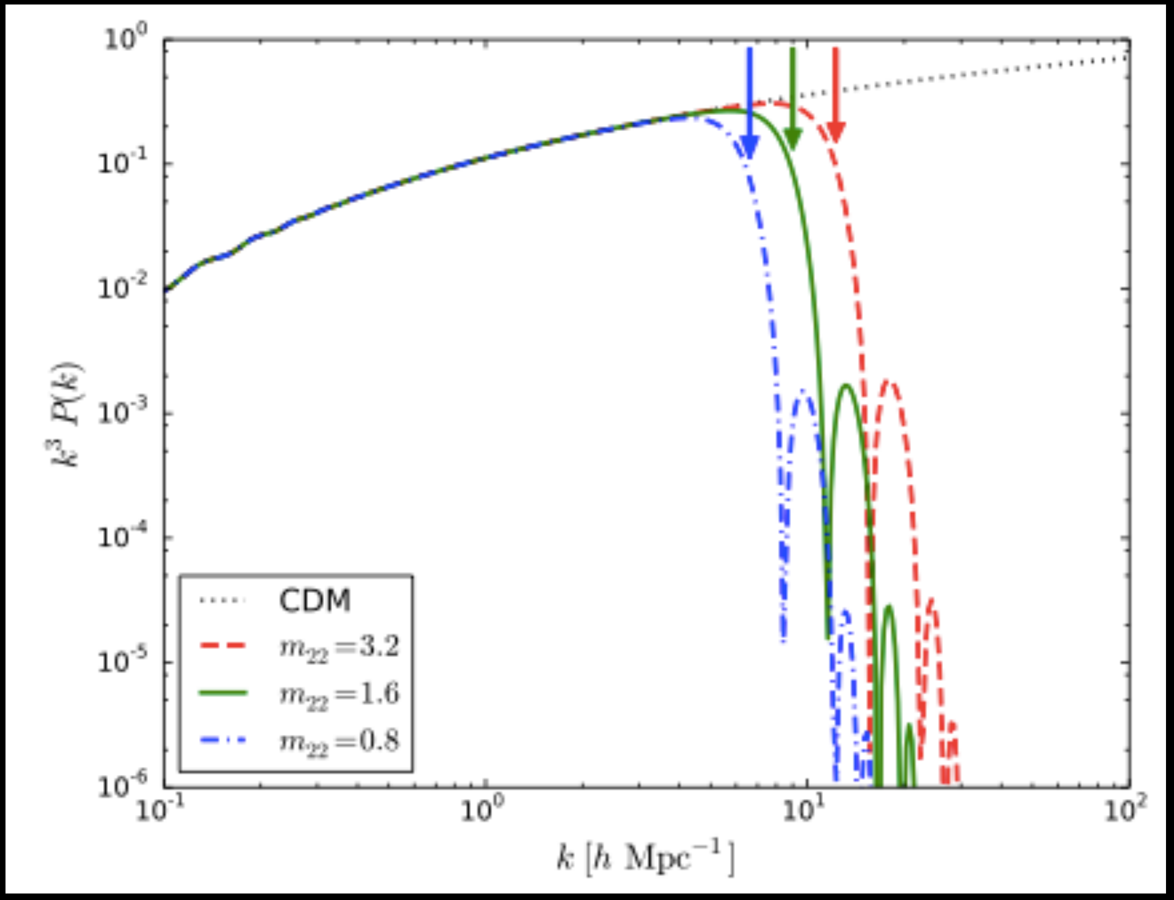

Wave DM - Fuzzy Dm: Bose condensate of ultra-light axion $m_X \sim 10^{-22}$ ev. Such class of models is ruled out

matching observed abundance of z=6 galaxies requires $m_{22}>10$
Matching the dwarf profiles requires $m_{22}<1.2$

Schive et al. 2016

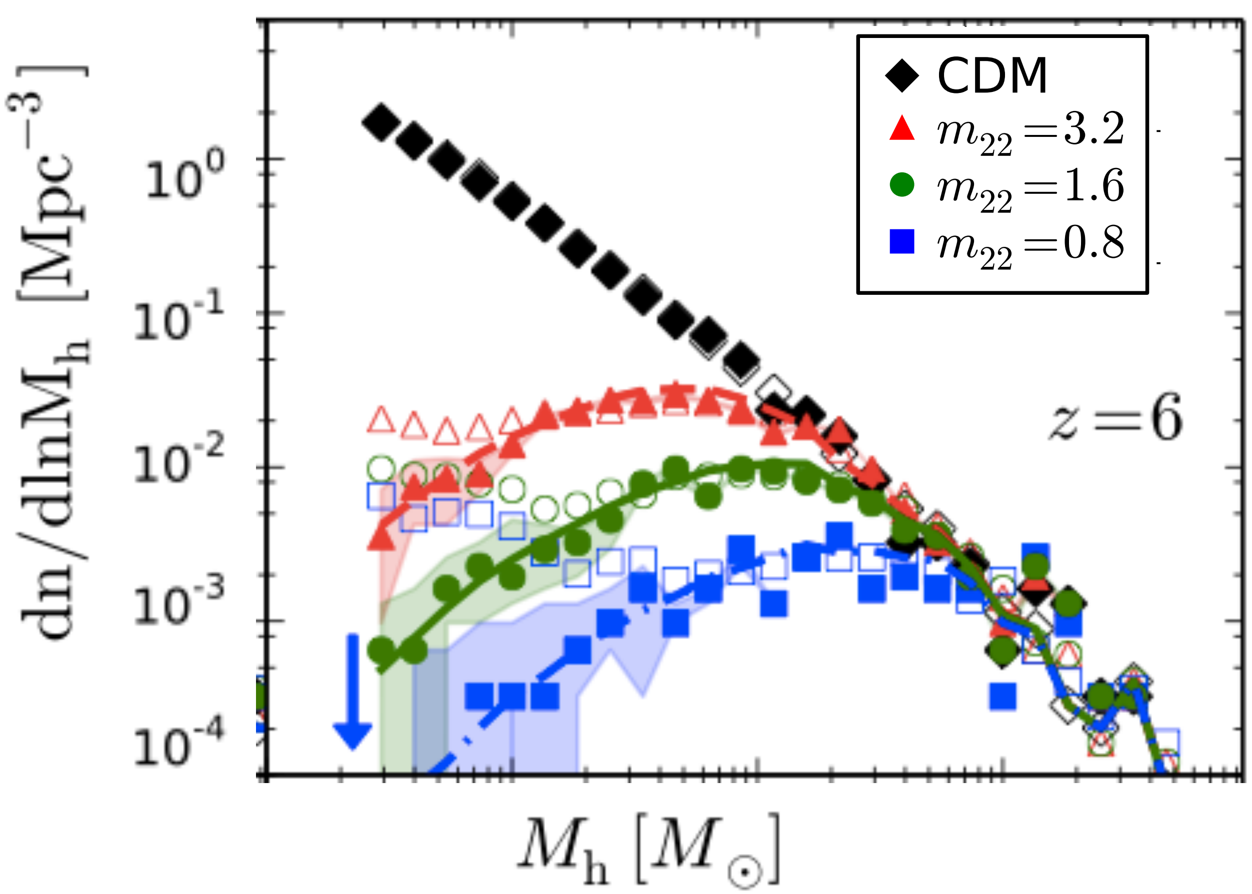

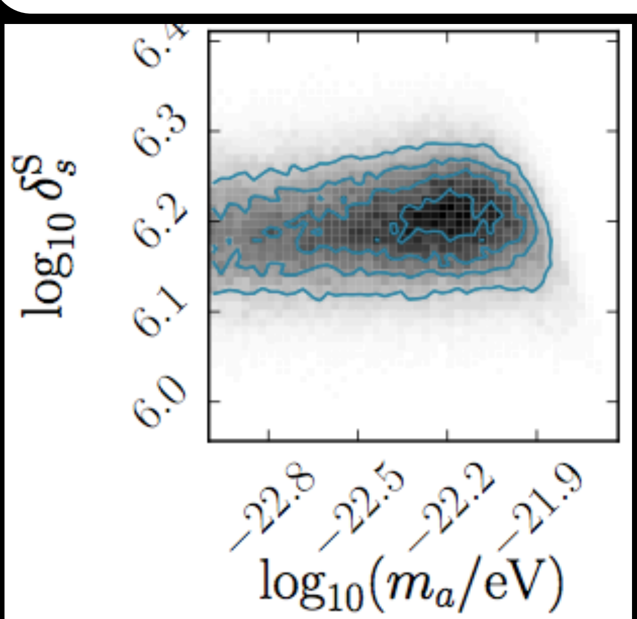

Marsch et al. 2015

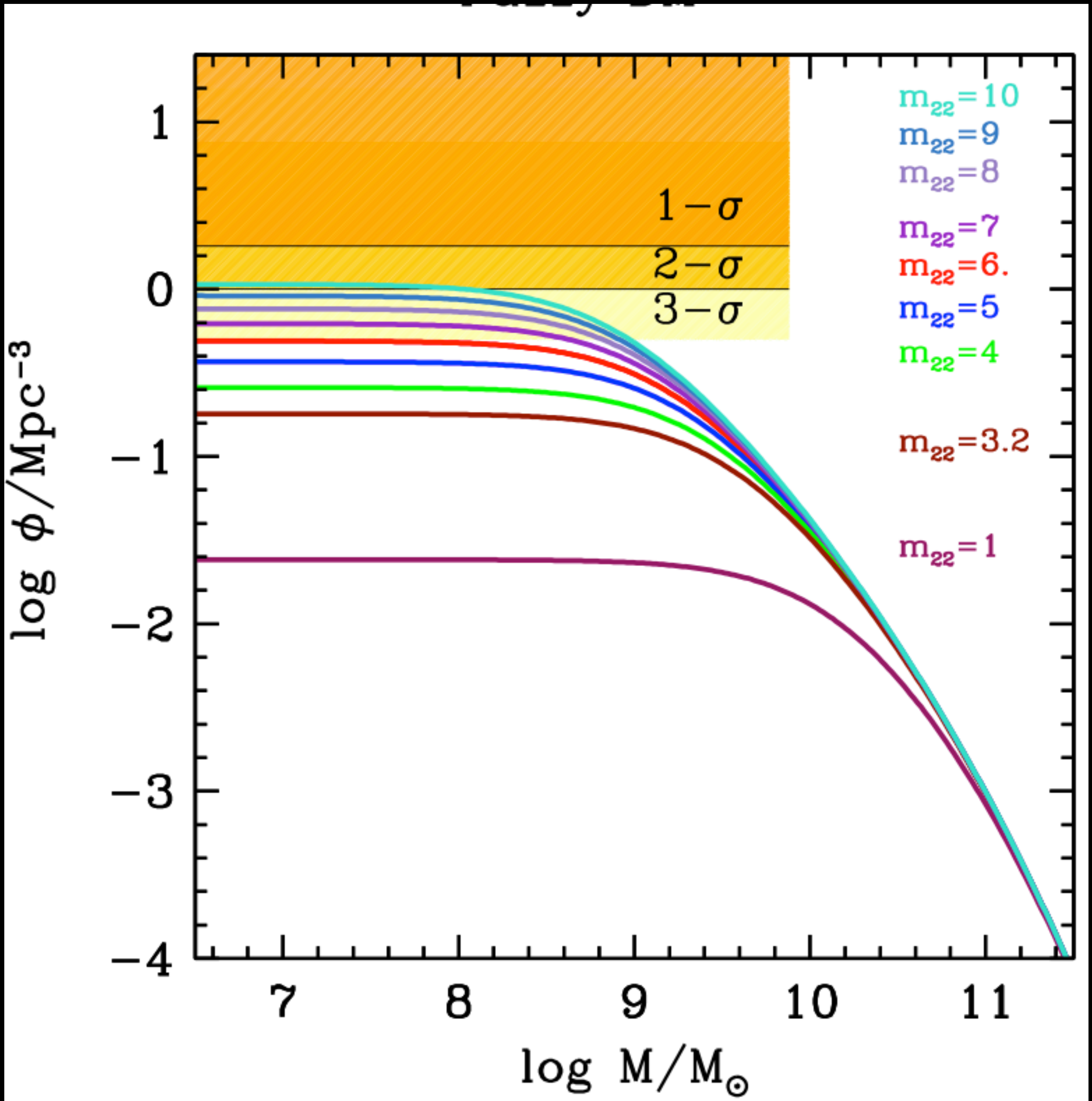

Conclusions

WDM models with spectra corresponding to thermal relic mass m_X~ keV constitute viable solutions provided $m_X < 4$ keV (models with larger m_X are undistinguishable from CDM as far as galaxy formation is concerned)

The tremendous improvement in the observations of faint galaxies at high redshift through WFC3+lensing (HFF) allows to measure the abundance of z=6 galaxies down to M_{UV}=-12.5. This allows to set strong constraints on DM models with suppressed power spectra

independent of the modeling of astrophysical processes involving baryons

- Thermal relics: $m_X > 2.4$ keV at 2-σ level

- Sterile neutrinos

  produced through Shi-Fuller: unprecedented lower limits for $\sin^2(2\vartheta)$ as a function of $m_{sterile}$.

  E.g., for $m_{sterile}$=7 keV we obtain $-10.4<\log \sin^2(2\vartheta)<-9.8$ at 2-σ level

  produced through scalar decay (for small Higgs portal coupling $\lambda \ll 10^{-6}$)

  $y>10^{-8}$ at 2-σ level for $m_{sterile}$=7 keV

- Bose condensate of ultra-light axion $m_X \sim 10^{-22}$ ev are ruled out: $m_X > 10^{-21}$ eV

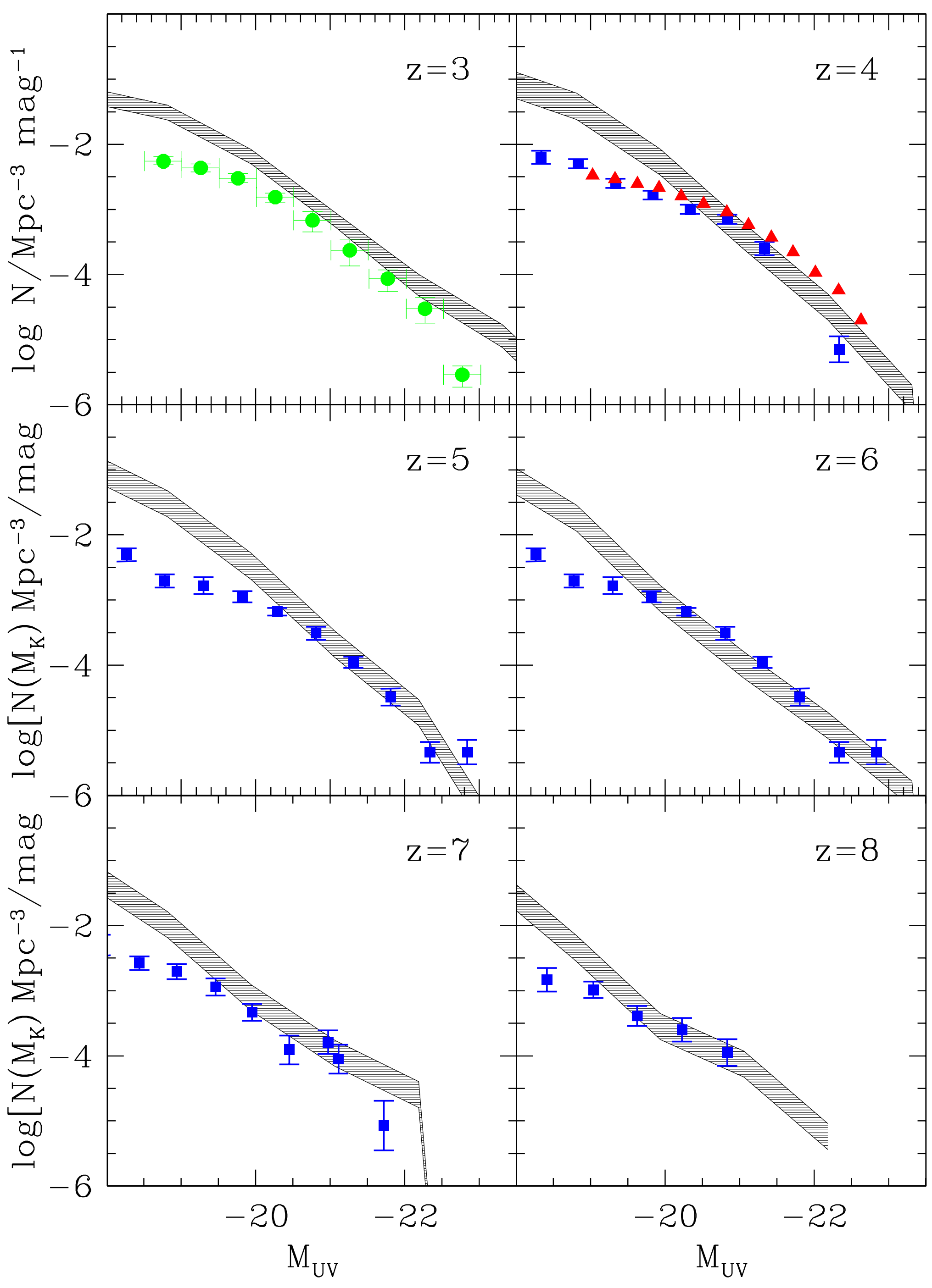

z=3
z=4
z=5
z=6
z=7
z=8
log N/Mpc⁻³ mag⁻¹
log[N(M_K) Mpc⁻³/mag
log[N(M_K) Mpc⁻³/mag
−2
−4
−6
−20
−22
M_UV

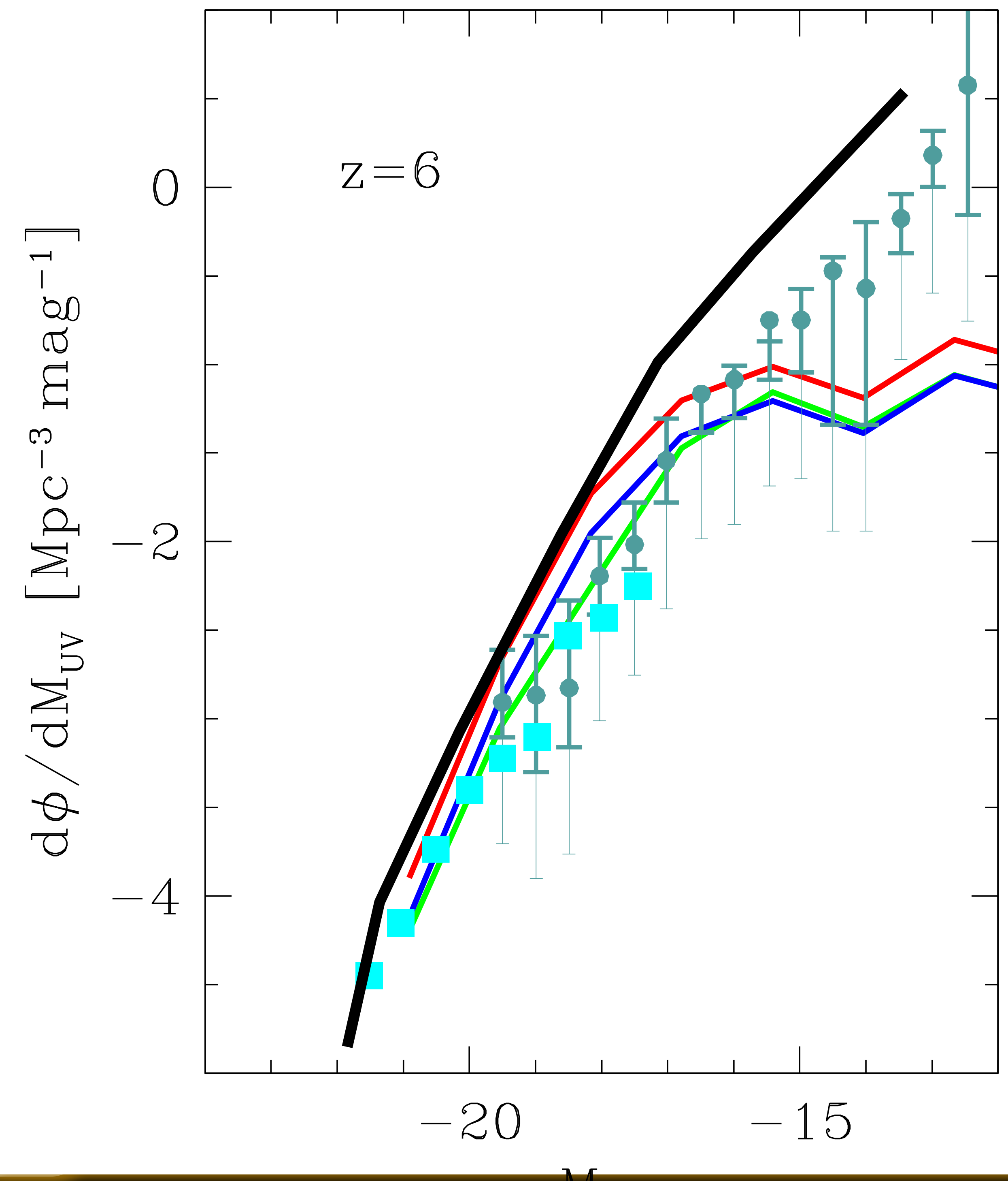

z=6
dφ/dM_UV [Mpc⁻³ mag⁻¹]
0
−2
−4
−20
−15

Mikheev–Smirnov–Wolfenstein

Constraints from X-ray emission from clusters and galaxies

if $m_s > m_\alpha$ the radiative decay $\nu_s \to \nu_\alpha + \gamma$ becomes allowed

$$E_\gamma = \frac{1}{2} m_s \left(1 - \frac{m_\alpha^2}{m_s^2}\right) .$$

Emission lines in X-rays from DM concentrations:
- clusters (large signal but also large background)
- galaxies

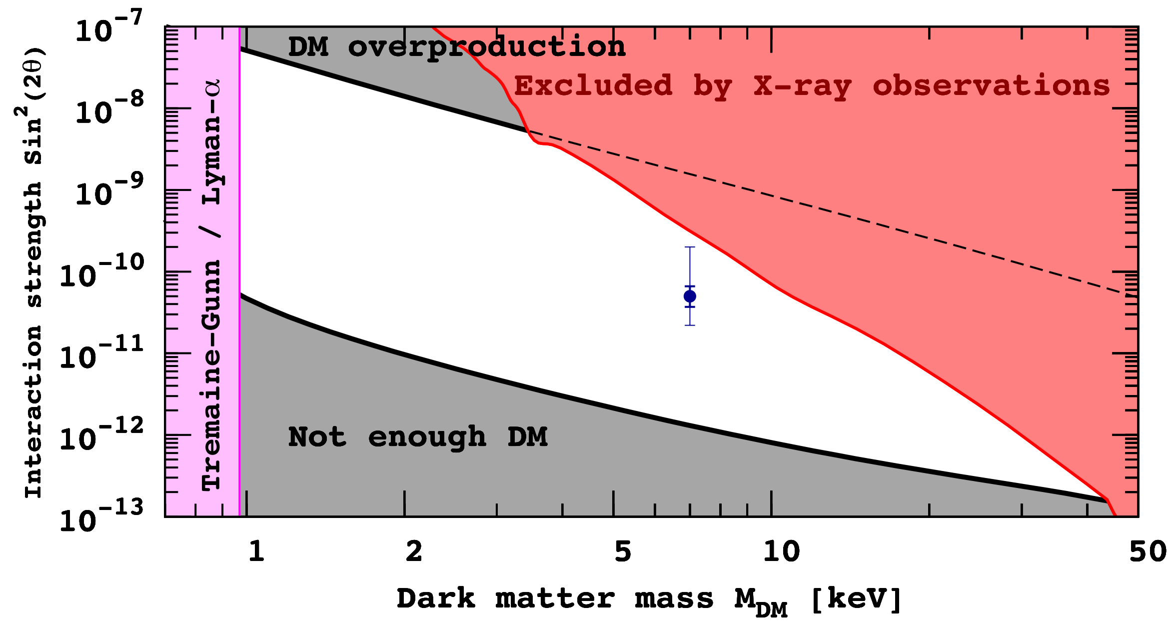

FIG. 4: Constraints on sterile neutrino DM within νMSM [4]. The blue point would corresponds to the best-fit value from M31 if the line comes from DM decay. Thick errorbars are $\pm 1\sigma$ limits on the flux. Thin errorbars correspond to the uncertainty in the DM distribution in the center of M31.

Boyarsky et al. 2014

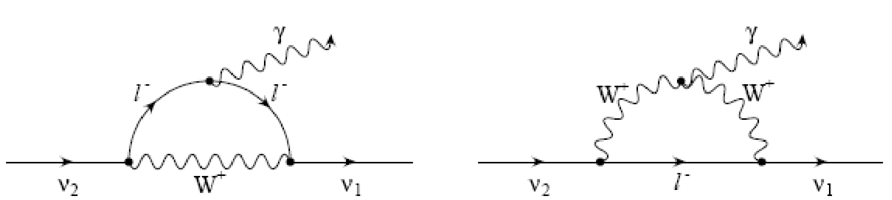

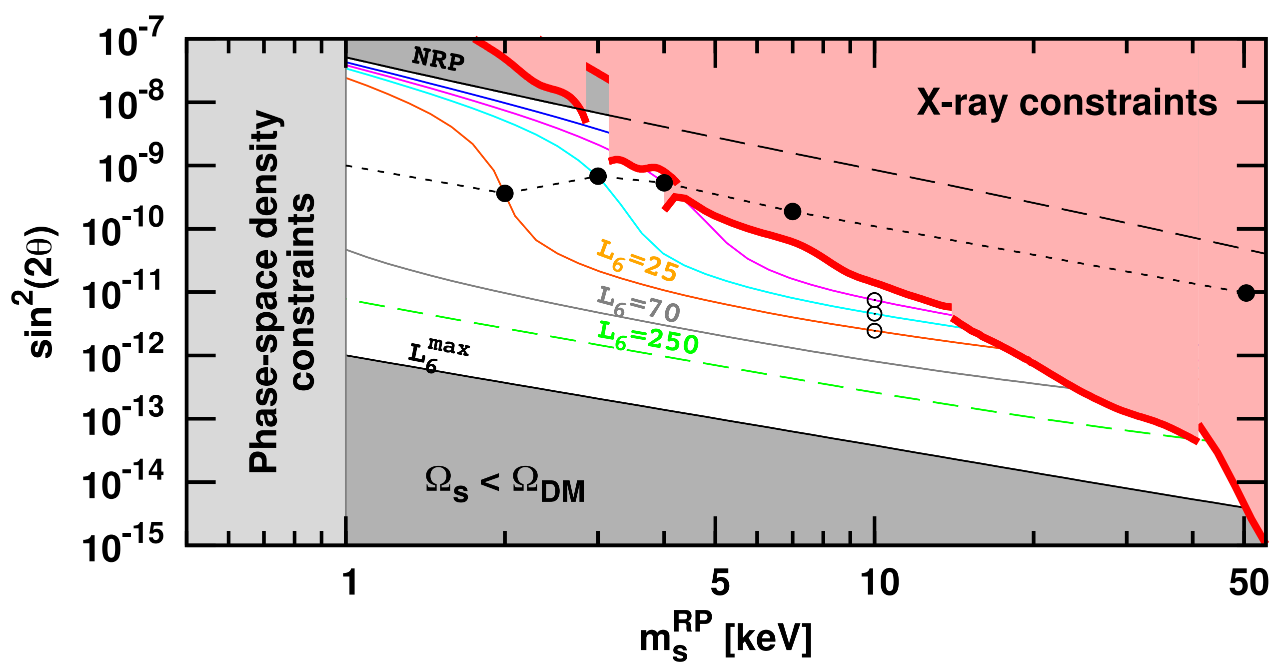

Abazajian et al. 2001-2005

Boyarsky et al. 2009

4.3 DM production in the νMSM

In the νMSM DM sterile neutrinos are produced in the early Universe due to their coupling to active neutrinos. An estimate of the rate of DM sterile neutrino production Γ_N at temperatures below the electroweak scale is given by [55]

$$\Gamma_N \sim \Gamma_\nu \theta_M^2(T) \,, \tag{24}$$

where $\Gamma_\nu \sim G_F^2 T^5$ is the rate of active neutrino production, and where $\theta_M(T)$ is a temperature- (and momentum-) dependent mixing angle:

$$\theta_1^2 \to \theta_M^2(T) \simeq \frac{\theta_1^2}{\left(1 + \frac{2p}{M_1^2}\left(b(p,T) \pm c(T)\right)\right)^2 + \theta_1^2} \,. \tag{25}$$

Here [56]

$$b(p,T) = \frac{16 G_F^2}{\pi \alpha_W} p (2 + \cos^2\theta_W) \frac{7\pi^2 T^4}{360}, \quad c(T) = 3\sqrt{2} G_F \left(1 + \sin^2\theta_W\right)(n_{\nu_e} - n_{\bar{\nu}_e}) \,, \tag{26}$$

where θ_W is the weak mixing angle, α_W is the weak coupling constant, and $p \sim$ few T is the typical momentum of created DM neutrinos. The term $c(T)$ in (25) is proportional to the *lepton asymmetry* and contributes with the opposite sign to the mixing of N_1 with active neutrinos and antineutrinos.

If the term $b(p,T)$ dominates $c(T)$ for $p \sim (2-3)T$ [which we refer to as non-resonant production *NRP*), the production rate (24) is strongly suppressed at temperatures above a few hundred MeV and peaks roughly at [28]

$$T_{peak} \sim 130 \left(\frac{M_1}{1\ \text{keV}}\right)^{1/3} \text{MeV} \,, \tag{27}$$

The production of sterile neutrino DM may substantially change in the presence of lepton asymmetry. If the denominator in Eq. (25) is small,

$$1 + 2p \frac{b(p,T) \pm c(T)}{M_1^2} = 0, \tag{29}$$

then resonant production (*RP*) of sterile neutrinos [29] occurs, analogous to the

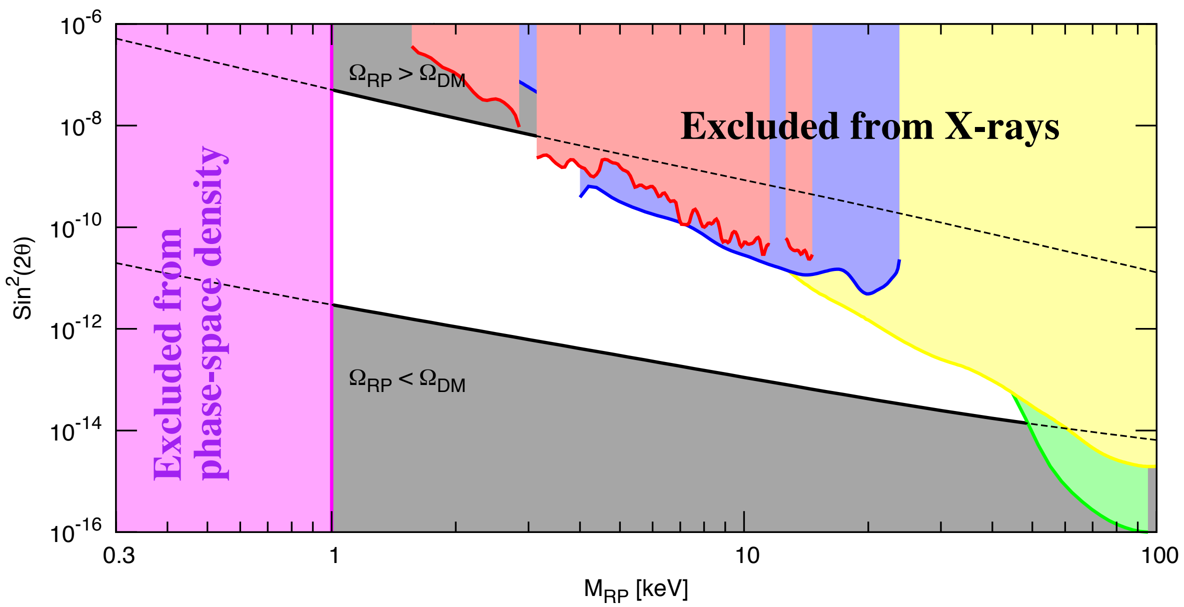

Window corresponds to resonant production

Upper boundary - zero lepton asymmetry

Lower boundary - maximal lepton asymmetry

Boyarsky et al 2009

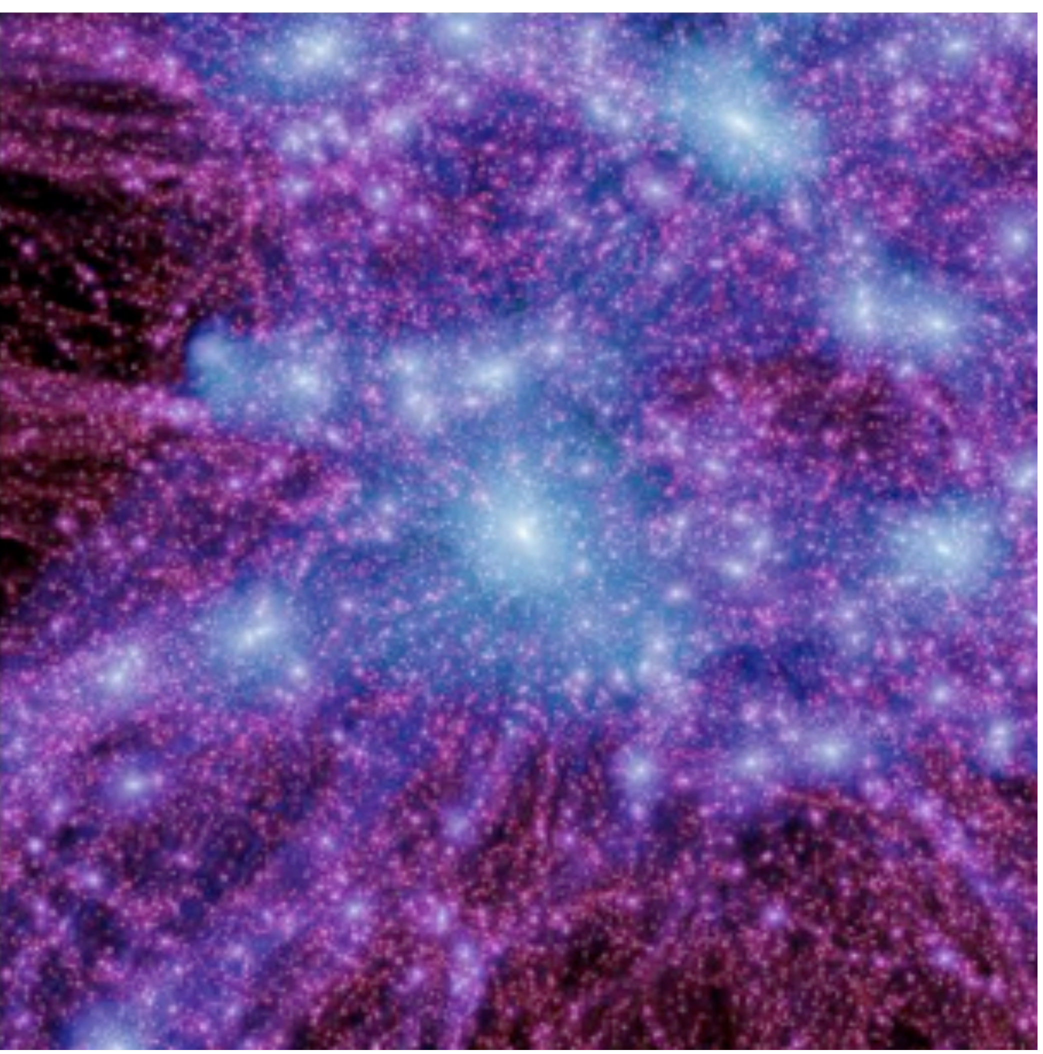

6 – Sterile neutrino resonant production

In presence of a large lepton asymmetry, $\mathcal{L} \equiv (n_\nu - n_{\bar\nu})/n_\gamma$, matter effects become important and the mixing angle can be resonantly enhanced. [Shi, Fuller, 1998; Abazajian et al., 2001

$$\boxed{\sin^2 2\theta_m = \frac{\Delta^2(p)\sin^2 2\theta}{\Delta^2(p)\sin^2 2\theta + D^2 + (\Delta(p)\cos 2\theta - \frac{2\sqrt{2}\zeta(3)}{\pi^2} G_F T^3 \mathcal{L} + |V_T|)^2}}$$

The mixing angle is maximal $\sin^2 2\theta_m = 1$ when the resonant condition is satisfied (with $\Delta(p) \equiv m_4^2/(2p)$)

$$\boxed{\Delta(p)\cos 2\theta - \frac{2\sqrt{2}\zeta(3)}{\pi^2} G_F T^3 \mathcal{L} + |V_T| = 0}$$

$$\boxed{\left(\frac{m_4}{1\mathrm{keV}}\right)^2 \simeq 0.08 \frac{p}{T} \frac{\mathcal{L}}{10^{-4}} \left(\frac{T}{100\,\mathrm{MeV}}\right)^4 + 2\left(\frac{p}{T}\right)^2 \frac{B}{\mathrm{keV}} \left(\frac{T}{100\,\mathrm{MeV}}\right)^6}$$

Sterile neutrinos are produced in primordial plasma through

- off-resonance oscillations. [Dodelson, Widrow; Abazajian, Fuller; Dolgov, Hansen;Asaka, Laine, Shaposhnikov et al.]
- oscillations on resonance, if the lepton asymmetry is non-negligible [Fuller, Shi]

- production mechanisms which do not involve oscillations

– inflaton decays directly into sterile neutrinos [Shaposhnikov, Tkachev] – Higgs physics: both mass and production [AK, Petraki]

Watson et al. 2012

Limits from the
X-ray emission from clusters and
galaxies

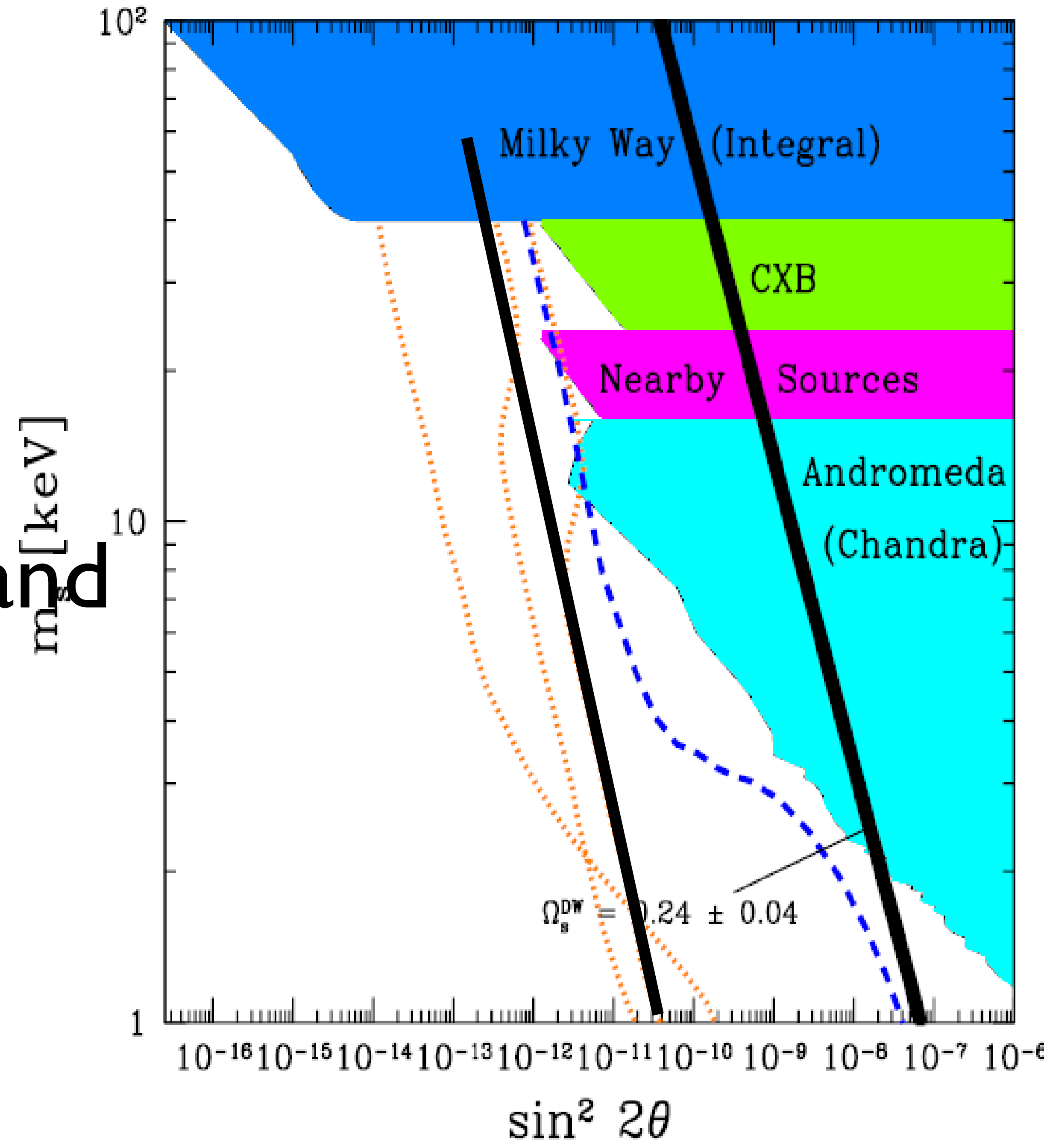

Very small mixing ($\sin^2 2\theta \lesssim 10^{-7}$) between

mass $|\nu_{1,2}>$ & flavor $|\nu_{\alpha,s}>$ states:

$$|\nu_\alpha\rangle = \cos\theta|\nu_1\rangle + \sin\theta|\nu_2\rangle$$
$$|\nu_s\rangle = -\sin\theta|\nu_1\rangle + \cos\theta|\nu_2\rangle$$

For $m_s < m_e$,

3ν Decay Mode Dominates:

$$\Gamma_{3\nu} \backsimeq 1.74 \times 10^{-30} s^{-1} \left(\frac{\sin^2 2\theta}{10^{-10}}\right)\left(\frac{m_s}{\text{keV}}\right)^5$$

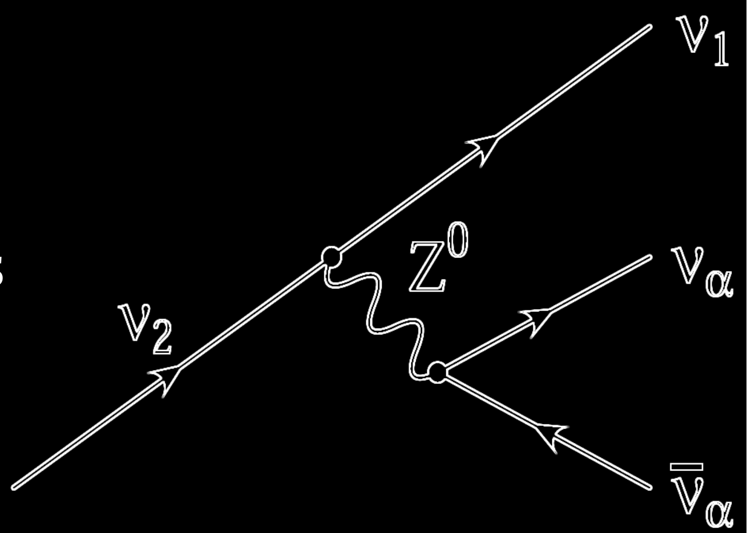

Radiative Decay Rate is:

$$\Gamma_s \backsimeq 1.36 \times 10^{-32} s^{-1} \left(\frac{\sin^2 2\theta}{10^{-10}}\right)\left(\frac{m_s}{\text{keV}}\right)^5 \quad \nu_s \longrightarrow \nu_\alpha + \gamma$$

WIMP

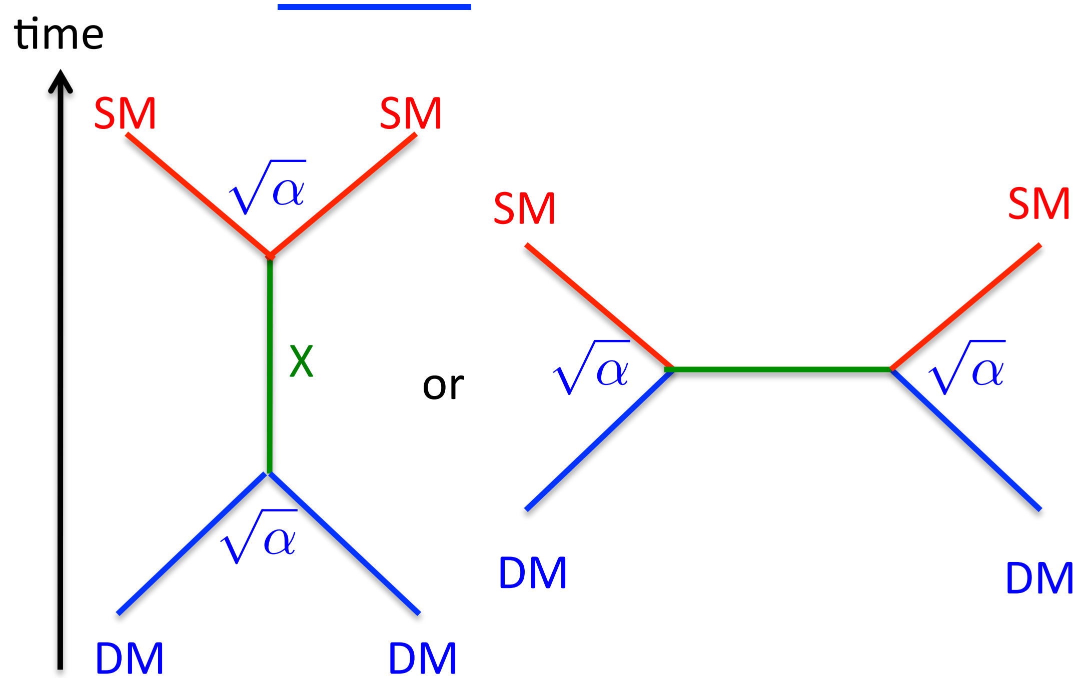

self-annihilation

freeze out

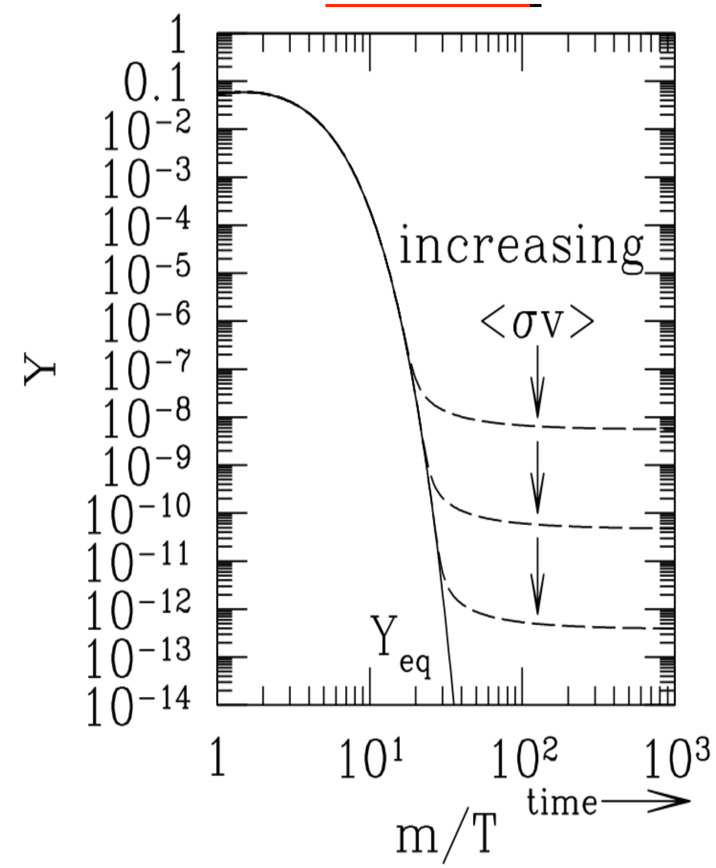

$$\Omega h^2 \approx \frac{3 \times 10^{-27}\ \mathrm{cm}^3/\mathrm{s}}{\langle \sigma_{\mathrm{ann}} v \rangle}.$$

$$\langle \sigma_{\mathbf{ann}} \mathbf{v} \rangle \sim \mathbf{10^{-25}} \mathrm{cm^3 s^{-1}} \left(\frac{\alpha}{\mathbf{10^{-2}}} \right)^{\mathbf{2}} \left(\frac{\mathbf{100GeV}}{\mathbf{m_X}} \right)^{\mathbf{2}}$$

➡ Electro Weak Scale(～100GeV) WIMP naturally explains the relic abundance.

TeV scale SUSY & neutralino dark matter

Dispersional relations for active and sterile neutrinos (from real part)

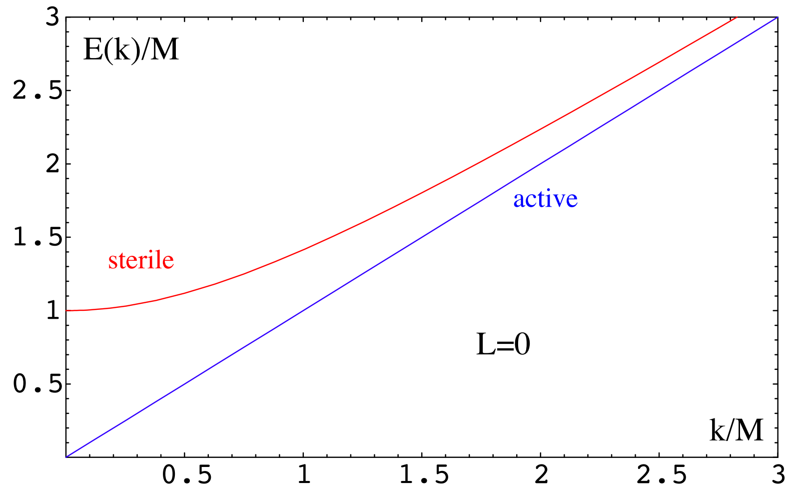

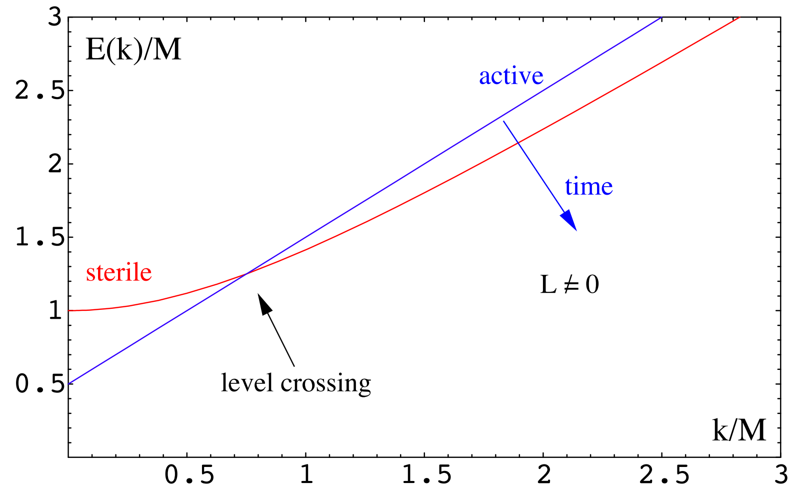

Transitions $\nu \to N_1$

Dodelson-Widrow

Zero lepton asymmetry

Resonant transitions

Shi-Fuller

Lepton asymmetry

created in $N_{2,3}$ decays

Dark matter and the Lyman-α forest.

The bounds depend on the production mechanism.

$$\lambda_{FS} \approx 1\,\mathrm{Mpc}\left(\frac{\mathrm{keV}}{m_s}\right)\left(\frac{\langle p_s\rangle}{3.15\,T}\right)_{T\approx 1\,\mathrm{keV}}$$

The ratio

$$\left(\frac{\langle p_s\rangle}{3.15\,T}\right)_{T\approx 1\,\mathrm{keV}} = \begin{cases} 0.9 & \text{for production off} - \text{resonance} \\ 0.6 & \text{for MSW resonance (depends on L)} \\ 0.2 & \text{for production at T} > 100\text{ GeV} \end{cases}$$

- Photon energy:

$$E_\gamma = \frac{M_1}{2}$$

- Radiative decay width

$$\Gamma = \frac{9\alpha_{\mathrm{EM}} G_F^2}{256\pi^4}\,\theta^2\,M_1^5$$

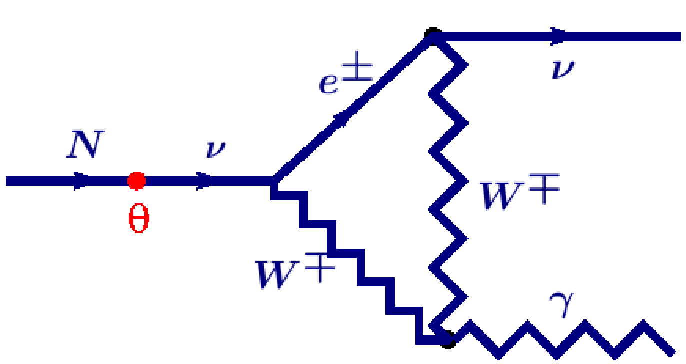

Dark matter made of sterile neutrino is not completely dark

Dolgov & Hansen (2000)

Where to look for DM decay line?

Extragalactic diffuse X-ray background (XRB)	Dolgov & Hansen, 2000; Abazajian et al., 2001 Mapelli & Ferrara, 2005; **Boyarsky et al. 2005**
Clusters of galaxies	Abazajian et al., 2001 **Boyarsky et al. astro-ph/0603368**
DM halo of the Milky Way. Signal increases as we increase FoV!	**Boyarsky et al. astro-ph/0603660** Riemer-Sørense et al. astro-ph/0603661 **Boyarsky, Nevalainen, O.R.** (in preparation)
Local Group galaxies	**Boyarsky et al. astro-ph/0603660** Watson et al. astro-ph/0605424
“Bullet” cluster 1E 0657-56	**Boyarsky, Markevitch, O.R.** (in preparation)
Cold nearby clusters	**Boyarsky, Vikhlinin, O.R.** (in preparation)
Soft XRB	**Boyarsky, Neronov, O.R.** (in preparation)

Need to find the best ratio between the DM decay *signal* and object’s X-ray emission

CDM as particle Dark Matter

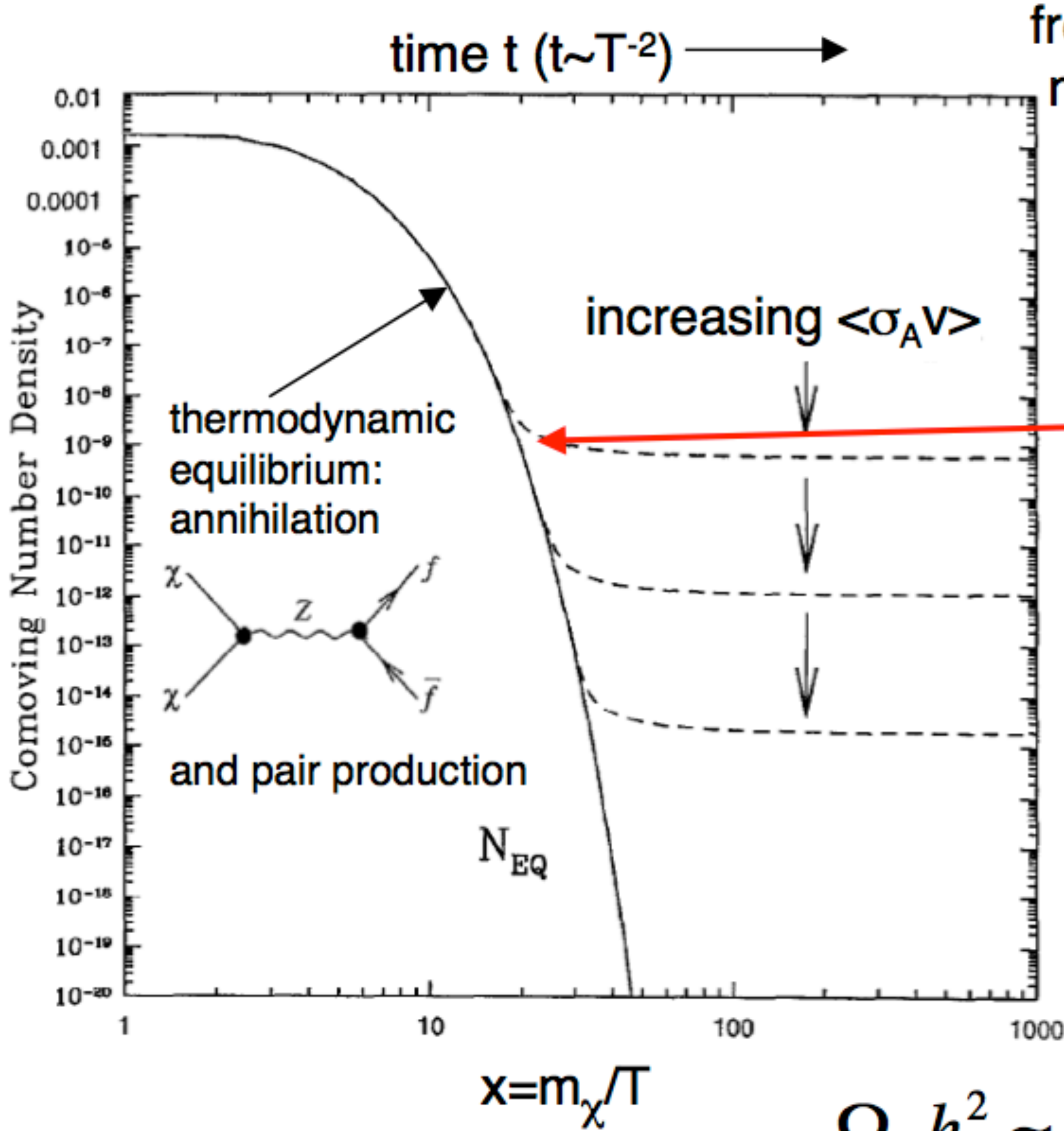

freeze-out of a weakly interacting massive particle (WIMP χ) when reaction rate drops below expansion rate

$T_{freeze\text{-}out}$~ 1/20 x m(WIMP)

Cold Dark Matter:

- non-relativistic

"survival of the weakest"

At or below the weak scale

$$\Omega_\chi h^2 \approx \frac{m_\chi n_\chi}{\rho_c} \approx \frac{3\times10^{-27}\,\mathrm{cm}^3/\mathrm{sec}}{\langle\sigma_A v\rangle}$$

Le Duc et al. 2013

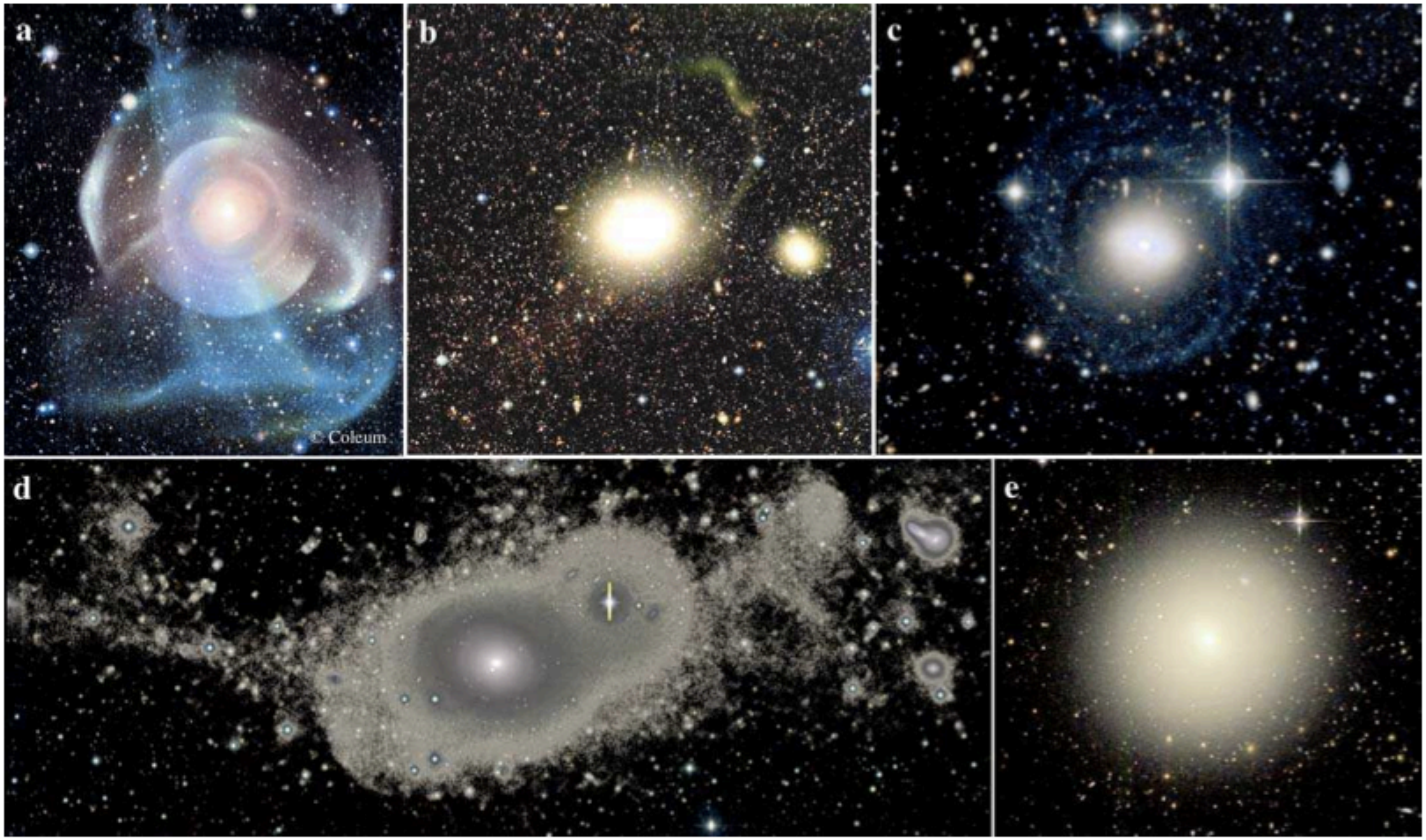

Figure 1. Deep optical images of a sub-sample of nearby Early-Type Galaxies obtained with MegaCam on the CFHT as part of the ATLAS^{3D} and Next Generation Virgo Cluster Survey. The figure illustrates the variety of low surface brightness structures that show up around these galaxies: long tidal tails and shells, telling us about past major mergers (a,d); narrow stellar filaments associated with disrupted dwarf satellites, revealing future minor mergers (b); regular low surface brightness star–forming disks (c); extended featureless stellar halos (e).

The Next Generation Virgo Cluster Survey. IV. NGC 4216: A Bombarded Spiral in the Virgo Cluster Paudel et al. 2014

FIG. 1.— Composite NGVS image of the field around NGC 4216. A monochromatic g–band image for which the faintest point-like stars have been subtracted is shown with a grey scale. For regions above a surface brightness level $\sim$24 mag arcsec^{-2}, and in empty sky regions far from the main galaxy, a true color image (composite of g, i, z-band images) is superimposed. North is up, East is left and the field of view is 20 $\times$ 17 arcmin. The image in the inset on the upper right corner is a zoom towards VCC 165, the closest companion of NGC 4216.